NASA Technical Memorandum 100713

An Improved Error Assessment for the GEM-T1 Gravitational Model

F. J. Lerch
J. G. Marsh
NASA/Goddard Space Flight Center
Greenbelt, Maryland

S. M. Klosko
E. C. Pavlis
EG&G/Washington Analytical Services Center
Lanham, Maryland

G. B. Patel
D. S. Chinn
STX
Lanham, Maryland

C. A. Wagner
NOAA/National Geodetic Survey
Rockville, Maryland

National Aeronautics
and Space Administration

Goddard Space Flight Center
Greenbelt, Maryland 20771

1988

PREFACE

An Improved Error Assessment for the GEM-T1 Gravitational Model

Several tests have been designed to determine the correct error variances for the GEM-T1 gravitational solution which was derived exclusively from satellite tracking data. The basic method employs both wholly independent and dependent subset data solutions and produces a full field coefficient by coefficient estimate of the model uncertainties. The GEM-T1 errors have been further analyzed using a method based upon eigenvalue-eigenvector analysis which calibrates the entire covariance matrix. Dependent satellite and independent altimetric and surface gravity data sets, as well as independent satellite deep resonance information, confirm essentially the same error assessment. These calibrations (utilizing each of the major data subsets within the solution) yield very stable calibration factors which vary by approximately 10% over the range of tests employed. Measurements of gravity anomalies obtained from altimetry were also used directly as observations to show that GEM-T1 is calibrated. Based upon these calibrated error estimates, GEM-T1 is a significantly improved solution which to degree and order 8 is twice as accurate as earlier satellite derived models. By being complete to degree and order 36, GEM-T1 is much larger than earlier gravitational solutions calculated from direct satellite tracking and has significantly reduced aliasing effects that were present in previous models. The mathematical representation of the covariance error in the presence of unmodeled systematic error effects in the data is analyzed and an optimum weighting technique is developed for these conditions. This technique yields an internal self-calibration of the error model, a process which GEM-T1 is shown to approximate. This geopotential field with calibrated error estimates, predicts 25 cm for the radial RMS uncertainty of the TOPEX orbit. The TOPEX Mission has a requirement for 10 cm radial orbital modeling which is needed to support the oceanographic applications of a high quality spaceborne altimeter.

TABLE OF CONTENTS

TABLE OF CONTENTS (cont.)

I. INTRODUCTION

The least-squares method yields a formal estimate of a solution's accuracy. This estimate is generally optimistic due to imperfections in the mathematical model employed and suspected, yet unmodeled, systematic error sources resulting in non-random observation residuals. Hence some form of verification and calibration of errors is required to reliably establish the "true" accuracy of the results. This verification is made difficult in circumstances where the solution output is a mathematical model of a physical phenomenon whose empirical coefficients taken individually are not directly observed. This situation applies here to the problem of estimating the accuracy of a geopotential field determined from satellite tracking data. Such models have grown in size and resolution as tracking instrumentation has advanced and many satellite orbits became available. It is desirable to validate such a solution completely and even though recent models now contain more than 1300 individual coefficients, this has become feasible with the main method employed here (Lerch, 1985) and the use of high speed vectorized computers. It is also desirable and feasible to validate the entire error covariance matrix through an eigenvector analysis as developed in this report.

We discuss here the error calibration of "satellite only" Goddard Earth Models (GEM). These fields have been computed from restricted observation sources sensitive only to satellite dynamics. To serve the objectives of error calibration, data rich in high frequency local information have been excluded when deriving these fields. An accuracy assessment of these models benefits from a direct comparison with such information derived from satellite altimetry and surface gravimetry which both independently describe the gravitational field over vast regions of the earth's surface with a resolution well beyond the limits of satellite dynamical sensitivity. Tests of the geopotential solution with global sets of these independent local observations have yielded important statistics on the true accuracy of the gravitational models. Historically, the Goddard Earth Models have been calibrated through the

use of these and other independent data as described in Lerch (1985), Lerch et al. (1974, 1979, 1985, and 1986), Wagner (1983), and Wagner and Lerch (1978). These calibrations were made using a variety of tests and comparisons including those already mentioned with surface gravimetry and altimetry, and also utilizing deeply resonant orbits and assessments of orbit solutions when fit to tracking data excluded from the solution. All such tests in the past used data sets that were essentially independent of the model.

For example, an earlier validation method, and one which has had some success, was to divide the final solution into independent pieces. Independent solutions were computed from these highly decimated portions of the original data set to assess solution weighting factors and scaled formal statistics. In the past, we have used this approach to compare the laser vs. optical contributions in the GEM models (Lerch et al., 1985). But this type of test has its limitations, for these subset solutions seldom approach the accuracy of the complete original field. Nonetheless, calibrations using this method have proven beneficial in establishing rough estimates of field accuracy while also testing data weighting approaches and locating suspect data contributions.

The fundamental objective of our analysis in the GEM models is to develop the most accurate and well resolved spherical harmonic expansion of the gravitational field, and at the same time, obtain reliable estimates of its uncertainty. As the work progresses, the information included in the models is upgraded and made more complete through the incorporation of additional data types. Independent data tests are more difficult to construct as these formerly independent observations are merged into the solution. Obviously, the most accurate and complete models require the best observations to resolve the geopotential. The final solution inevitably contains all of the strongest data sets. Therefore, independent data are increasingly more difficult to find and the desired accuracy of the model outweighs the needs of specific error calibrations which require the exclusion of independent test data subsets. Our latest GEM-T1 solution (Marsh et al., 1988) has been developed

to serve as the base model for a whole new series of comprehensive geopotential solutions. Future solutions will contain virtually all significant satellite tracking data sets, and combination models will also contain surface gravimetry and satellite altimetry.

In anticipation of the need to verify the accuracy of increasingly more comprehensive and precise gravitational models, a new technique was sought to achieve reliable full field calibrations. This new method developed by Lerch (1985) uses major dependent subsets of the full solution and is described further in the report on GEM-T1 (Marsh et al., 1987). This method of calibrating a solution is the main focus of this paper. We will show that in addition to the verification of the model uncertainties, this technique yields valuable information on the proper weighting of the data subsets comprising the field, and on the proper relative weighting of new data when they are introduced into existing models.

This calibration technique is based upon the comparison of the complete model with a nearly equivalent one lacking the specific contribution of an individual observation subset. In this case, the subset field is not substantially reduced in performance and the complete complementary data set and the original model undergo simultaneous calibration. Since an individual data subset of GEM-T1 does not significantly span all of the eigenvectors of GEM-T1, it is important to test the calibration on each of the major data subsets individually. Hence, this report shows the error assessment of GEM-T1 using all of the major subsets comprising the solution. Furthermore, since GEM-T1 lacks gravimetry, altimetry and deep resonant satellite information, the calibrations obtained through this analysis are compared with that obtained through more traditional calibrations using independent data. Finally, given that the solution uncertainties (error variances) alone of a satellite-derived model are insufficient to predict the performance of the field on specific orbits, a more complete calibration and validation of the error covariance matrix of the geopotential solution was required. This analysis was extended to the calibration of the

eigenvectors of the GEM-T1 error covariance matrix which is a major element developed within this report.

Since the primary method of calibration subtracts a pair of solutions with and without a given subset of data, there is concern that a bias due to some unmodeled effect may exist in each of the solutions which would be eliminated through the subtraction and therefore remain undetected. In order to account for this type of problem, calibrations were also made which test the gravitational solutions directly with independent surface based and deep resonant observations. Gravity anomalies obtained from altimeter data and deep satellite resonant passage observations were employed for this purpose.

A principal interest in these error assessments is to predict the performance of the geopotential on the yet-to-be-flown TOPEX satellite. Gravitational modeling error is the dominant error source which can degrade the precise ephemerides sought for this mission. An accuracy level of 10cm in the radial component of the TOPEX orbit is required which is substantially beyond the capabilities of any existing gravitational models. GEM-T1 is a preliminary model developed for the TOPEX Project and has reduced the field uncertainty for this mission. An assessment of TOPEX orbit modeling capabilities will also be presented based upon the calibration of the full GEM-T1 covariance matrix since the covariance terms significantly affect this error estimate.

An Appendix in three sections (A1, A2, A3) is presented to elaborate on the estimation theory employed in GEM-T1 and in this report. Because of the systematic error effects in the data and other unmodeled force effects, the mathematical validity of the representation of the covariance error is analyzed in Appendix A. Also included in the Appendix is an optimum process for simultaneously converging on all data subset weights. These weights compensate for the unmodeled systematics and provide an automatic self-calibration of the error covariance internal to the solution. It is shown that the method of solution for GEM-T1 approximates this process.

II. GEM-T1 CALIBRATION OVERVIEW

GEM-T1 was derived from about 800,000 tracking observations on 17 satellites (Table 1) consisting of laser, optical and Doppler data. When combining data from different instruments and different orbits whose sensitivity to non-gravitational signals vary widely, strategies must be developed and tested to obtain optimal data weighting factors. And to account for the general problem of optimistic formal statistics, we have found it necessary to scale down considerably the entire data set of the solution in order to yield a properly calibrated solution.

The solution is obtained by simultaneously solving for a 36x36 gravitational model, 66 dynamic tidal terms having long period orbital perturbations and earth orientation parameters for the post-1979 time period. A total of nearly 2500 unknowns comprised the solution after back-substitution of approximately 7000 satellite-arc-dependent parameters (e.g., orbit elements, drag and solar radiation pressure coefficients and doppler biases).

The post-fit performance of a solution on the tracking data--the so called "residual analyses"--plays a significant role in the design of the solution, the selection of data weights, and in the final error assessments. Marsh et al., (1987) discuss this problem and show in considerable detail relatively large orbit residuals for laser systems as compared to their precision level. In Appendix A2 these tracking residuals are analyzed on a pass-by-pass basis for some of the laser systems and show considerable biases which are unmodeled in GEM-T1. Hence, this verifies the need for the downweighting factors to compensate for unmodeled biases and to test the calibration of the error covariances.

This report utilizes all of the major data sets and will more completely verify the GEM-T1 accuracy assessments through a comprehensive calibration of the solution variances and through a new technique utilizing eigenvector analyses which will test the entire

TABLE 1

SATELLITE DATA IN GEM-T1

SATELLITE	SEMI MAJOR AXIS (km.)	ECC	INCL DEG	DATA TYPE	# OF ARCS	# OF OBS	RMS RESID.	SIGMA* WEIGHTS
1 LAGEOS	12273.	.0038	109.85	LASER	57	144527	10cm.	112cm.
2 STARLETTE	7331.	.0204	49.80	LASER	46	57356	20cm.	224cm.
3 GEOS-3	7226.	.0008	114.98	LASER	36	42407	70cm.	816cm.
4 PEOLE	7006.	.0164	15.01	LASER	6	4113	90cm.	816cm.
5 BE-C	7507.	.0257	41.19	LASER	39	64240	50cm.	577cm.
				CAMERA	50	7501	2 arcsec	5.6 arcsec
6 GEOS-1	8075.	.0719	59.39	LASER	48	71287	70cm.	667cm.
				CAMERA	43	60750	1 arcsec	8.9 arcsec
7 GEOS-2	7711.	.0330	105.79	LASER	28	26613	80cm.	816cm.
				CAMERA	46	61403	1 arcsec	8.9 arcsec
8 DI-C	7341.	.0532	39.97	LASER	4	7455	150cm.	816cm.
				CAMERA	10	2712	2 arcsec	7.3 arcsec
9 DI-D	7622.	.0848	39.46	LASER	6	11487	100cm.	816cm.
				CAMERA	9	6111	2 arcsec	8.9 arcsec
10 SEASAT	7170.	.0021	108.02	LASER	14	14923	70cm.	707cm.
				DOPPLER	14	138042	.5cm/sec	7cm/sec
11 OSCAR-14	7440.	.0029	89.27	DOPPLER	13	63098	1cm/sec	8cm/sec
12 ANNA-1B	7501.	.0082	50.12	CAMERA	30	4463	2 arcsec	4.5 arcsec
13 BE-B	7354.	.0135	79.69	CAMERA	20	1739	2 arcsec	4.5 arcsec
14 COURIER-1B	7469.	.0161	28.31	CAMERA	10	2476	2 arcsec	4.5 arcsec
15 TELSTAR-1	9669.	.2429	44.79	CAMERA	30	3962	2 arcsec	4.5 arcsec
16 VANGUARD-2RB	8496.	.1832	32.92	CAMERA	10	686	2 arcsec	4.5 arcsec
17 VANGUARD-2	8298.	.1641	32.89	CAMERA	10	1299	2 arcsec	4.5 arcsec

* $SIGMA\ (\sigma) = \left(\frac{1}{w}\right)^{\frac{1}{2}}$

covariance matrix. To do so convincingly, different accuracy estimates and error calibrations will be undertaken and compared spanning the spectrum of eigenvectors in GEM-T1. The stability of results across this spectrum will give insight into realistic field accuracy and will demonstrate the reliability of this determination. The coefficient uncertainties for GEM-T1 are shown in Figure 1.1. They are also presented as an rms coefficient error by degree in Figure 1.2.

A review of the solution technique (Section III) utilized to achieve the weighting factors employed in the computation of GEM-T1 is useful to the discussion of the calibration method which is presented in Section IV.

ERRORS X 10^9

RMS	DEGREE	0	1	2	3	4	5	6	7	8	9	10	11	12	13	14	15	16	17	18	19	20	21	22	23	24	25	26	27	28	29	30	31	32	33	34	35	36
0	2	0		0																																		
1	3	0	1	1	1																																	
1	4	1	1	2	1	1																																
2	5	0	3	3	2	2	2																															
2	6	2	2	3	3	2	1	1																														
3	7	1	4	5	4	3	3	0	2																													
3	8	2	3	5	5	4	3	2	2	4																												
5	9	1	6	7	7	6	4	3	3	3	6																											
5	10	3	4	7	7	6	5	3	3	3	4	4																										
6	11	2	7	8	8	9	7	5	4	4	4	4	6																									
6	12	4	6	7	9	9	8	6	5	3	4	3	3	3																								
7	13	4	6	10	9	11	10	8	6	5	4	5	4	2	1																							
7	14	4	6	7	9	10	10	9	8	5	5	3	4	2	1	2																						
7	15	4	6	10	9	10	12	10	9	7	6	5	4	3	1	1	3																					
7	16	4	7	9	8	11	11	11	10	8	6	4	4	2	1	1	4	7																				
8	17	4	9	9	11	10	11	12	10	9	7	6	5	4	1	1	1	6	8																			
8	18	4	6	10	10	9	12	11	11	11	8	6	4	2	1	1	4	4	7	11																		
8	19	3	10	9	11	11	11	11	11	11	9	7	5	2	1	1	3	5	4	9	11																	
8	20	5	7	10	11	9	11	11	11	11	10	8	4	3	1	2	3	4	7	6	9	13																
8	21	3	9	9	11	10	11	10	11	11	10	9	5	5	2	1	3	4	6	8	6	10	11															
8	22	5	7	9	10	10	11	10	11	10	10	9	5	4	1	2	3	5	6	7	8	8	10	13														
8	23	3	8	9	10	10	11	10	10	10	10	9	6	6	3	2	4	5	6	6	8	8	6	10	11													
8	24	5	7	9	9	10	10	10	10	10	10	9	6	5	2	3	4	6	6	6	7	8	8	8	10	11												
8	25	3	8	9	9	10	10	10	9	9	9	8	7	6	4	3	4	5	6	7	7	7	8	8	8	6	9	8										
7	26	5	7	8	9	9	9	9	9	9	9	9	7	6	3	4	5	6	6	7	7	7	7	8	8	7	7	8	8									
7	27	4	7	8	9	9	9	9	8	9	8	8	7	6	4	4	5	6	6	7	7	7	7	7	7	7	6	5	6	3								
7	28	5	7	8	8	8	8	8	8	8	8	8	7	6	4	4	6	6	7	7	7	7	6	7	7	6	6	6	5	5								
7	29	5	7	8	8	8	8	8	8	8	8	8	7	6	4	5	6	6	7	7	7	7	6	6	6	6	5	6	8									
6	30	5	6	7	7	7	7	7	7	7	7	7	6	6	5	5	6	6	7	7	7	7	6	6	6	6	6	6	6	7								
6	31	5	7	7	7	7	7	7	7	7	7	7	6	6	5	4	6	6	6	6	6	6	6	6	6	5	5	5	5	4	4	4	6	7				
6	32	4	6	6	6	6	6	6	6	6	6	6	6	6	5	5	6	6	6	6	6	6	6	6	6	6	5	5	5	4	4	4	5	6	7			
5	33	4	6	6	6	6	6	6	6	6	6	6	6	6	5	4	5	6	6	6	6	6	6	6	6	6	5	5	5	4	3	3	4	6	6	6		
5	34	5	6	6	6	6	6	6	6	6	6	6	6	5	5	4	5	6	6	6	6	6	6	6	6	6	5	5	5	4	4	3	4	4	5	6	6	
5	36	4	5	5	5	5	5	5	5	5	5	5	5	5	4	4	5	5	5	5	5	5	5	5	5	5	5	4	3	2	3	4	5	5	5	6	6	5
		0	1	2	3	4	5	6	7	8	9	10	11	12	13	14	15	16	17	18	19	20	21	22	23	24	25	26	27	28	29	30	31	32	33	34	35	36
																	ORDER																					
RMS		4	6	7	8	8	8	8	8	8	7	7	6	5	3	3	5	6	6	7	7	7	7	7	7	6	6	5	4	4	5	5	6	6	6	6	6	5

ESTIMATED ERRORS FOR GEM-T1 COEFFICIENTS

Figure 1.1

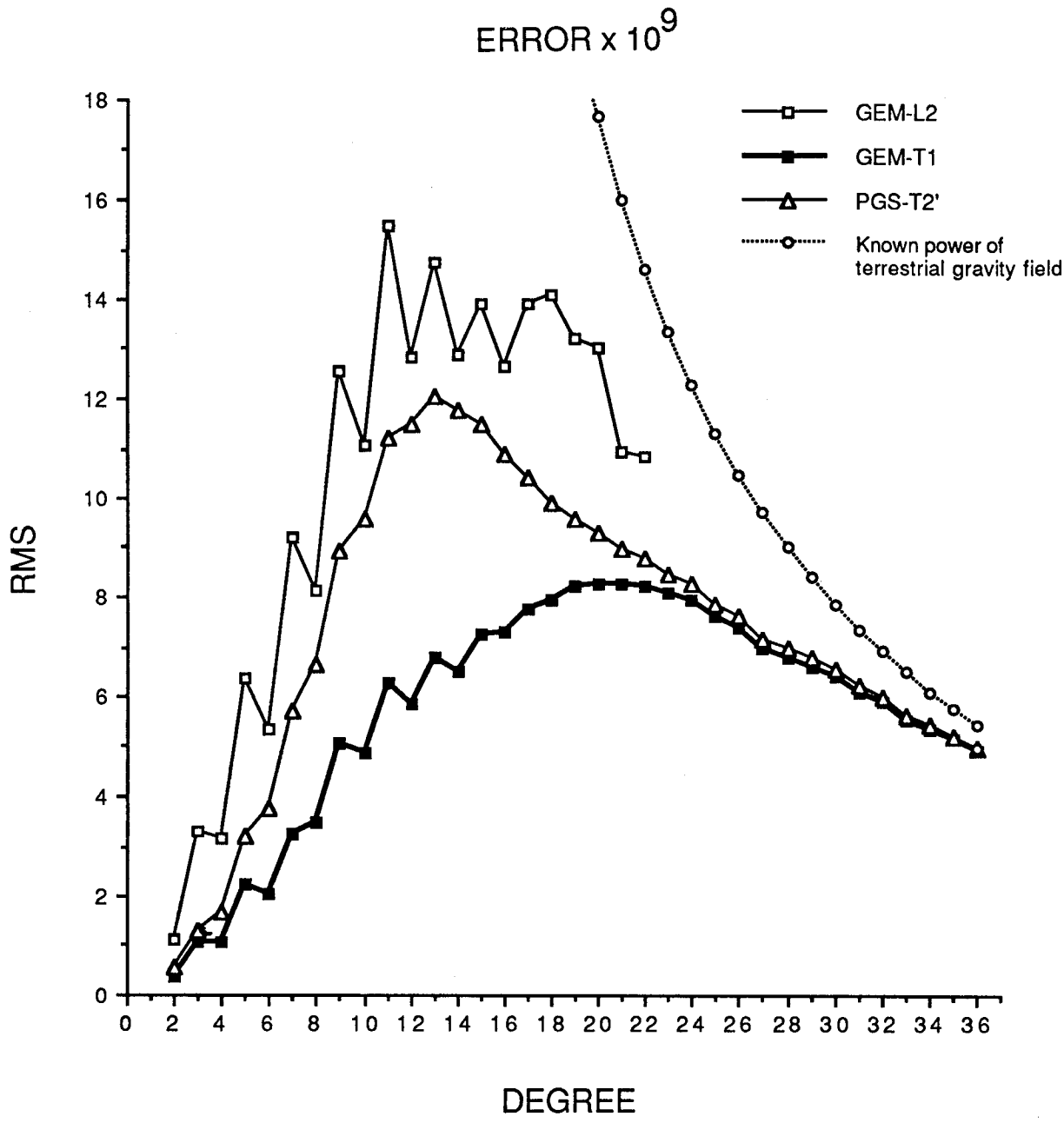

GEM-L2 - - - Previous gravity model (20 x 20 field)

GEM-T1 - - - TOPEX gravity model (36 x 36 field)

PGS-T2' - - - TOPEX model: GEM-T1 without low inclination satellites

RMS Coefficient Error per Degree

Figure 1.2

III. TECHNIQUE AND DATA WEIGHTING FOR THE GEM-T1 SOLUTION

The method of solution is a modified-least squares process which minimizes the sum (Q) of signal and noise as follows:

$$Q = \sum_{\ell,m} \frac{C^2_{\ell,m} + S^2_{\ell,m}}{\sigma^2_\ell} + f \sum_t \sum_{\substack{obs \\ i}} \frac{r^2_{it}}{\sigma^2_t} \qquad (3.1)$$

- where the signal is given by

$C_{\ell,m}$, $S_{\ell,m}$: spherical harmonics comprising the solution coefficients; and

σ_ℓ: $\frac{1}{\sqrt{2}} \times \frac{10^{-5}}{\ell^2}$ is rms of the coefficients of degree ℓ (a priori rule) and is introduced to permit larger solutions to degree and order 36x36. This law, based upon Kaula's rule, has been obtained independently from studies of the spectra of the Earth's gravity field and is used here to represent the observed power within the geopotential.

- and the noise by

r_{it} : observation residual (observed-computed) for the ith observation of satellite tracking data set (type) t; and

σ_t : RMS of observation residuals (generally significantly greater than a priori data precision)

f : downweighting factor to compensate for unmodeled error effects in the data (ideally f=1).

The weighting factor f is used to scale the data contributions; unmodeled errors remain in the data and this scale factor is utilized to obtain realistic error estimates from the solution statistics (variance-covariance matrix). A proper combination of the data normals with the well-known size of the a priori signal (σ_ℓ) is the result. Since f is

not well known, as it depends upon the biases in the data (see Appendix A1), it must be estimated in the development of the solution from the data itself. The value of f was obtained from an extensive calibration procedure which we describe in what follows. Presently we have found that the value f = .02 is required since residuals in the tracking data are systematic and highly correlated particularly within a given tracking pass.

When minimizing Q in (3.1) using the least-squares method, the normal metric equation and error covariance is obtained as follows:

$$Nz = R$$ are the normal equations, where z is the solution, R is the vector of residuals, and

$$V_{zz} = N^{-1}$$ is the approximate form for the variance-covariance error matrix which must be calibrated. (3.2)

The complete expression for V_{zz} is given in Appendix A2 which accounts for systematic unmodeled effects. It is shown therein that, with the proper downweighting factors, N^{-1} is a reasonable approximation.

Certain characteristics of the solution are important. The relative weighting factors $(1/\sigma_t^2)$ are first obtained as the rms (σ_t) of the observation residuals from the solution for each satellite data type t. In converging σ_t, a few test arcs of each satellite data type are employed. A value of f is also iterated upon and is obtained principally by comparing the solution with independent gravity anomalies in the usual calibration procedure. For example, we have found (Marsh, et al., 1988) the overall weighting factor, f = .02, provides for realistic error estimates of the coefficients in GEM-T1. It is shown also (Appendix A1.2 and A1.3) that this downweighting accounts for the systematic trends in the data residuals which are not random and are strongly correlated over a pass of tracking data. The residuals in post-fit analyses (Appendix A1.1) are predominantly trended and typically fall on a straight line over time for a given tracking interval. If the residuals were random then f=1 (which is the ideal case) would be realized for the least-squares weighting. The need to

use f=.02 for the solution scaling factor is interpreted as an indication that non-gravitational signals must be better accommodated. Usually a few iterations of combining and fine-tuning the weights for the normals for each satellite data type are required to converge on proper weighting factors. In Appendix A3 an optimal technique is developed allowing $f(f_t)$ to converge simultaneously on all subset data types. This was applied to a certain extent in the development of GEM-T1 as indicated by the weights given in Table 1.

Another important aspect of the error estimation process is the effect of the a priori signal on the solution (in the minimization of Q in (3.1)). The signal consists of the gravitational coefficients with an a priori estimate of their size, σ_ℓ, like the modified version of Kaula's rule $(\frac{1}{\sqrt{2}}\, 10^{-5}/\ell^2)$ which is used here. The normal least squares adjustment solely minimizes the noise (observation residuals) to obtain the solution. The process used here is a modified least squares adjustment which minimizes both the signal (the size of the potential coefficients which are constrained with an a priori power spectrum) and the noise simultaneously. This latter approach (Lerch et al., 1977 and 1985) permits a more satisfactory and accurate estimation of high degree and order terms. This process is also referred to as collocation (Moritz, 1978, 1980). The process is necessary for solution stability especially in the determination of the high degree portion of the field. While there is some sensitivity within the data to these high degree terms, there is a lack of separability for the entire set.

With the normal least squares approach (noise-only minimization) there is a problem of separability due to the strong correlation between many of the high degree coefficients. The absence of collocation (GEM-T1 without the Kaula constraint) results in excessively large power in the adjustment of the potential coefficients. Figure 2 illustrates the instability of the least-squares solution when collocation is not used. A satellite-derived gravity solution has been solved without collocation which is evaluated using a global set of independent gravity

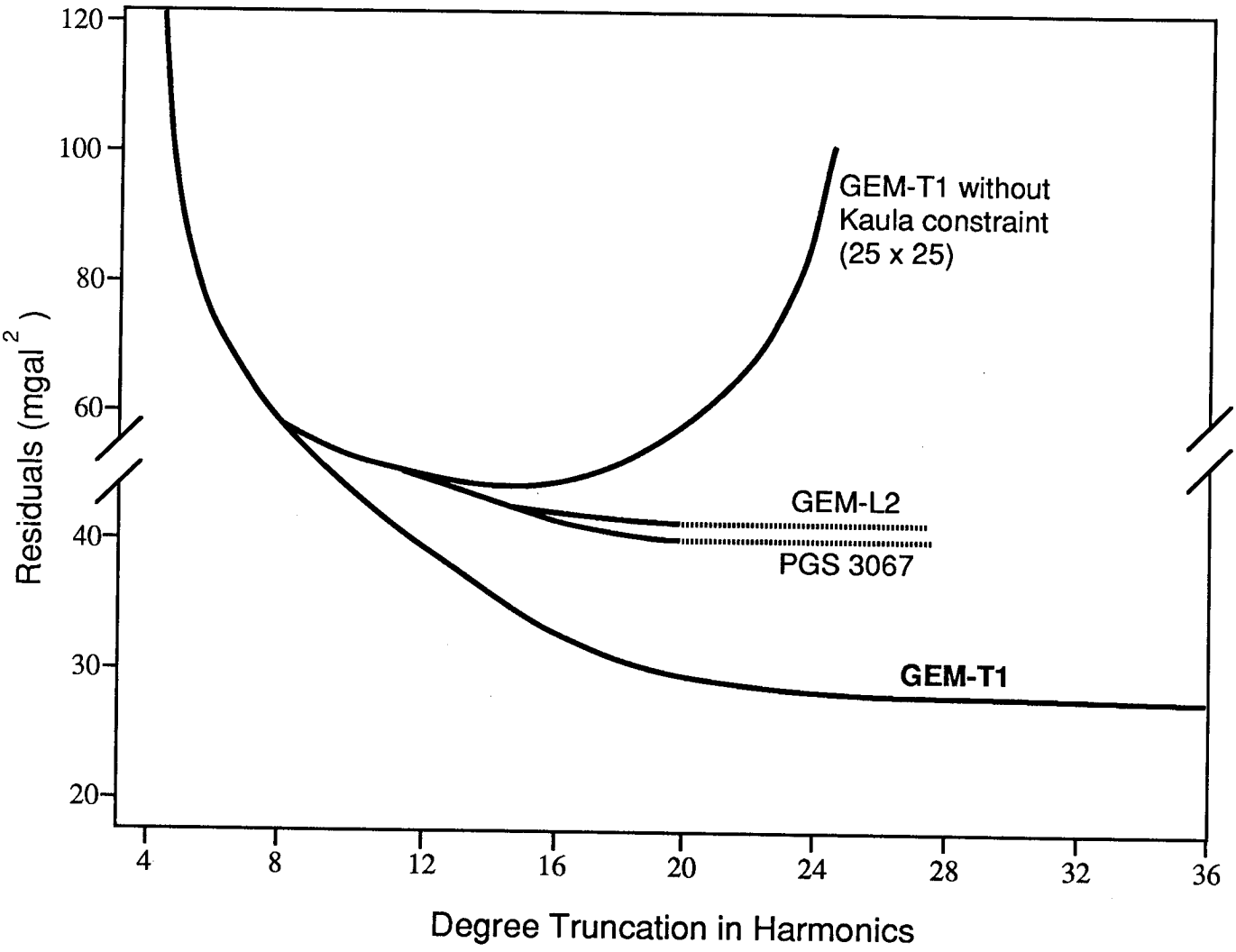

Gravity Model Comparison with 1114 5°x5° SEASAT Gravity Anomalies

Figure 2

anomalies. An unrestricted high degree field performs poorly due to excessively large adjustment in the coefficients which is normally circumvented in the standard least-squares method by solving for a smaller sized field. Unfortunately, by restricting the size of the field, one also is requiring the higher degree terms above the field limits to be constrained absolutely to zero. Figure 2 also shows the disadvantage of this approach where the smaller sized field (PGS-3067) contains aliasing in its coefficients and does not perform well. (The abbreviation PGS stands for Preliminary Gravity Solution.) The aliasing signal sensed in the data above the field limits is absorbed into the adjustment of the lower degree coefficients. The best approach is seen with the least-squares collocation (or constrained) solution, GEM-T1, with a complete solution of a 36x36 field in harmonics.

Since the a priori signal matrix contains only diagonal terms which are added to the data normals, it is interesting to compare the relative size of their contribution to the overall data normals. As seen in Table 2, the satellite normal equations have considerably larger diagonal terms than does the collocation matrix. At lowest degree, the ratio of the two contributions indicates that the collocation contribution is barely visible. It is only at highest degree that the collocation contributions become a large percent (30%) of the diagonal terms. Since collocation stabilizes the entire solution, it does so by indirectly controlling ill-conditioning due to correlation within the system of observation equations.

Table 2

Ratio of Diagonal Elements of GEM-T1 vs. Signal (Kaula) * Matrix

Degree (ℓ)	ratio** of diagonal elements for specific terms: Order m=1	Sectorial m=ℓ
2	400,000,000	4,000,000,000
5	5,000,000	1,700,000
10	400,000	200,000
15	30,000	30,000
20	1,500	10
25	300	7
30	50	6
35	7	3

* Collocation/ Kaula Weight = $\dfrac{1}{\left[\dfrac{1}{\sqrt{2}}\dfrac{10^{-5}}{\ell}\right]^2} = 2\text{x}10^{10}\ell^4$

** $= \left[\dfrac{\text{DIAG}_{\text{GEM -T1}}}{\text{DIAG}_{\text{Kaula}}}\right]$

IV. MATHEMATICAL DESCRIPTION OF ERROR CALIBRATION BASED UPON FIELD SOLUTIONS

The most direct method of calibration entails the computation of a field solution wholly independent of the data used in GEM-T1 and a comparison of GEM-T1 with its results. The coefficient differences ($\Delta C_{\ell m}$) combined with the error estimator ($e_{\ell m}$) between GEM-T1 and this test solution will be used to compute the following quantity as a sample calibration factor for each spherical harmonic as follows:

$$k_{\ell m} = \frac{\Delta C_{\ell m}}{e_{\ell m}} \qquad (4.1)$$

The ensemble of the sample will be utilized to determine a calibration factor for terms of degree ℓ or order m in GEM-T1 together with the test field from the formulae developed in this section. An overall calibration factor can then be obtained from the rms average of the sample calibration factors.

GEM-T1 will also be compared to dependent solutions using the GEM-T1 data set with individual subsets eliminated. Calibrations of the same form as shown in (eq. 4.1) will be developed using these models. Since the estimated errors $e_{\ell m}$ in both of these approaches will involve both GEM-T1 and the test field in a mutual calibration, it is important for reliability of the entire error spectrum that a significant number of test solutions based upon a variety of data sets be employed.

The models which will be tested are complete to degree and order 36 containing 1363 terms. A separate calibration factor for each harmonic is computed and for overall model assessments, these factors are statistically combined by both degree and order.

A mathematical description of the error calibration is now presented with a derivation of its components.

First, let x and $\bar{x}$ be the respective errors in two gravitational models F and $\bar{F}$ consisting of coefficients C and $\bar{C}$ respectively and let E( ) define the expected value. It follows that:

$$C = C_{true} + x$$

$$\bar{C} = C_{true} + \bar{x}$$

and

$$\left| \bar{C} - \bar{\bar{C}} \right| = x - \bar{x}$$

represent the coefficient differences. Both x and $\bar{x}$ are errors within each solution of unknown magnitude. The covariance matrix of these errors is:

$$V_{\bar{x}\,\bar{x}} = E(\bar{x}\,\bar{x}^T) \quad \text{for solution } \bar{F}$$

and similarly

$$V_{x\,x} = E(x\,x^T) \quad \text{is the covariance matrix for solution F.}$$

The cross covariance for x and $\bar{x}$, non-zero when they share observations, is $V_{x\,\bar{x}}$. The covariance V for the difference in the two solutions is obtained as:

$$V = E[(x-\bar{x})\,(x-\bar{x})^T] = E(x\,x^T - 2x\,\bar{x}^T + \bar{x}\,\bar{x}^T)$$

$$= V_{x\,x} - 2V_{x\,\bar{x}} + V_{\bar{x}\,\bar{x}} \qquad (4.2)$$

For solutions which are completely independent (i.e. they share no data subsets) as noted above

$$V_{x\,\bar{x}} = 0$$

Therefore, from (4.2) we find

$$V = V_{x\,x} + V_{\bar{x}\,\bar{x}} \tag{4.3}$$

For cases where the data in $\bar{F}$ is totally contained within the F solution, we will show that:

$$V_{x\,\bar{x}} = V_{x\,x}$$

Then, again using (4.2) the variance of the difference solution $(C-\bar{C})$ is simply:

$$V = V_{\bar{x}\,\bar{x}} - V_{x\,x} \tag{4.4}$$

The complete solution has (n + n1) observations while the subset solution only contains n observations. Let the contribution of the least-squares normal equations be denoted as Nx = R and N1x = R1 respectively for the set of n and n1 observations. Then for the combined set of observations n + n1:

$$(N + N1)x = R + R1 \tag{4.5}$$

are the set of complete normal equations whose covariance for the case of random noise is:

$$(N + N1)^{-1} = V_{xx} \tag{4.6}$$

Likewise, for the subset solution

$$(N)\bar{x} = R \tag{4.7}$$

with a covariance

$$(N)^{-1} = V_{\bar{x}\,\bar{x}} \tag{4.8}$$

See Appendix A2 where this is shown to be an approximation.

From (4.5) and (4.7)

$$\bar{x}x^T = N^{-1}R\,(R + R1)^T\,(N + N1)^{-1} \tag{4.9}$$

and

$$\bar{x}x^T = N^{-1}(RR^T + RR1^T)\,(N + N1)^{-1} \tag{4.10}$$

Since R and R1 are based upon independent observations they are uncorrelated

$$E(R\,R1^T) = 0 \tag{4.11}$$

The expected value for $E(x\,\bar{x})$, using (4.10) and (4.11) is then

$$E(x\,\bar{x}^T) = V_{x\,\bar{x}} = N^{-1}\,N\,E(\bar{x}\,\bar{x}^T)\,N\,(N + N1)^{-1}$$

$$= (N + N1)^{-1} = V_{xx} \tag{4.12}$$

since $E(\bar{x}\,\bar{x}^T) = N^{-1}$. Thus we have the general result for V (the covariance of solution differences)

$$V = V_{\bar{x}\,\bar{x}} + V_{x\,x}$$

for C and $\bar{C}$ being independent solutions, and

$$V = V_{\bar{x}\,\bar{x}} - V_{x\,x} \qquad \text{for } \bar{C} \text{ with data wholly contained within the data of } C \tag{4.13}$$

Since these results (4.13) are approximations based upon random noise, they need to be calibrated which is done in the remainder of this report. To this end, we define several quantities used in our field calibrations:

For two fields F and $\bar{F}$:

$F : C_{\ell m}, S_{\ell m}, \quad \sigma$'s (coeff. errors)

$\bar{F} : \bar{C}_{\ell m}, \bar{S}_{\ell m}, \quad \bar{\sigma}$'s

$$RMS_{\ell}(\Delta F) = \left[\sum_{m=0}^{\ell} \frac{\Delta C^2_{\ell,m} + \Delta S^2_{\ell,m}}{2\ell + 1} \right]^{1/2} \tag{4.13a}$$

$$\sigma_{\ell} = \left[\sum_{m=0}^{\ell} \frac{\sigma^2(C_{\ell,m}) + \sigma^2(S_{\ell,m})}{2\ell + 1} \right]^{1/2}$$

since there are $2\ell+1$ coefficients per degree. Further, for order m

$$RMS_m(\Delta F) = \left[\sum_{\ell=m}^{36} \frac{\Delta C^2_{\ell m} + \Delta S^2_{\ell m}}{\delta_m (36-m+1)} \right]^{1/2}, \qquad \delta_m = \begin{cases} 1, & m=0 \\ 2, & m\neq 0 \end{cases}$$

$$\sigma_m = \left[\sum_{\ell=m}^{36} \frac{\sigma^2(C_{\ell m}) + \sigma^2(S_{\ell m})}{\delta_m (36-m+1)} \right]^{1/2}$$

since, for a 36x36 field, there are $\delta_m(36-m+1)$ coefficients per order. From the derivation given we know that the expected value of the average coefficient differences for a given degree, e_ℓ, is:

$$e_\ell^2 = E(RMS_\ell)^2 .$$

When F is independent of $\bar{F}$ as in (eq. 4.2), the derivation (4.13) shows that

$$e_\ell^2 = \sigma_\ell^2 + \bar{\sigma}_\ell^2 \qquad (4.14)$$

and when data in $\bar{F}$ is wholly contained within F as in (eq. 4.4), the derivation shows that

$$e_\ell^2 = \bar{\sigma}_\ell^2 - \sigma_\ell^2 \qquad (4.15)$$

Based on the above equations and (eq. 4.1), the calibration factors we will use throughout the next section are defined by:

$$k_\ell = \frac{rms_\ell}{e_\ell} \quad \text{for degree } \ell \qquad (4.16)$$

$$k_m = \frac{rms_m}{e_m} \quad \text{for order } m \qquad (4.17)$$

$$k_{\ell,m} = \frac{rms_{\ell,m}}{e_{\ell,m}} \quad \text{for an individual coefficient pair} \qquad (4.18)$$

V. CALIBRATION OF GEM-T1 USING DEPENDENT SUBSET AND INDEPENDENT TEST SOLUTIONS

5.0 Introduction

Many investigations utilizing the gravity model also require a validated geopotential error model. To assess the error of the field by wavenumber, over different geographic regions, or in terms of orbit error, a detailed knowledge of model errors is required. Independent data needs to be obtained and calibration techniques need to be improved. This is especially important when assessing the separation of oceanographic and gravitational signals simultaneously contained within satellite altimeter observations. It is of critical importance when evaluating the accuracy of models for reaching the precision orbit determination (POD) performance objectives of future missions like TOPEX. In this latter case, actual observations are absent, and assessments rely solely on statistical considerations. Those statistics, which is found in the calibrated full solution covariances, need to be reliable. The uncertainty reported for the GEM-T1 geopotential solution which are to be verified herein have been given as an RMS coefficient error by degree in Figure 1a and for each coefficient individually in Figure 1b.

Obtaining detailed knowledge of the geopotential errors is made difficult due to the lack of a perfect force model, measurement model, and correction algorithms which enter into the solution. Although it may appear that we are limited to providing a single overall scaling factor (f in eq. 3.1) to account for systematic errors (σ_t) per data type (t) in order to obtain realistic error statistics, the factor σ_t may be varied somewhat to account for variations in f for different data types (see Appendix A2.6). We know that each error is unlikely to contaminate the model uniformly in a way representable by a single scale factor. However, only through a detailed and rather complete analysis directed at a total field calibration can the effects of each error source be isolated through the resulting behavior of subset calibrations. Appendix A3 derives an optimal weighting process where each data type is adjusted for a weighting factor f_t.

In earlier gravitational modeling efforts, the inversion of the 2500x2500 parameter matrix for GEM-T1 would have represented a considerable computational burden. On the IBM 360/95, which was the fastest mainframe available at GSFC until the late 1970's, such a solution would have taken in excess of 100 CPU minutes. In 1982 the Cyber 205 vector computer was installed at GSFC. Our geopotential modeling efforts have benefitted substantially from the advent of this new "supercomputing" environment. On the Cyber, the inversion of the GEM-T1 normal matrix requires less than 2.5 minutes of CPU time. Given this enhanced capability, it is now possible to compute a variety of test solutions complete to degree and order 36 which will calibrate a broad spectrum of the errors in GEM-T1. If this extensive testing yields comparable results to those which we found earlier (Marsh et al., 1988), then we will have a more reliable verification of our estimates of the accuracy of the GEM-T1 model.

In Table 3 the major data subsets of the GEM-T1 solution, as well as independent data used for calibration, are reviewed. The GEM-T1 normal matrix is formed by summing the modularized contribution of each of these observation groupings. It is therefore a relatively simple task to manipulate these contributions and solve for models which either lack specific subset contributions or combine GEM-T1 with new independent observations such as altimetry and surface gravimetry. GEM-T2 and GEM-T3 are under development and will be models which optimally combine GEM-T1 with new data in this way.

From equations (4.14) through (4.18) we have defined two methods for calibrating model errors from potential coefficient solutions; the first when the fields F and $\bar{F}$ are independent and share no common data; the second when the data within $\bar{F}$ are wholly contained within F. The test solutions made in conformance with the requirements of these calibration methods are given in Table 4.

For each individual spherical harmonic, the calibration factors (eq. 4.18) tend to have random variations. To better assess the overall

TABLE 3

MAJOR DATA SETS USED FOR THE CALIBRATION OF GEM-T1 COEFFICIENT ERRORS

MAJOR DATA SUBSETS WITHIN THE GEM-T1 SOLUTION

- SATELLITE TRACKING DATA

  LASER - 10 SATELLITES

  DOPPLER - 2 SATELLITES

  OPTICAL - 11 SATELLITES

- COLLOCATION CONSTRAINTS - MODIFIED KAULA'S RULE $\left[\frac{10^{-5}}{\sqrt{2}\,\ell^{2}}\right]$

INDEPENDENT DATA COMBINED WITH GEM-T1 FOR CALIBRATION PURPOSES

- SEASAT ALTIMETER

  GLOBAL COVERAGE (OCEANS)

- SURFACE GRAVITY

  OSU '86 NORMALS
  GLOBAL COVERAGE

- 60 DEEP RESONANT SATELLITE LUMPED HARMONICS

Table 4

Independent and Dependent Subset Solutions* for GEM-T1 Error Calibration

Independent Data Solutions

- GEM-T1 vs. Surface Gravimetry + SEASAT Altimetry
- GEM-T1 minus LAGEOS vs. Surface Gravimetry + SEASAT Altimetry + LAGEOS

Subset Data Solutions

GEM-T1 vs. GEM-T1 *minus*

- The laser data from GEOS-1, GEOS-2, GEOS-3 andBE-C; this data set is referred to elsewhere as "4-LASERS".
- The laser data from STARLETTE.
- The SEASAT and OSCAR Doppler data.
- The optical observations acquired on 11 different satellites.
- The laser data from LAGEOS

GEM-T1 as a *Subset Solution*

- Combining GEM-T1's data with surface gravimetry.
- Combining GEM-T1's data with surface gravimetry and SEASAT alitmetry.
- Combining GEM-T1's data with satellite deep resonant spherical harmonic constraints.

* All solutions are complete to degree and order 36x36 and solve for ocean tidal and Earth orientation parameters.

quality of the calibration, we present the average calibration factors for terms of the same degree and terms of the same order separately. These are the k_ℓ and k_m values given in eqs. (4.16) and (4.17) respectively. The size of the sample used to calculate these average calibration factors contributes to their overall stability whether they are collected by degree or order. Those sampling a larger set of terms tend to be better behaved across the spectrum within the model. This is probably why more stable results are generally found in the assessment by order for the low order terms and by degree for the high degree terms. Anomalous behavior of the calibration factors for averages taken by order are particularly useful for locating aliasing problems within the gravitational model arising from satellite dynamic sensitivities to terms above the 36x36 limits of the field. Performance of data sets from satellites experiencing larger atmospheric drag and other non-conservative forcing effects are also scrutinized to assess possible field contamination arising from these error sources.

Briefly, Subsection 5.1 details the calibration of the GEM-T1 solution, specifically the optimization of data weights, through a calibration of the solution variances. Gravitational models formed from completely independent data are evaluated by comparing their respective uncertainties with their coefficient differences. Subsection 5.2 shows a more direct calibration of GEM-T1 through a mutual calibration analysis where GEM-T1 is calibrated against other models which either lacked specific data subsets or added additional data to the GEM-T1 field. Subsection 5.3 tests the sensitivity of the calibration methodology to the data weighting factor, f given in (eq. 3.1). A field which falsely reports superior results by having f increased by a factor of ten is evaluated in this subsection. Section 5.4 provides an overall summary of this calibration technique and the results obtained when evaluating GEM-T1.

5.1 Gravitational Model Calibrations Using Independent Data

Turning first to calibrations using independent data, Figure 3 shows the calibration factors, k_ℓ and k_m, obtained when comparing GEM-T1 with a field computed solely from a combination of SEASAT altimetry (where the altimeter ranges are treated as tracking observations) and block areal mean values of surface gravimetry. The gravimetry were provided to us by Pavlis (1988) in the form of compatible normal equations. These normal equations from gravimetry were developed under the direction of R. Rapp of The Ohio State University and have been scaled for consistency with the GEM-L2 geopotential. Here they will be used to calibrate GEM-T1. As noted in Marsh et al. (1988) the data in GEM-T1 is largely independent of GEM-L2. The calibration factors, as shown in Figure 3, cluster around the ideal where $k_\ell=1$ and $k_m=1$. This indicates that the overall uncertainties estimated within these independent models agree well with their coefficient variations. However, one of the limitations of this particular calibration test is revealed in Figure 4, which shows a large disparity in low degree coefficients between GEM-T1 and this model computed solely from altimetry and surface gravimetry. A better test of GEM-T1's long wavelength harmonics was made by removing the Lageos data from GEM-T1 and combining them with the normals of the altimetry/gravimetry model. The resulting two models were again composed of independent data, but both were now more equal in accuracy at low degree and closer to the uncertainty level of GEM-T1 itself. In Figure 5 the coefficient differences between GEM-T1 lacking Lageos and this altimetry/gravimetry/Lageos solution are compared. The two solutions resulting from this shift of the LAGEOS information are compared in terms of their estimated uncertainty and rms coefficient differences in Figure 6. It is interesting to note that these uncertainties reverse if the optical data were also removed from GEM-T1 and included in the independent test field.

These "Lageos-shifted" models were then calibrated with one another. Figure 7 gives the average calibration factors (k_ℓ and k_m)

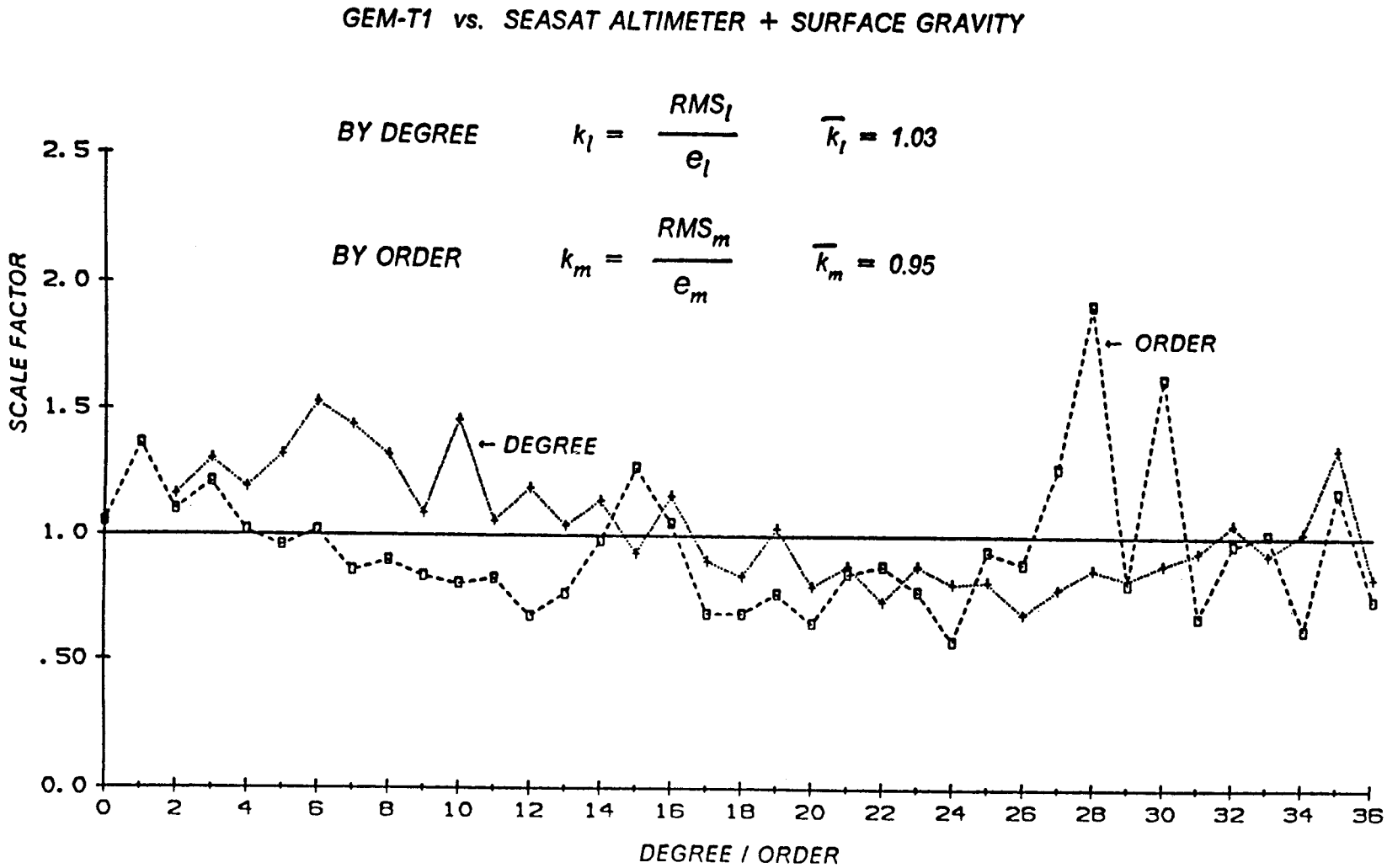

CALIBRATION OF ERROR ESTIMATES BASED UPON INDEPENDENT SOLUTIONS

FIGURE 3

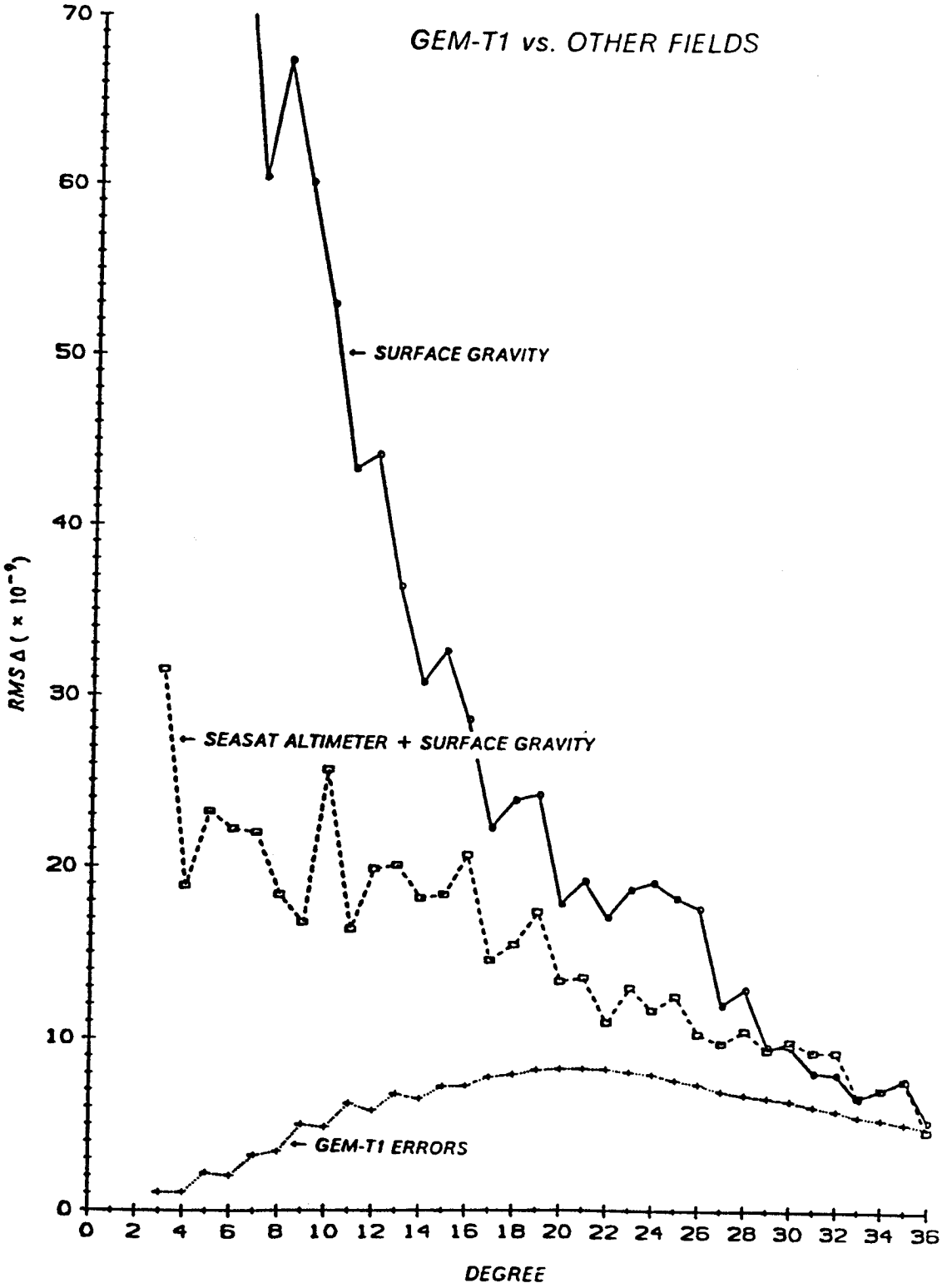

RMS COEFFICIENT DIFFERENCE BY DEGREE

FIGURE 4

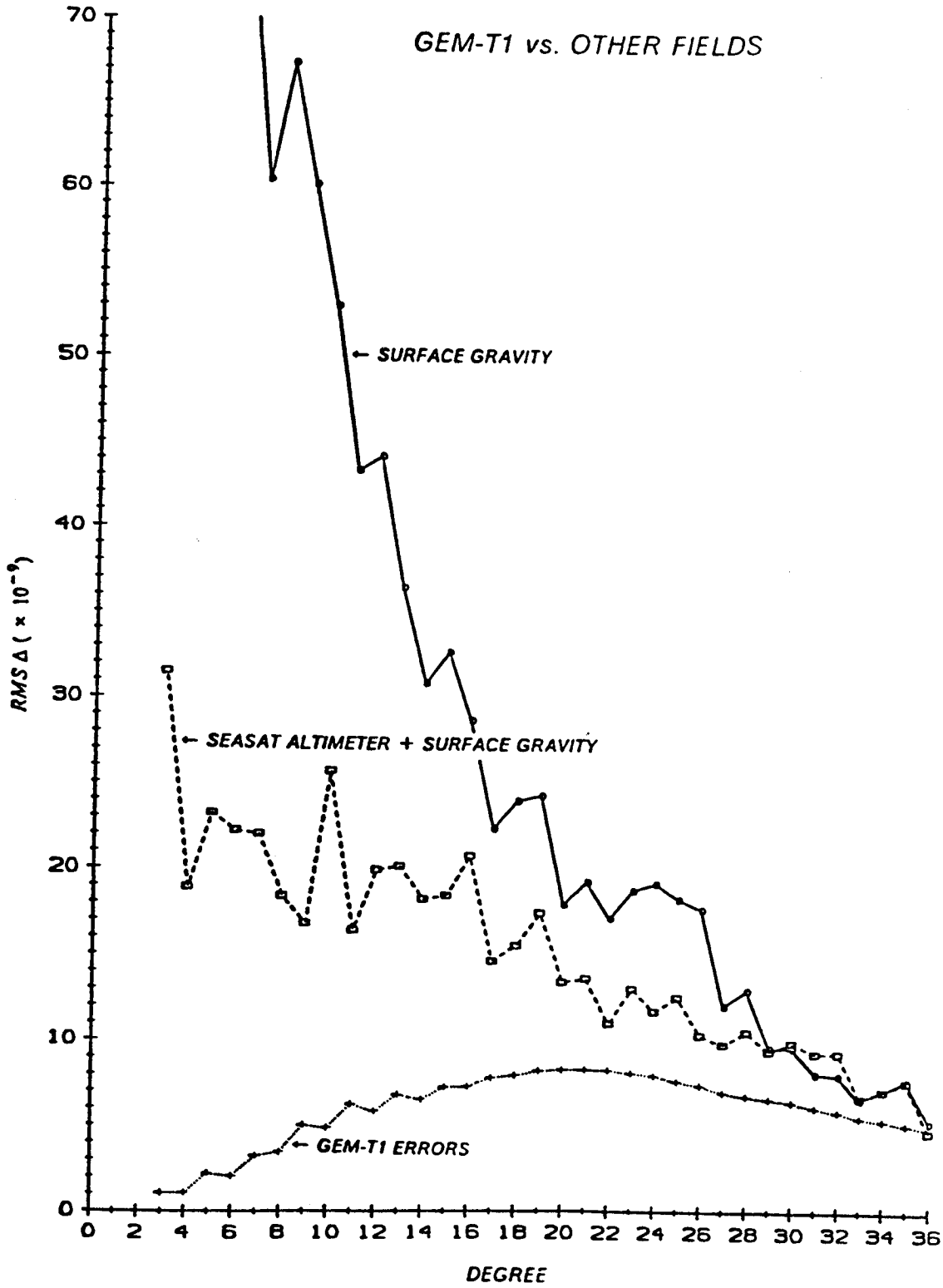

RMS COEFFICIENT DIFFERENCE BY DEGREE

FIGURE 4

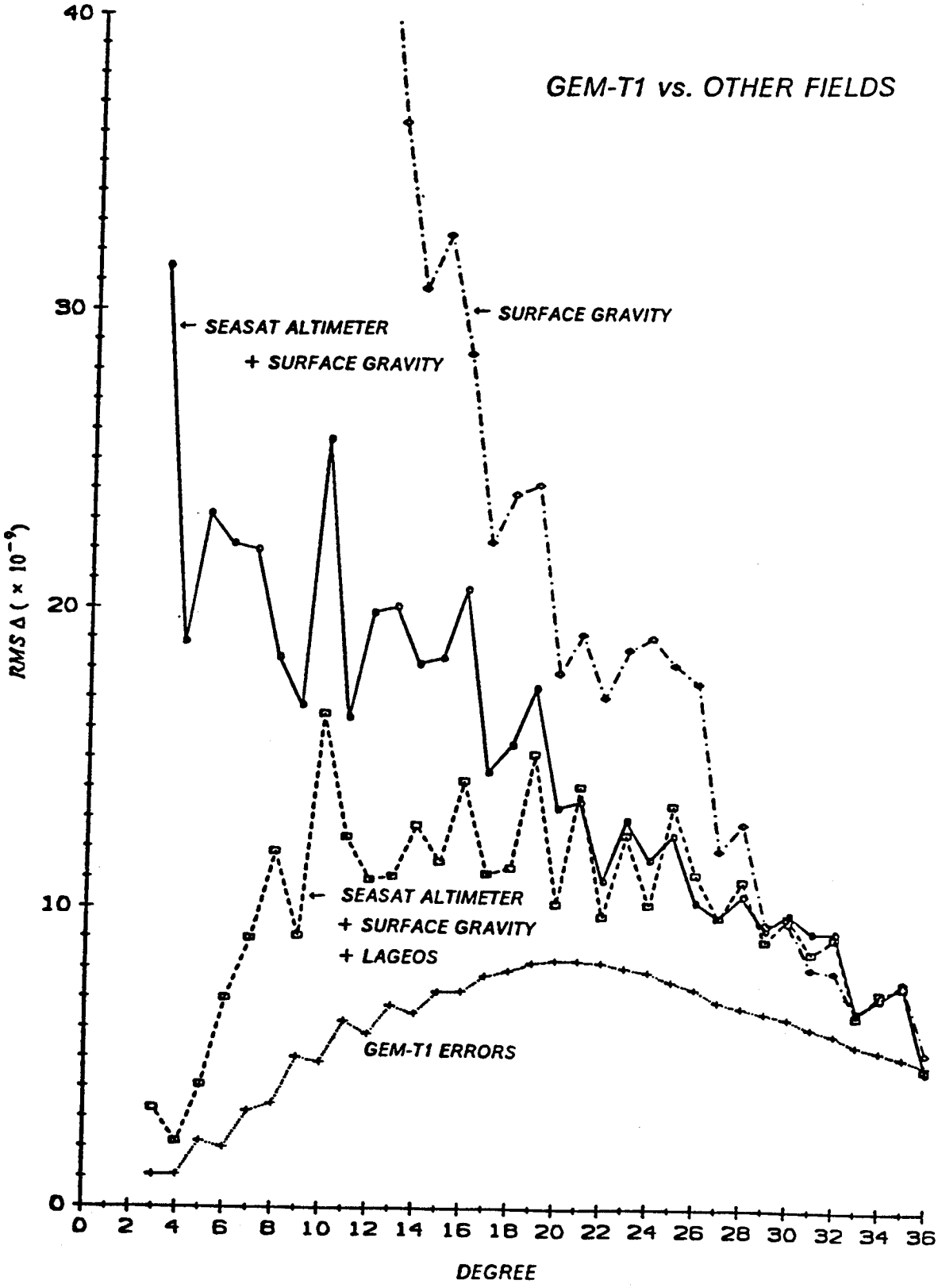

RMS COEFFICIENT DIFFERENCE BY DEGREE

FIGURE 5

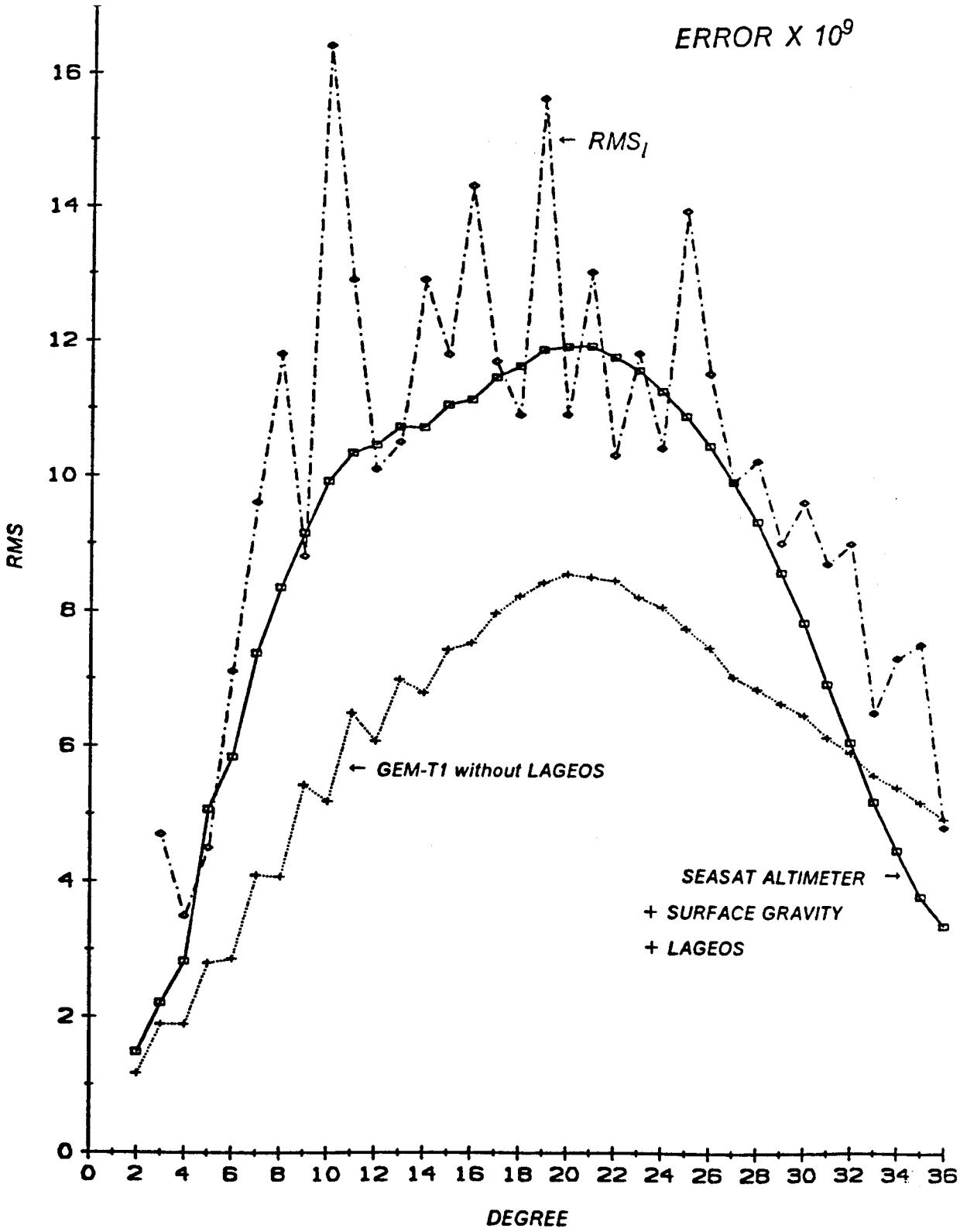

RMS COEFFICIENT ERROR PER DEGREE

FIGURE 6

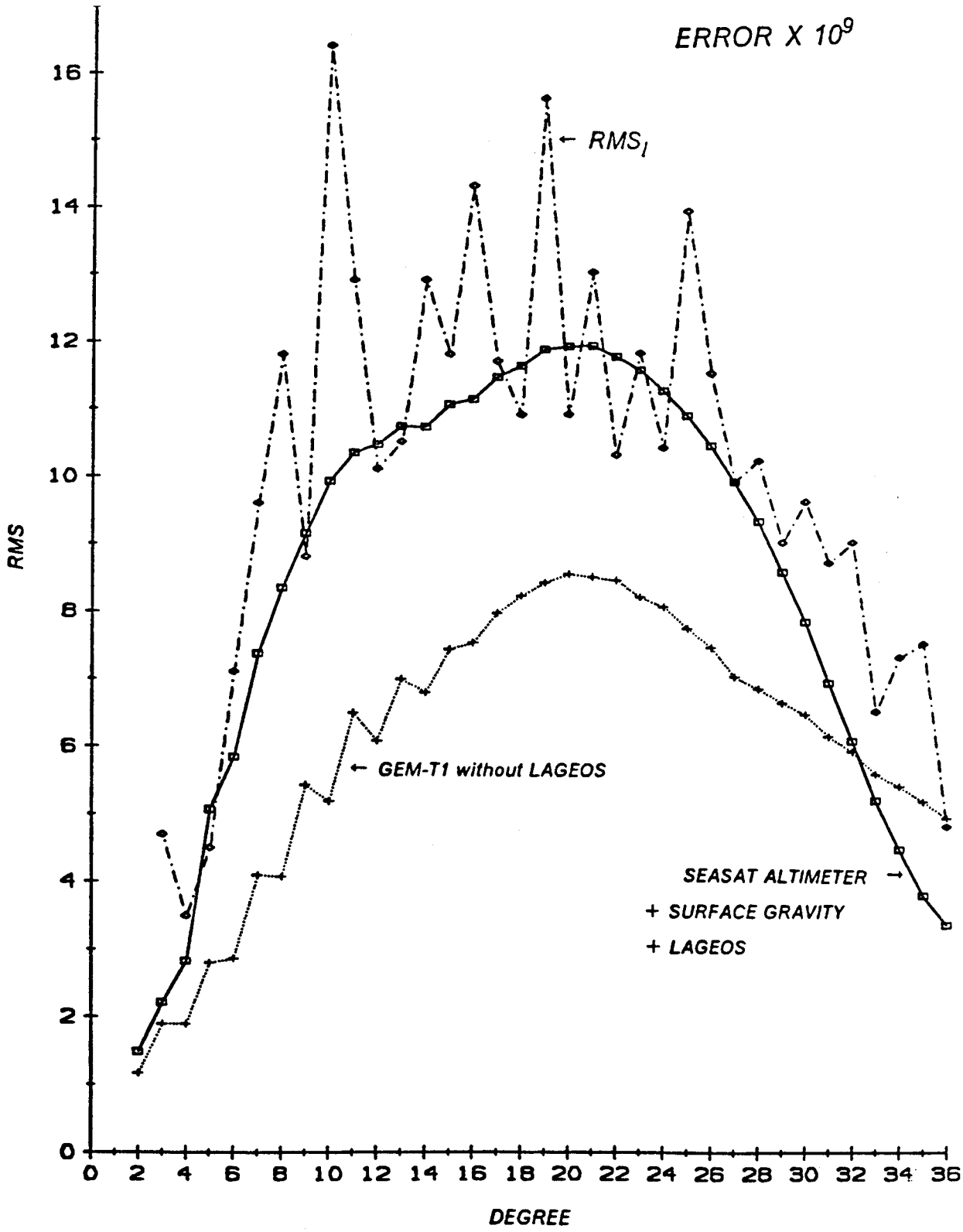

RMS COEFFICIENT ERROR PER DEGREE

FIGURE 6

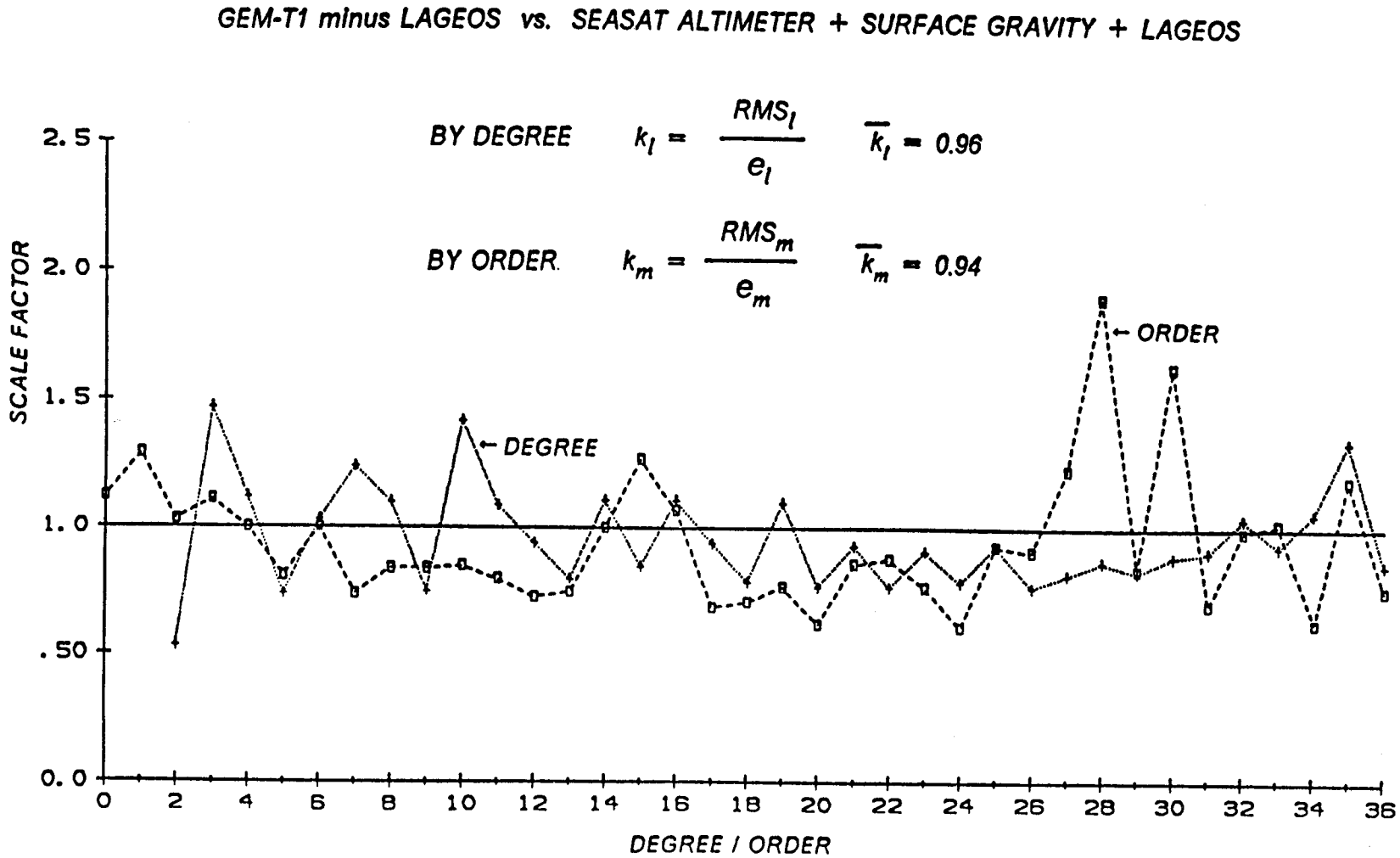

CALIBRATION OF ERROR ESTIMATES BASED UPON INDEPENDENT SOLUTIONS

FIGURE 7

which were obtained. Again, the results are well centered about 1, indicating that the model uncertainties are reasonably well calibrated. Furthermore, the calibration factors are more stable than those shown in Figure 3 although only marginally so. In summary, for these calibration procedures where geopotential models were composed of independent data sources, excellent overall calibration results have been obtained. The variances and model differences are consistent. These results indicate that the error estimates shown for GEM-T1 in Figures 1.1 and 1.2 are supported by independent global altimetry and surface gravimetry.

The large variation of k_m from unity for high orders around m=28 is due to the truncation at degree 36 for satellite resonant perturbations. Hence, this variation will consistently show up in the calibration plots for k_m and will be discussed later in more detail.

5.2 Gravitational Model Calibrations Using Dependent Solution Subsets

Returning to Table 3, tracking data from 17 different satellites contribute data to GEM-T1. These observations have been divided into several independent subsets. For each experiment which follows, the data was divided in such a way that the subset contributed significantly to the GEM-T1 solution. In some cases this required combining observations from several satellites into a single subset. A solution was made after removing each of the data subsets individually, and all of these subset fields were used in an extensive evaluation of the uncertainties published for the GEM-T1 coefficients.

A typical example of the variations found among the individual harmonic calibration factors, $k_{\ell m}$, is shown in Figure 8 for the case where GEM-T1 is calibrated against the model which removed the laser data contributions from GEOS-1,-2,-3 and BE-C. As expected, there is a good deal of variation in these calibration factors when going from term to term. However, the values overall fall into an approximate

AVERAGE PER DEGREE = 1.05 AVERAGE PER ORDER = 1.07

$$k_{l,m} = \frac{RMS_{l,m}}{e_{l,m}}$$

* 4-LASER satellites = GEOS-1, GEOS-2, GEOS-3 and BE-C

RMS	DEG	0	1	2	3	4	5	6	7	8	9	10	11	12	13	14	15	16	17	18	19	20	21	22	23	24	25
0.9	2	0.3		0.8																							
1.4	3	0.5	0.6	2.1	1.4																						
1.7	4	0.0	1.9	2.1	0.7	2.0																					
1.0	5	0.4	0.6	0.6	0.9	0.5	1.8																				
1.2	6	0.5	0.4	0.9	0.6	2.0	0.5	1.5																			
0.7	7	0.2	0.3	0.5	0.6	0.1	0.2	1.0	1.0																		
1.2	8	0.6	1.1	0.4	0.4	1.1	1.8	1.4	0.9	1.1																	
0.9	9	0.8	1.0	0.6	0.5	0.7	0.6	0.5	0.8	0.5	1.0																
0.9	10	0.6	0.8	0.6	1.5	0.5	0.2	0.5	1.0	0.9	0.6	0.3															
1.0	11	0.0	0.2	1.5	0.7	0.3	1.4	1.3	0.6	0.7	0.3	1.7	0.4														
1.1	12	1.3	0.9	2.0	0.5	0.8	0.9	0.5	0.4	0.3	0.8	1.3	1.0	1.0													
0.9	13	0.6	0.9	0.6	0.5	0.3	0.7	0.6	0.4	1.4	0.6	0.9	1.4	0.2	0.9												
0.9	14	0.4	1.0	0.6	0.8	1.4	0.8	0.7	0.6	0.7	1.6	0.1	0.2	0.2	0.3	0.2											
0.9	15	0.2	0.9	0.7	0.8	0.7	1.1	0.3	0.3	1.6	0.9	1.6	0.8	0.3	0.5	0.7	0.6										
0.9	16	0.3	0.7	1.4	1.5	0.1	1.1	1.1	0.5	0.4	0.9	0.7	0.6	0.4	1.0	0.5	0.6	0.3									
0.8	17	0.5	0.3	0.1	0.3	0.9	0.3	0.7	0.6	1.2	0.7	0.4	0.8	0.6	0.6	1.5	0.9	0.4	0.7								
0.9	18	0.3	0.4	1.5	0.3	1.2	0.6	0.3	1.1	0.8	0.9	0.5	0.6	0.6	0.5	0.7	1.1	0.1	0.6	1.2							
0.7	19	0.9	0.4	0.1	1.7	0.1	0.7	0.1	0.7	0.4	0.6	1.0	0.7	0.5	0.6	0.2	0.3	0.8	1.1	0.6	0.1						
1.0	20	0.7	1.4	1.3	0.9	1.2	1.2	0.6	0.5	0.7	1.0	0.5	1.2	0.3	0.7	0.7	0.4	0.3	1.4	0.9	0.6	0.9					
1.0	21	0.7	1.0	0.7	1.7	1.5	0.6	1.2	0.5	1.1	1.1	0.2	0.9	0.6	0.7	1.8	0.5	0.8	0.6	1.0	0.8	0.4	0.2				
1.1	22	0.6	2.5	1.7	0.7	1.5	1.1	1.2	0.6	0.8	0.4	0.3	0.6	0.9	1.6	0.5	0.8	0.8	0.4	0.2	1.0	0.3	0.4	0.6			
1.1	23	0.4	0.9	1.6	0.6	0.3	1.7	1.4	1.4	1.5	0.5	1.4	0.5	0.7	1.8	1.0	0.7	1.1	0.3	0.3	0.5	0.4	0.5	0.7	0.6		
0.9	24	0.5	1.8	1.6	1.5	1.3	0.9	0.6	0.5	0.4	0.5	0.3	0.9	0.4	0.1	1.0	1.1	0.5	0.1	0.6	0.7	0.4	0.6	0.9	0.1	0.3	
1.0	25	1.0	0.8	0.8	0.7	1.4	1.0	0.6	0.9	1.2	1.1	0.1	0.6	0.5	1.1	1.1	0.4	0.9	1.1	1.2	0.6	0.6	0.7	1.6	0.4	0.2	0.5
0.8	26	0.4	1.2	0.9	0.5	1.2	1.4	0.5	0.7	0.2	0.2	0.4	0.9	0.5	0.4	1.0	0.6	0.5	0.4	0.2	1.0	0.9	1.0	0.4	0.6	0.6	0.6
1.1	27	1.1	0.6	2.0	0.2	0.6	0.4	1.0	1.5	0.9	0.1	0.9	0.8	1.5	1.7	0.7	0.8	0.4	0.2	0.3	0.2	0.4	0.6	1.7	1.0	0.5	0.2
1.0	28	0.9	1.1	2.6	0.4	0.4	1.7	0.7	0.5	1.0	1.0	0.3	0.1	0.7	0.3	0.3	0.8	1.0	0.9	0.6	0.5	0.2	0.4	1.1	0.9	1.5	0.6
1.3	29	0.4	0.6	1.9	1.1	1.3	1.3	0.6	1.8	1.0	0.8	0.7	1.0	0.4	0.9	1.5	1.3	0.7	0.4	0.4	0.6	0.2	1.3	1.0	1.1	0.7	1.7
1.0	30	0.5	0.2	1.4	0.7	1.2	0.9	1.2	1.2	0.8	0.7	0.1	0.2	0.6	1.6	0.3	1.5	0.3	0.3	0.4	0.8	0.8	0.8	0.8	0.5	1.1	0.5
1.4	31	0.9	1.2	1.1	2.2	1.3	1.3	0.8	0.8	0.1	1.5	0.5	0.1	1.4	1.2	1.7	1.1	0.8	0.9	1.2	0.5	0.5	1.0	1.6	0.8	1.0	1.6
1.2	32	2.1	1.1	1.7	0.8	2.3	0.9	1.4	0.8	1.2	1.1	0.2	0.5	0.9	1.2	0.4	1.2	1.0	1.3	0.6	0.5	0.1	1.2	1.0	1.0	1.6	0.5
1.2	33	1.0	0.6	0.8	1.3	0.6	0.9	2.0	0.2	0.3	0.2	0.2	1.3	0.5	0.9	1.5	0.4	1.0	0.8	0.5	0.7	0.1	0.6	1.0	1.5	0.9	1.3
1.2	34	0.4	1.4	2.9	1.4	2.3	0.6	1.2	0.9	0.2	1.1	0.1	0.6	0.1	0.8	0.5	1.0	1.2	0.8	0.8	0.5	0.2	0.8	0.9	0.1	1.0	0.2
1.3	35	0.2	1.4	0.6	0.9	1.6	0.5	0.5	1.0	0.7	1.3	0.3	0.6	0.4	0.8	1.1	0.8	0.4	1.4	0.7	0.9	0.4	1.0	0.5	1.0	0.8	0.4
1.3	36	0.5	3.0	0.9	0.6	1.3	2.0	0.9	1.4	0.6	1.1	0.2	0.4	0.5	0.3	0.7	0.7	1.4	1.1	0.6	0.5	0.7	0.6	1.1	0.7	1.1	0.6
																ORDER											
RMS		0.7	1.2	1.5	1.1	1.3	1.2	1.1	0.9	0.9	1.0	0.8	0.8	0.7	1.1	1.1	1.0	0.8	0.9	0.8	0.8	0.5	0.9	1.2	0.9	1.1	1.0

CALIBRATION RATIO($k_{l,m}$) BASED UPON GEM-T1 AND GEM-T1 WITHOUT 4-LASER*

FIGURE 8

range of 0.2 to 2.0 and seldom depart by more than a factor of two from the degree and order average values which are shown in Figure 9. With the exception of the high order resonances of order 26 through 29, these average calibration factors are well behaved and centered about 1. As mentioned previously, the misbehavior at the high orders indicate that these satellites are sensitive to resonance terms beyond the 36th degree at these specific orders, and that there is some aliasing from these unmodeled higher degree contributions. When altimetry and surface gravity are introduced into the solution, these satellite data sets will contribute to the determination of higher degree resonance terms out to degree 50 and this source of aliasing will be eliminated. The normal equations from these and the other laser satellites are complete to degree 50 for all zonal, 1st and 2nd order, and resonance terms although they have not been used in GEM-T1 beyond degree 36.

These calibration tests have been repeated for each of the subset solutions. Table 5 summarizes the overall calibration factors (defined as the mean of the $\overline{k_\ell}$ and $\overline{k_m}$ terms) from these assessments. With the exception of the model leaving out Lageos contributions, the overall calibration factors were all found to be highly consistent and close to the ideal value of 1. The less consistent Lageos results are somewhat understandable. The Lageos satellite orbits at nearly 6000 km altitude and senses little of the gravitational field beyond degree 8. It is easy to understand how this subset solution may be ineffective for calibrating a full 36x36 model. The low degree portion of the field (to 6x6) however, gives essentially the same Lageos calibration factor of 1.2 which is satisfactory. Also of note, the Lageos calibration is sensitive to the polar motion adjustment, and the calibration improves if the pole position is fixed. Also in Figure 7 the solution for Lageos with altimetry and surface gravity data result in a consistent calibration with the solution for GEM-T1 minus Lageos data.

Additional tests were performed where GEM-T1's data became a subset of larger solutions--combination gravitational models which are being investigated as preliminary versions of GEM-T2 and GEM-T3. At this time, these more comprehensive models were solved only to degree

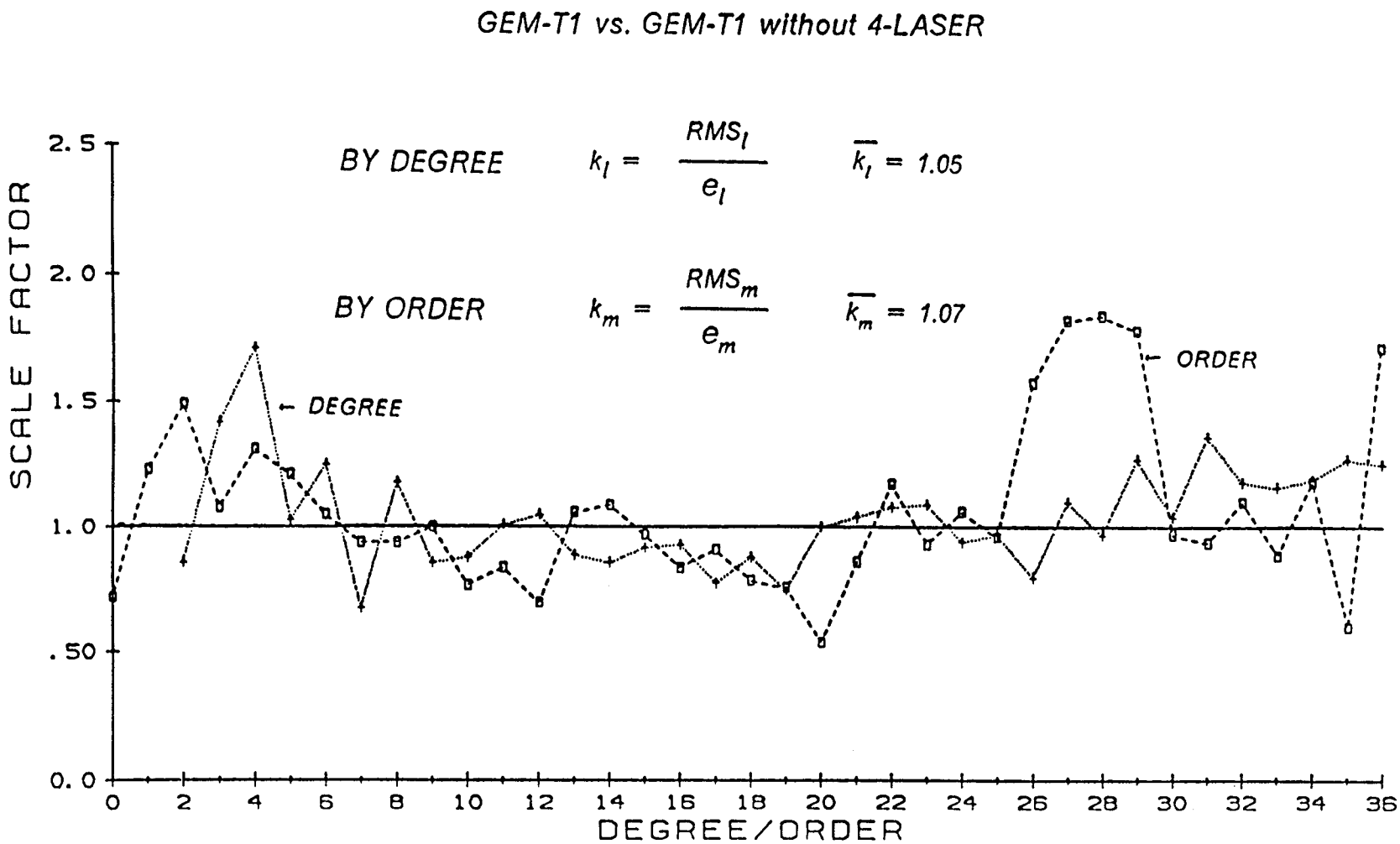

CALIBRATION OF ERROR ESTIMATES BASED UPON SUBSET SOLUTIONS

FIGURE 9

TABLE 5

SUMMARY OF RESULTS FOR ERROR CALIBRATION

• GEM-T1 vs. GEM-T1 minus DATA SUBSET	CALIBRATION FACTOR
4 LASER SATELLITES (GEOS 1,2,3, BE-C)	1.06
STARLETTE LASER	1.10
OSCAR + SEASAT DOPPLER	1.09
OPTICAL (11 SATELLITES)	0.84
LAGEOS LASER	1.45
• GEM-T1 vs. GEM-T1 + SURFACE GRAVITY	0.95
• GEM-T1 vs. GEM-T1 + SURFACE GRAVITY + SEASAT ALTIMETRY	0.94
• GEM-T1 vs. GEM-T1 + SATELLITE RESONANCE DATA	1.05
• GEM-T1 vs. SURFACE GRAVITY + SEASAT ALTIMETRY	0.99
• GEM-T1 minus LAGEOS vs. LAGEOS + SURFACE GRAVITY + SEASAT ALTIMETRY	0.95

and order 36. Before the TOPEX work is completed, the limits of these fields will be extended to degree and order 50. These combination models were developed by adding new normal equations which were produced from SEASAT satellite altimetry and surface gravimetry to the GEM-T1 solution and truncating the final solution through parameter suppression at degree 36. Figure 10 presents one such calibration comparing GEM-T1 with the GEM-T1/surface gravimetry combination solution. Again, a good calibration centering about 1 was obtained.

Another source of independent satellite information was also used to calibrate GEM-T1. Lumped harmonics representing the long term orbit changes of satellites undergoing deep resonant passages were utilized. In the first calibration method we compared the observed lumped harmonics directly with computed values of them using GEM-T1. All of these observations were from unique orbits not found in GEM-T1. The observations used, their estimated accuracies and their projected GEM-T1 errors are listed in Table 6. These observations provide a reliable error estimate for GEM-T1 since only lumped harmonics were used with errors considerably less than projected for GEM-T1. We have computed an average calibration factor for GEM-T1 errors necessary to resolve the residuals of these observations with GEM-T1 predictions - namely:

$$\bar{K} = \left| \frac{\sum_{i=1}^{60} (O_i - C_i)^2 - \Delta T_i^2 - \sigma^2 O_i}{\sum_{i=1}^{60} \sigma^2 C_i} \right|^{1/2}$$

where O_i, σO_i, C_i and σC_i are respectively the observations, their estimated errors, GEM-T1 computed quantities and GEM-T1 predicted errors based on its variance-covariance matrix. ΔT_i is the estimated truncation error for the ith observation for a model truncated at degree 36. Over this set of observations (note that $\sigma O_i \leq \frac{1}{3} \sigma C_i$; for all i) we find that

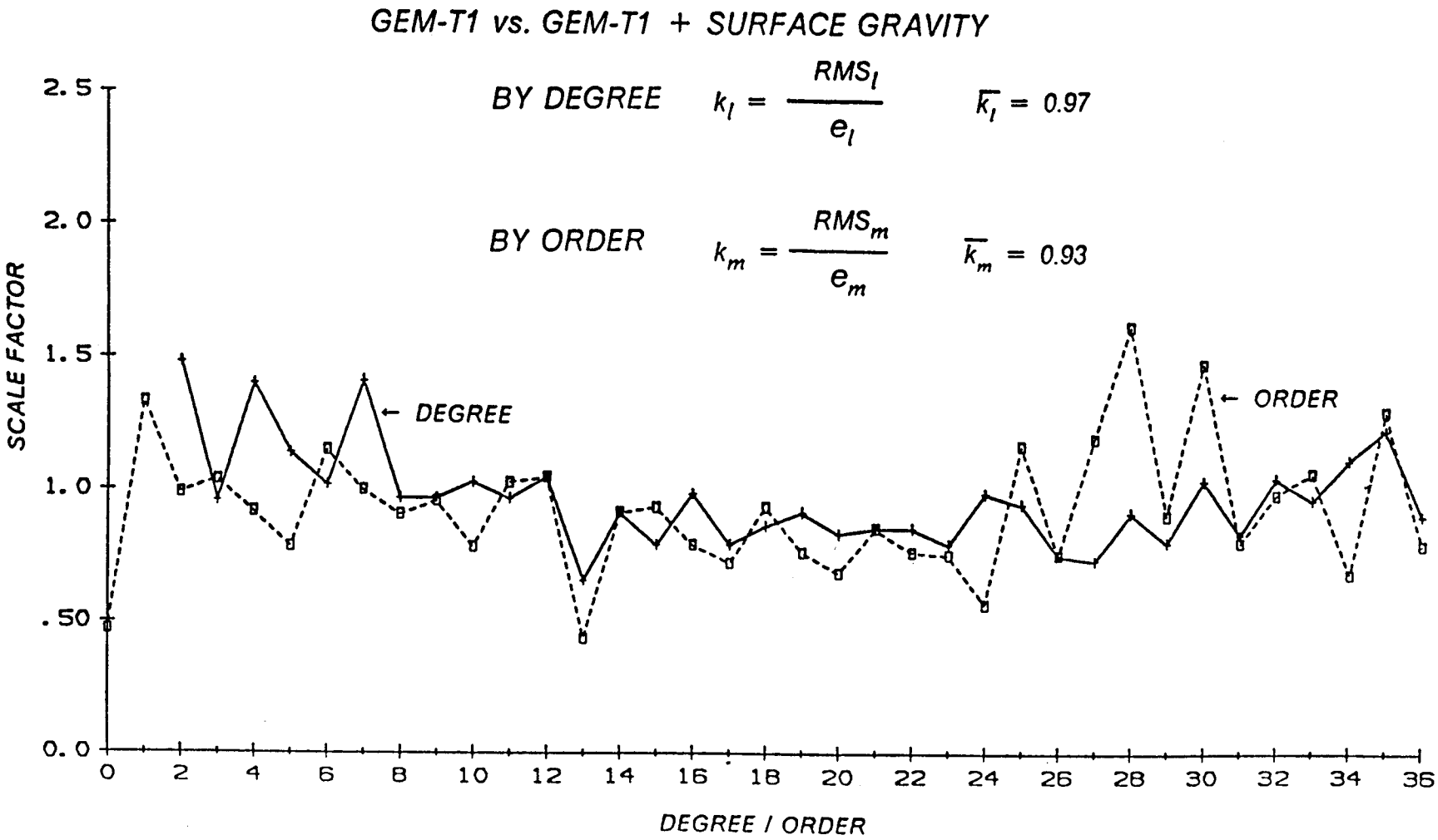

CALIBRATION OF ERROR ESTIMATES BASED UPON SUBSET SOLUTIONS

FIGURE 10

TABLE 6. COMPARISON OF GEM-T1 WITH THE BEST INDEPENDENT SATELLITE RESONANT HARMONICS FOR CALIBRATION PURPOSES

					(1)	(2)	(3)	(4) x 10^{-9}	(5)	(6)	(7)	(8)		
RESONANCE ≠					GEM-T1								Satellite	
REF	m	q	k		Obs	σ_o	Comp.	σ_c	ΔT	RES (O-C)	RES/ σ_c	RES/ ε	Name	Incl.	Ecc.
(1)	11	-2	1	C	-38.1	1.0	-45.7	5.6	1.0	7.6	7.6	1.28	VANGUARD 3	33.35	.188
				S	-33.4	1.2	-17.6	5.6	1.0	-15.8	-13.2	-2.64	VANGUARD 3		
(1)	11	-1	1	C	-30.6	1.0	-35.0	5.2	0.6	4.4	4.4	0.80	VANGUARD 3/2R	33.13	.184
				S	0.3	2.1	1.9	5.3	0.6	-1.6	-0.8	-0.27	VANGUARD 3/2R		
	11	0	1	C	26.1	2.2	25.9	6.6	0.6	0.2	0.1	0.03	VANGUARD 3/2R		
				S	52.6	1.1	53.7	6.7	0.6	-1.1	-1.0	-0.15	VANGUARD 3/2R		
	11	1	1	C	-42.9	1.5	-40.7	8.6	0.8	-2.2	-1.4	-0.23	VANGUARD 3/2R		
				S	-13.9	2.9	-8.2	8.0	0.8	-5.7	-2.0	-0.64	VANGUARD 3/2R		
	11	2	1	C	13.6	1.5	6.5	9.9	1.2	7.1	4.8	0.68	VANGUARD 3/2R		
				S	24.5	1.4	47.0	10.8	1.2	-22.5	-16.1	-1.96	VANGUARD 3/2R		
(1)	12	0	1	C	-4.2	2.0	-0.5	7.0	0.9	-3.7	-1.7	-0.48	D-1A & D-1A ROC	34.10	.139
				S	38.4	1.4	40.4	7.0	0.9	-2.0	-1.2	-0.27	D-1A & D-1A ROC		
	12	1	1	C	-42.4	1.4	-29.2	10.3	1.2	-13.2	-7.2	-1.20	D-1A & D-1A ROC		
				S	-23.4	2.4	-15.3	9.9	1.2	-8.1	-3.0	-0.76	D-1A & D-1A ROC		
(1)	12	1	1	C	19.2	0.5	16.9	4.1	0.5	2.3	3.1	0.52	EX.9 ROC.	38.90	.121
				S	42.2	1.5	39.1	4.2	0.5	3.1	2.0	0.67	EX.9 ROC.		
(1)	12	0	1	C	-44.3	2.1	-34.1	6.2	0.1	-10.2	-4.8	-1.48	TIROS 9	96.40	.117
				S	101.9	1.3	100.8	6.3	0.1	1.1	0.8	0.16	TIROS 9		
	12	1	1	C	-1.1	1.2	2.3	3.9	0.1	-3.4	-2.8	-0.80	TIROS 9		
				S	-14.0	1.1	-23.1	3.8	0.1	9.1	8.2	2.20	TIROS 9		
(1)	14	0	1	C	-31.6	1.1	-31.0	9.5	1.3	-0.6	-0.4	-0.06	OV2-1 ROC.	32.10	.013
				S	-4.8	1.1	17.8	9.8	1.3	-22.6	-13.2	-2.17	FRAGMENTS		
(2)	14	0	1	C	-1.8	0.6	-2.0	2.2	0.3	0.2	0.2	0.07	METEOR 10	81.23	.007
				S	-19.5	0.5	-17.0	2.2	0.3	-2.5	-4.3	-1.06	METEOR 10		
(1)	14	0	1	C	-2.3	0.3	-0.3	2.3	0.1	-2.0	-6.2	-0.83	LANDSAT 1	99.10	.001
				S	-22.5	0.5	-24.4	2.3	0.1	1.9	3.8	0.80	LANDSAT 1		
(2)	14	0	1	C	-2.8	0.3	-0.3	2.2	0.1	-2.5	-7.8	-1.05	LANDSAT 1	99.10	.002
				S	-22.6	0.1	-24.4	2.2	0.1	1.8	12.1	0.77	LANDSAT 1		
(3)	15	0	1	C	-26.3	1.7	-3.1	13.0	3.0	-23.2	-6.8	-1.65	1965-9A	31.76	.007
				S	-11.5	0.8	4.5	13.0	3.0	-16.0	-5.1	-1.14	1965-9A		
(3)	15	0	1	C	26.3	1.0	2.4	12.4	2.9	23.8	7.9	1.78	1969-68B	32.97	.004
				S	8.1	1.2	-4.9	12.4	2.9	13.0	4.2	0.97	1969-68B		
(1)	15	0	1	C	28.3	1.5	2.4	12.2	2.9	25.9	8.0	1.96	TETR-3	33.10	.012
				S	7.4	1.5	-4.9	12.3	2.9	12.3	3.8	0.93	TETR-3		
(3)	15	-1	1	C	-46.5	2.7	-50.1	11.2	1.8	3.6	1.1	0.30	1970-111A	74.00	.001
				S	-40.5	4.0	-46.5	11.2	1.8	6.0	1.4	0.48	1970-111A		
	15	0	1	C	-26.0	1.0	-21.2	6.0	0.6	-4.8	-4.2	-0.75	1970-111A		
				S	-5.2	1.3	-9.8	6.0	0.6	4.6	3.3	0.72	1970-111A		
(3)	15	-1	1	C	-45.5	2.0	-50.2	11.3	1.8	4.7	1.8	0.39	1971-131B	74.05	.002

			S	-35.2	1.0	-46.6	11.3	1.8	11.4	5.6	0.95	1971-131B	
	15	0	1 C	-24.6	1.3	-21.3	6.0	0.6	-3.3	-2.3	-0.51	1971-131B	
			S	-6.1	1.0	-9.8	6.0	0.6	3.7	3.2	0.58	1971-131B	
(3)	15	0	1 C	-23.0	1.6	-20.7	5.5	0.3	-2.4	-1.5	-0.39	1967-42A	80.17 .007
			S	-8.6	1.3	-6.9	5.5	0.3	-1.7	-1.3	-0.29	1967-42A	
	15	1	1 C	-54.6	3.2	-45.6	10.8	0.9	-9.0	-2.7	-0.76	1967-42A	
			S	-37.1	2.6	-45.7	10.7	0.9	8.6	3.1	0.74	1967-42A	
(3)	15	-1	1 C	-62.9	2.6	-49.0	13.7	1.2	-13.8	-4.8	-0.95	1971-54A	90.23 .002
			S	-53.4	1.6	-56.3	13.6	1.2	2.9	1.5	0.20	1971-54A	
	15	0	1 C	-16.0	0.2	-15.8	2.7	0.1	-0.2	-0.8	-0.07	1971-54A	90.21 .002
			S	-6.9	0.2	-6.8	2.6	0.1	-0.1	-0.5	-0.04	1971-54A	
(4)	27	0	1 C	-14.5	2.0	-13.4	6.2	1.4	-1.1	-0.5	-0.16	NAVSATS	89.80 .010
			S	+10.0	2.0	6.8	6.1	1.4	3.2	1.3	0.47	(1967-48A,	
												70-67A, 73-81A)	
(5)	28	0	2 C	7.0	1.1	2.9	4.7	1.0	4.1	2.8	0.80	METEOR 10	81.23 .007
			S	1.5	1.1	0.4	4.7	1.0	1.1	0.7	0.21	METEOR 10	
(6)	28	0	2 C	-9.3	0.9	-14.3	9.2	1.6	5.0	2.7	0.51	LANDSAT 1	99.10 .002
			S	-21.7	0.9	-7.4	9.2	1.6	-14.3	-7.8	-1.45	LANDSAT 1	
(3)	30	0	2 C	-9.8	0.6	0.6	8.2	0.4	-10.4	-14.8	-1.21	1971-54A	90.23 .002
			S	9.0	0.7	0.1	8.2	0.4	8.9	10.5	1.03	1971-54A	
(7)	31	0	2 C	-2.9	1.2	0.4	6.9	2.2	-3.3	-1.3	-0.43	1961-α1	97.20 .005
			S	9.0	2.2	-2.4	6.9	2.2	11.4	3.6	1.44	1961-α1	

Column Notes:

(1),(2) For all of these observation pairs C/S: $\sigma_o(C) + \sigma_o(S) < [\sigma_C(C) + \sigma_S(C)]/3$.

Thus the comparisons are all dominated by the estimated model error σ_C and hence they serve principally to calibrate the model.

†The resonances are all of periods $\geq$ 14 days with most passing through perfect commensurability with the earth's rotation. Their frequencies are:

$$\dot{\psi}_{m,q,k} = \dot{\omega}q + (\dot{\omega}+\dot{M})\,k + m\,(\dot{\Omega}-\dot{\theta}_e)$$

where m=geopotential order and $\dot{M},\dot{\Omega},\dot{\omega}$ are the satellite's mean motions of mean anomaly, argument of perigee and node. $\dot{\theta}_e$ is the earth's rotation rate. C and S are the cosine and sine terms of the lumped harmonic observed for these resonances. The definition of these harmonics is from Ref. (1). Harmonics from all other references have been converted to this definition which normalizes the observation with respect to the geopotential harmonic ($\bar{C}_{\ell m}$) of greatest sensitivity to the orbit element whose resonance is observed. Here the elements are mainly inclination but equivalently semi-major axis eccentricity and along track perturbation, covering all cases.

(3),(4) Computed observation and estimated commission error from GEM-T1 and its covariance matrix as presented in this report (precalibrated or formal errors)

(5) Estimate of truncation error for resonant harmonic of GEM-T1 for terms ℓ>36 using a power law for the geopotential signal.

(6) Residual = (1) - (3)

(7) Residual ÷ $\left| \sqrt{\sigma_o^2 + \Delta T^2} \right|^{1/2}$: weighted residual if model were perfect for the terms in its solution

(8) Residual ÷ $\left| \sqrt{\sigma_o^2 + \Delta T^2 + (K\ \sigma_c)^2} \right|^{1/2}$: weighted residual accounting for calibrated commission error.

Here the calibration factor was found by solving for K from

$$\sum_{i=1}^{60} RES_i^2 \div (\sigma_{o,i}^2 + \Delta T_i^2 + K^2\ \sigma_{c,i}^2) = 60$$

The result was : K=1.05. The resulting statistics in (8) yield : #>2σ : 3 (expected from unit normal : 3)
#>1σ : 17 (expected from unit normal : 19)

References for Resonant Data

1. Wagner, C.A. and F.J. Lerch, "The Accuracy of Geopotential Models," Planet. & Sp. Sci., 26, 1081-1140, 1978.

2. King-Hele, D.G. and D.M.C. Walker, "14th Order Harmonics in the Geopotential From Analysis of Satellite Orbits at Resonance," Planet & Sp. Sci., 34, 183-195, 1986.

3. King-Hele, D.G. and D.M.C. Walker, "Individual Geopotential Coefficients of Order 15 and 30 from Resonant Orbits," Planet & Sp. Sci., 33, 223-238, 1987.

4. Bowman, B.R., "Analysis of Mean Elements of Three U.S. Navy Navigation Satellites for the Period 1974-76," Celest. Mech., 19, 203-211, 1979.

5. Walker, D.M.C., "Analysis of 208 Navy Orbits for the Satellite 1970-47B at 14th Order Resonance," Rac Tech. Report 85015, Farnborough, Hants., England, 1985.

6. Dunn, P., "Geopotential Resonance in a Landsat Orbit," Bull. Geod., 55, 143-158, 1981.

7. King-Hele, D.G., "Geopotential Harmonics of Order 29, 30 and 31 from Analysis of Resonant Orbits," Planet & Sp. Sci., 30, 411-425, 1982.

$\bar{K} = 1.14$.

To test this calibration of the lumped harmonics of GEM-T1 with the dependent data set method in terms of the specific geopotential harmonics in GEM-T1 (instead of the lumped harmonic observables) we have combined the lumped harmonics data with GEM-T1. This new solution was then compared to GEM-T1. As expected from the small set of 60 lumped coefficients, only a limited number (about 280) of resonant harmonics (ℓ,m) in GEM-T1 were changed appreciably by these new data. The rms average calibration factor $\bar{K}_{\ell m}$ (Eq. 4.18) for these 60 observations was found to be 1.05 and agrees well with the 1.14 calibration factor obtained above for the 60 lumped harmonics. The importance of these resonance tests is that they show the capability of GEM-T1 over a wide range of "new orbits" with respect to the dominant perturbations of those orbits. Furthermore, since the computed errors for these lumped harmonic "observations" used the full variance-covariance matrix of GEM-T1, these are direct tests of the validity of that matrix, a task essential to reliable radial error prediction for TOPEX. Many more such full matrix calibrations will be presented in Section VI.

Table 5 (last five entries) also summarizes the overall calibration factors which were determined for GEM-T1 from these tests using more advanced gravitational models. In all cases tested, the overall calibration factors indicated satisfactory error estimates for both GEM-T1 and these more advanced gravitational field coefficients.

5.3 Tests of Overall Observation Scaling Factor

Tests were also made to determine the sensitivity of our calibrations to the overall scaling factor f of the solution (eq. 3.1). Clearly, the overall formal uncertainties of the model are strongly affected by the adopted value of f used in combining the signal and observation matrices. By design in GEM-T1 and previously in GEM-9 (Lerch et al., 1979), the scaling of f was found to produce solution uncertainties which reflected the true accuracy of the field. For

GEM-T1 we found f=.02. To test this assignment using our more comprehensive calibration methods both GEM-T1 and the GEM-T1 subset model which lacked data from the 4-Laser satellite group were recomputed with f increased by a factor of 10 to f=0.2 while leaving the signal matrix weight for the Kaula constraints (σ_ℓ) unchanged. This increased the satellite data weight in the solution by a factor of 10, and as expected, the overall parameter standard deviations improved by approximately $\sqrt{10}$. This was expected since, as we previously mentioned, (Section III) tests with global sets of gravimetry and other independent data gave f=0.02 as the optimum scale for the satellite data relative to the a priori constraint information. Here, we deliberately corrupted this weighting and attempted to confirm this estimate with reference only to the solution's own satellite contribution.

As shown in Figure 11, when calibrated using the subset solution technique, the calibration factors k_ℓ and k_m were both found to yield values approximately equal to $\sqrt{10}$ for these test models indicating that f=.02 is indeed close to optimum. The subset solution method is thereby shown to be capable of revealing both a poorly calibrated model and also showing the correct approximate level at which these errors were improperly reported.

5.4 Summary of the Calibration Based Upon GEM-T1 Variances

Clearly from the results shown within this section, the calibration method we have developed is sensitive to overly optimistic solution statistics and is consistent across many data subsets as they are individually tested against the complete GEM-T1 field. These results therefore confirm the coefficient uncertainties of GEM-T1 for the diagonal terms of the covariance matrix. We will now proceed to test the full covariance matrix for this solution.

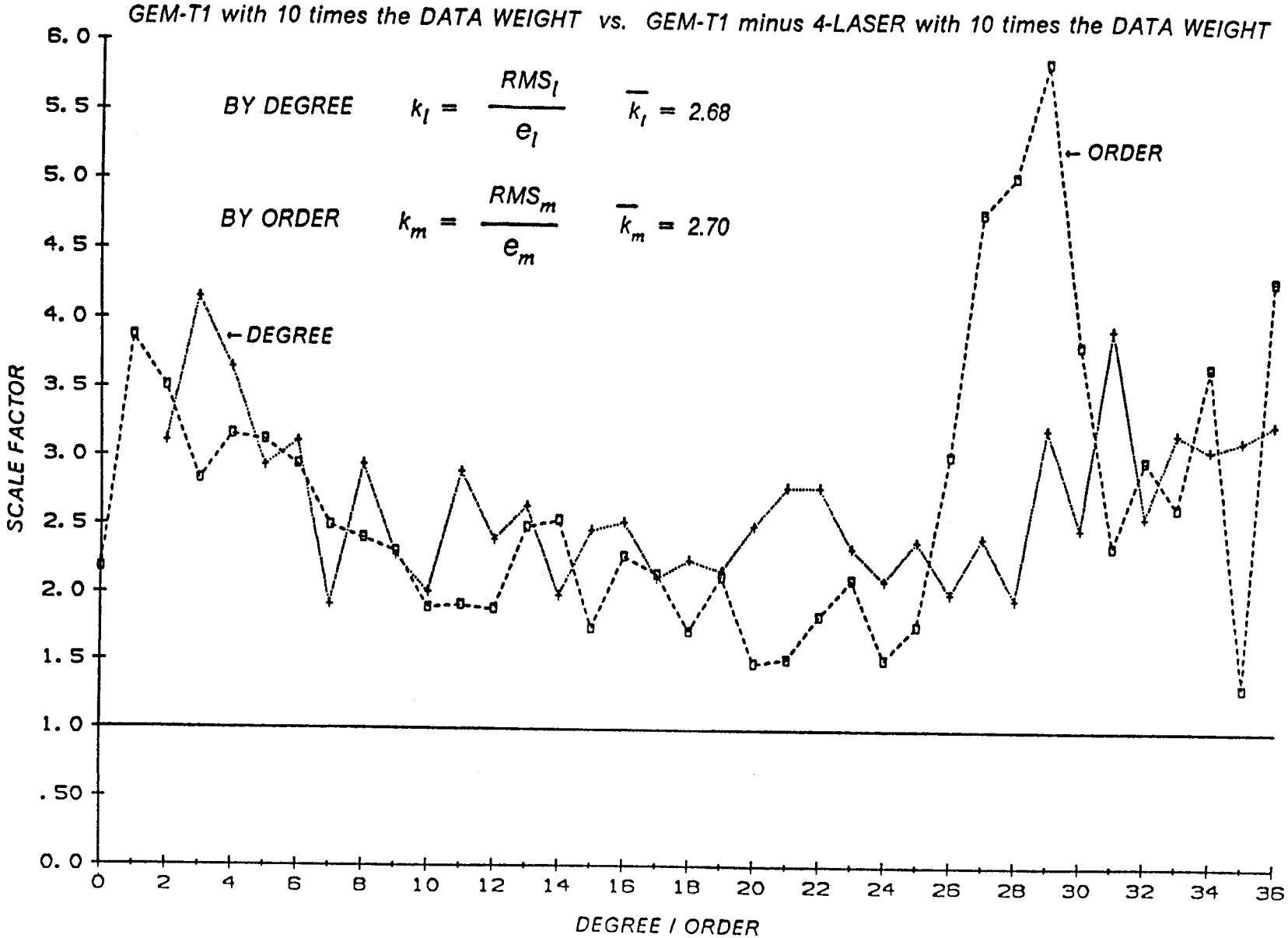

CALIBRATION OF ERROR ESTIMATES BASED UPON SUBSET SOLUTIONS

FIGURE 11

VI. GRAVITY MODEL CALIBRATION BY EIGENVALUE-EIGENVECTOR ANALYSIS

6.0 Introduction

One of the major objectives of this research effort is to produce gravitational models capable of supporting the stringent orbit determination requirements of the TOPEX Mission. However, to fully assess the performance of a gravitational model on a satellite orbit (prior to launch), knowledge of only the error variances of the field is insufficient to make a reliable projection. For example, consecutive even and odd zonal harmonics are correlated by .95 and significant correlation exists for coefficients in all orders (particularly resonance orders). For TOPEX, the predicted radial error based upon the GEM-T1 covariance matrix (as more fully described later) gives about 25 cm while using the variances alone predicts radial errors for TOPEX exceeding 80 cm RMS.

Any given satellite orbit samples the earth's gravitational field in a way which causes it to sense certain perturbative frequencies. Each of these perturbations can be mathematically described as some linear combination of the spherical harmonics used to represent the gravitational field (see for example Wagner and Klosko, (1977) or Reigber, (1974) who base their analyses on the linear perturbation theory given in Kaula, (1966)). These sums (or "lumped-harmonics") can be very accurately determined, even more so than the individual harmonic coefficients, but they are satellite-specific and tend to reflect the distribution of orbital characteristics sampled when forming the model. Therefore, our pre-launch analysis was directed at estimating the errors in the "lumped-harmonics" which are TOPEX specific and TOPEX sensitive. In particular, we are most interested in those that represent significant radial perturbations.

While it is correct to assume that highly correlated parts of our gravitational model have degraded variances due to significant off-diagonal terms in the normal matrix, only these cross-correlations allow

one to properly sum the effects within a given order to calculate errors in these "lumped-harmonics". Specific knowledge of the full covariance (not merely the standard errors) of the solution, especially the cross-correlation of the coefficients with odd and even parity within the same orders is therefore essential to predict orbit errors. Acknowledging this, we wondered, for example, whether the Kaula constraint matrix within our solution (which artificially reduces the cross-correlation between high degree terms) would yield a seriously distorted covariance matrix. In any case, it is necessary to provide a calibration of the complete GEM-T1 covariances before covariant orbital accuracy projections on TOPEX can be considered reliable.

Our approach to the covariance calibration of GEM-T1 was through the eigenvectors of its error covariance matrix. Again, we were fortunate that we had a supercomputer available for calculating the eigenvectors within the GEM-T1 solution. The full covariance matrix for each of the solutions described in Table 4 were calculated and provided the means for calibrating the GEM-T1 covariance. First, in Section 6.1, we review the mathematical development of this calibration technique which strongly parallels that given in Section IV. We then discuss the projection of the eigenvectors from various dependent models onto those of GEM-T1 using the differences in their respective covariances (Section 6.2). Section 6.3 shows the calibration of the model using all of the major data subsets within GEM-T1 and results obtained after introducing surface gravimetry and satellite altimetry into the model. Here an approach which projects the difference of the coefficients directly on the eigenvectors of the main or subset field is employed.

6.1 Calibration by Eigenvector Analysis: Direct Method

Given two fields F and $\bar{F}$, let their corresponding coefficient solutions be C and $\bar{C}$, and their corresponding error-covariance matrices be V and $\bar{V}$, respectively.

Since we are interested here in assessing only the gravity model uncertainties and their effects on orbital trajectories, the full error-covariance matrices were truncated to include only the geopotential parameters. Thus the eigenvector technique of calibration (to be discussed herein) considers the previously ignored covariances.

Let λ and $\bar{\lambda}$ be the diagonal eigenvalue matrices of the now truncated V and $\bar{V}$ matrices, respectively. By convention, λ and $\bar{\lambda}$ are arranged in descending order. Thus, the matrices take on the form

$$\begin{bmatrix} \lambda_{1,1} & 0 & 0 & 0 & \cdots & 0 \\ 0 & \lambda_{2,2} & 0 & 0 & \cdots & 0 \\ 0 & 0 & \lambda_{3,3} & 0 & \cdots & 0 \\ 0 & 0 & 0 & \lambda_{4,4} & \cdots & 0 \\ 0 & 0 & 0 & 0 & \cdots & \lambda_{1363,1363} \end{bmatrix} \qquad (6.1)$$

Let B and $\bar{B}$ correspond to the ordered eigenvector matrices, where the individual normalized eigenvectors form the columns of B and $\bar{B}$. Therefore,

$$V = B \lambda B^T \qquad (6.1a)$$

$$\bar{V} = \bar{B} \bar{\lambda} \bar{B}^T \qquad (6.1b)$$

The eigenvectors of the error-covariance matrix represent the independent combined harmonics unique to the solution while the corresponding eigenvalues represent the variance of the error in estimating each of these combinations. These combined harmonics C' are defined from C as: $C' = B^T C$. Thus, a small eigenvalue means that a particular combination (corresponding approximately to a "lumped" harmonic of all terms in the field) is well-determined by the solution while a large eigenvalue means that a particular combination is poorly-determined.

Now we can derive eigenvector calibration factors in analogy to equation (4.1)

$$k_{\ell,m} = \Delta C_{\ell,m} \; / \; e_{\ell,m}$$

Let

$$\Delta C = \bar{C} - C = (\bar{C} - C_{true}) - (C - C_{true}) \qquad (6.2)$$

$$\Delta V = \bar{V} - V \qquad (6.3a)$$

when the data included in $\bar{F}$ is a subset of the data included in F. Also, again by analogy, when models are compared based exclusively on independent data,

$$\Delta V = V + \bar{V} \qquad (6.3b)$$

By equation (6.1), where the D subscript represents the difference in the covariances as in (6.3a), we get

$$\Delta V = B_D \, \lambda_D \, B_D^T \qquad (6.4)$$

While equation (6.4) is similar to equation (6.1), the interpretations of the eigenvalue sizes are quite different. Small eigenvalues derived from V or $\bar{V}$ indicate that the associated eigenvectors are well-determined by the data used to form the respective F or $\bar{F}$ gravity fields. In contrast, small eigenvalues derived from ΔV imply that the parameters associated with the eigenvectors are not significantly altered due to the presence or absence of a specific data subset which delineates the difference between the main (F) and subset field solutions ($\bar{F}$). Hence, significant effects of the data subsets are found

with the largest eigenvalues of λ_D. In this case, the magnitude of the eigenvalues is a measure of the improvement in the variances achieved through the inclusion of these data.

The direct eigenvector projection Δy of the difference in the actual harmonics ΔC of the two solutions can be obtained through the eigenvector matrix B_D by the relation

$$\Delta y = B_D^T \Delta C \tag{6.5}$$

We shall refer to Δy as the eigenvector parameters whose variance is given by $E(\Delta y\ \Delta y^T)$:

$$E(\Delta y\ \Delta y^T) = B_D^T\ E(\Delta C\ \Delta C^T)\ B_D \tag{6.6}$$

We are now in a position, by analogy to (4.1), to define the eigenvector calibration factors where $\Delta C_{\ell,m}$ becomes $|\Delta y|$ while $e_{\ell m}$ becomes $(E(\Delta y\ \Delta y^T))^{1/2}$ as follows:

$$CF_i = |\Delta y| \ / \ [E(\Delta y\ \Delta y)^T]^{1/2}$$

From (4.3) and (4.4) we have shown that

$$E(\Delta C\ \Delta C^T) = \Delta V \tag{6.7}$$

Thus,

$$E(\Delta y\ \Delta y^T) = B_D^T\ \Delta V\ B_D \tag{6.8}$$

Now

$$B_D^T\ B_D = B_D\ B_D^T = I \tag{6.9}$$

from the definition of the eigenvector matrix. Using these identities, equation (6.4) can be transformed to

$$B_D^T \, \Delta V \, B_D = \lambda_D \tag{6.10}$$

so that

$$E(\Delta y \, \Delta y^T) = \lambda_D \tag{6.11}$$

The direct eigenvector calibration factor then becomes

$$CF_i = \left[(\Delta y \, \Delta y^T)_{ii} \, / \, (\lambda_D)_{ii} \right]^{1/2} \tag{6.12}$$

where i = 1 to 1363, the number of geopotential parameters in GEM-T1 type solutions.

Table 7A shows the results of three calibration tests. For simplification purposes and to average over individual samples, the individual calibration factors are divided into groups of 50 beginning with the CF_i associated with the largest eigenvalue. An RMS of the CF_i's

$$\langle CF_k \rangle = \left| \sum_{i=n}^{n+49} (CF_i)^2 \, / \, 50 \right|^{1/2} \tag{6.13}$$

and an average of the $\langle \lambda_D \rangle_k$

$$\langle \lambda_D \rangle_k = \sum_{i=n}^{n+49} (\lambda_D)_{ii} \, / \, 50 \tag{6.14}$$

where n = 50(k-1) + 1, are obtained for each group. Finally, an rms of the CF_k's (k = 1 to 27) for the complete sets of CF_i's,

$$\text{rms} = \left[\sum_{k=1}^{27} \langle CF_k \rangle^2 \; / \; 27 \right]^{1/2} \qquad (6.15)$$

and a weighted rms

$$\text{Wrms} = \left[\sum_{k} \langle \lambda_D \rangle_k \; \langle CF_k \rangle^2 \; / \; \sum_{k} \langle \lambda_D \rangle_k \right] \qquad (6.16)$$

are computed for each of the three tests. Note, the weighted rms gives added weight to the eigenvector parameters which are more significantly affected by the data.

The exponential fall off in average eigenvalue size shown in Table 7A led directly to the computation of the weighted rms calibration factor in equation (6.16). Using this formula, the overall weighted calibration factor now more closely reflects the significant differences in the errors of the two solutions.

The size of the average eigenvalues in Table 7A is a measure of how much a tested data set improves the main field over the subset model lacking these data. In general, the average eigenvalues for the surface gravity and altimeter data set are larger than the corresponding average eigenvalues for the other two tested data sets. Furthermore, the data subset from the 4 laser satellites ("4-LASERS") improves the solution more than the solitary Starlette data set. Since four unique orbital geometries are sampled in the 4-LASER case, this result is expected.

Note that there are only 25 (instead of 27) eigenvalue groups of 50 samples for the case of [GEM-T1] vs. [GEM-T1 minus STARLETTE data]. The algorithm which computed the eigenvalues produced about 100 negative but small eigenvalues. Negative eigenvalues have no physical significance but reflect numerical properties of the computation environment. The positive eigenvalues have a range of about 10^{12}. The computer arithmetic, however, was done using only 14 digits. Therefore these negative eigenvalues undoubtedly result from machine round-off errors. Thus, for all practical purposes, they can be treated as zeros. The

TABLE 7.A

DIRECT EIGENVECTOR CALIBRATION
FACTORS $\langle CF_k \rangle$ AND AVERAGE EIGENVALUES $\langle \lambda_{D_k} \rangle$

GEM-T1 vs. GEM-T1 Minus/Plus the following data sets

EIGENVALUE	(-)STARLETTE		(-) 4 LASERS		(+) SURFACE GRAVITY + ALTIMETER	
GROUP NO(k)	$\langle CF_k \rangle$	$\langle \lambda_{D_k} \rangle$	$\langle CF_k \rangle$	$\langle \lambda_{D_k} \rangle$	$\langle CF_k \rangle$	$\langle \lambda_{D_k} \rangle$
1	0.87	.11E-15	0.92	.11E-15	0.73	.28E-15
2	1.15	.60E-16	0.86	.54E-16	0.85	.14E-15
3	1.13	.36E-16	1.10	.36E-16	0.82	.11E-15
4	1.55	.21E-16	1.26	.24E-16	0.88	.83E-16
5	1.24	.95E-17	1.03	.15E-16	0.95	.68E-16
6	1.00	.33E-17	1.19	.94E-17	0.85	.57E-16
7	0.72	.10E-17	0.98	.55E-17	0.79	.50E-16
8	0.66	.36E-18	1.26	.30E-17	0.83	.45E-16
9	0.64	.14E-18	1.08	.15E-17	1.16	.40E-16
10	0.52	.53E-19	0.96	.81E-18	1.12	.36E-16
11	0.52	.20E-19	0.88	.43E-18	1.06	.32E-16
12	0.44	.84E-20	0.65	.23E-18	1.03	.30E-16
13	0.45	.36E-20	0.80	.12E-18	0.84	.27E-16
14	0.40	.16E-20	0.60	.66E-19	0.93	.24E-16
15	0.35	.71E-21	0.82	.35E-19	1.04	.20E-16
16	0.38	.31E-21	0.60	.19E-19	1.04	.16E-16
17	0.33	.13E-21	0.59	.10E-19	1.11	.11E-16
18	0.39	.54E-22	0.73	.52E-20	1.27	.76E-17
19	0.39	.21E-22	0.58	.27E-20	1.52	.46E-17
20	0.27	.74E-23	0.64	.14E-20	1.69	.26E-17
21	0.34	.24E-23	0.59	.67E-21	1.74	.14E-17
22	0.27	.76E-24	0.58	.31E-21	1.31	.65E-18
23	0.31	.22E-24	0.63	.13E-21	1.64	.26E-18
24	0.28	.49E-25	0.56	.51E-22	2.03	.81E-19
25	0.36	.63E-26	0.56	.17E-22	1.85	.19E-19
26			0.61	.37E-23	1.91	.25E-20
27			0.67	.35E-24	2.01	.14E-21
RMS	0.69		0.89		1.30	
WEIGHTED RMS	1.08		1.00		0.88	

weighted rms calibration factors for the three test cases presented in Table 7A show that the data in GEM-T1 is approximately weighted correctly. Calibration factors less than 1 mean that the errors have been over-estimated. Thus, for the cases of [GEM-T1] vs. [GEM-T1 minus STARLETTE data] and of [GEM-T1] vs. [GEM-T1 minus 4 LASER data], the attributed errors are actually slightly too large, but only if all the eigenvector parameters are weighted the same.

For the case of [GEM-T1 plus surface gravity + altimeter data] vs. [GEM-T1], the rms calibration factor indicates that at certain frequencies the attributed errors have been under-estimated. However, a close look at Table 7A shows that all of the large calibration factors are associated with small average eigenvalues. In this case, the small eigenvalues generally correspond to eigenvectors of primarily long-wavelength combination terms or zonal and resonance effects. Surface gravity and altimeter data cannot resolve these dynamically resolved terms nearly as well as the direct satellite tracking (see Figure 4). Therefore, it is not surprising that these eigenvector calibration factors for the best determined eigenvectors are all significantly larger than 1 using surface gravimetry and the radially-sensitive satellite altimetry. Hence, the weighted calibration factor (0.88) should give the more reliable estimate.

The average geoid height error Δh_i implied by each eigenvalue is

$$\Delta h_i = \sqrt{\lambda_{ii}}\, R_e \qquad (6.17)$$

where R_e is the mean radius of the earth.

Thus, the contribution of these long wavelength eigenvalue errors is insignificant compared to the contribution of the large shorter wavelength eigenvalue errors. Therefore, if the attributed errors (for the surface gravity/altimeter case) for these longest wavelength terms were increased to reduce their calibration factors to approximately 1, there would be little change in the total predicted orbit determination error produced by GEM-T1.

Of the calibration factors associated with large average eigenvalues, only a few of them are exceptionally high, such as the 1.55 in the case of [GEM-T1] vs. [GEM-T1 minus STARLETTE data]. A close look at the components of the associated eigenvectors shows that the largest components are higher order resonant and near-resonant terms, such as C(33,27) and S(33,28). The primary resonance order of STARLETTE is 14 with strong secondary resonances with 27th and 28th order terms. STARLETTE senses terms beyond the degree 36 cutoff of GEM-T1 for these resonance orders. Therefore it appears that these large calibration factors are due to aliasing arising from these neglected coefficients. Thus, if the gravity field model is expanded to degree and order 50 as is planned when altimetry and surface gravimetry are fully utilized, STARLETTE will contribute significantly to the recovery of these higher degree harmonics. Therefore, this aliasing problem and the large calibration factors for these vectors would be expected to disappear.

When the weighed rms calibration factors are computed for each of the three cases, the results are all approximately 1. Thus, as far as the significant errors in the GEM-T1 gravity field model are concerned, especially for the more significant larger errors, a satisfactory calibration is indicated.

6.2 Calibration by Eigenvector Analysis: Projection Method

Calibration can also be done by an indirect projection method using eigenvector analysis. Instead of converting ΔC into combined-harmonics using the eigenvectors of the difference of the two error-covariance matrices by equation (6.5), ΔC can be projected onto the combined-harmonics of either the main gravity field solution or the subset gravity field solution using either B or $\bar{B}$, respectively.

$$\Delta y_P = B^T \Delta C \qquad (6.18a)$$

$$\Delta\bar{y}_P = \bar{B}^T \Delta C \qquad (6.18b)$$

Thus, we have

$$E\ (\Delta y_P\ \Delta y_P^T) = B^T\ \Delta V\ B \qquad (6.19a)$$

$$E\ (\Delta\bar{y}_P\ \Delta\bar{y}_P^T) = \bar{B}^T\ \Delta V\ \bar{B} \qquad (6.19b)$$

The calibration factors of the projection are then

$$PCF_i = \left[(\Delta y_P\ \Delta y_P^T)_{ii} \ /\ (B^T\ \Delta V\ B)_{ii}\right]^{1/2} \qquad (6.20a)$$

$$\overline{PCF}_i = \left[(\Delta\bar{y}_P\ \Delta\bar{y}_P)_{ii} \ /\ (\bar{B}^T\ \Delta V\ \bar{B})_{ii}\right] \qquad (6.20b)$$

The eigenvectors of any GEM-T1-type field completely span the 1363 geopotential parameter space. Thus, mathematically, Δy and its associated eigenvector calibration factors can be computed using either B or $\bar{B}$. Projecting ΔC and ΔV into the combined-harmonics of either the main or subset fields (rather than onto the harmonics of the difference field) yields additional insight for assessing the errors in the gravity field solutions.

Table 7B shows the results of the projection method when applied to the three test cases shown in Table 7A. Individual calibration factors were calculated for each eigenvector and averaged in groups of 50 as before. However, for the sake of brevity, only the rms and weighted rms of the projected eigenvector calibration factors are presented in the table.

The results show again that the data in GEM-T1 is basically well-calibrated. When projections are made onto the main field, both the rms and weighted rms projected calibration factors are found to be approximately 1.

TABLE 7.B

PROJECTED EIGENVECTOR
CALIBRATION FACTORS <PCF_k>

GEM-T1 vs. GEM-T1 Minus/Plus the following data sets

	(-) STARLETTE		(-) 4 LASERS		(+)SURFACE GRAVITY +SEASAT ALTIMETRY	
	PROJECTED ONTO (GEM-T1)		PROJECTED ONTO (GEM-T1)		PROJECTED ONTO (GEM-T1)	
	SUBSET FIELD	MAIN FIELD	SUBSET FIELD	MAIN FIELD	SUBSET FIELD	MAIN FIELD
RMS	1.30	1.03	1.15	.99	1.22	.87
WTED. RMS	1.09	.99	1.00	.94	.89	.97

However, when projections are made onto the subset field, the rms projected calibration factors depart markedly from 1. This result should not be surprising since the subset field does not contain any of the data whose errors are being assessed. Thus, the eigenvectors of the subset field are not likely to align with the errors of the data being calibrated, resulting in less reliable projections. On the contrary, projections onto the main field which contain the data being calibrated are likely to align with the data errors yielding more reliable calibration results.

A closer look at the projected calibration factors when using the subset solution for each group of 50 also shows that all of the high calibration factors are associated with small average eigenvalues. The weighted rms projected calibration factors which favor more significant model differences are all reasonably close to 1. Therefore, as far as the significant errors in the data are concerned, the GEM-T1 gravity field is still calibrated correctly even when the errors are projected onto the subset field. We thereby have another useful method for further assessing the errors in GEM-T1 through this projection method utilizing subset solutions.

6.3 Calibration by Means of Eigenvector Projections onto GEM-T1

A total of 1363 projected eigenvector calibration factors were computed for each of the subset test solutions. To reiterate, the PCF_i's were then ordered so that the PCF_1 term came from the best determined eigenvector found within the GEM-T1 solution. Likewise, PCF_{1363} was from the poorest determined eigenvector. To more easily evaluate the behavior of these calibration factors (as was done for the calibration factors k_ℓ and k_m), the CPF_i factors have been averaged over groups of 50 taken from this ordering. The first group contained the best determined eigenvectors, while the 27th group had the worst. Table 8 presents the results of these average projected eigenvector calibration factors from tests using:

Case (A) a GEM-T1 subset solution that lacks the contribution of GEOS 1, 2, 3 and BE-C laser data: "4 LASERS" and also

Case (B) GEM-T1 as the subset of a GEM-T1 plus altimeter/surface gravimetry model.

Shown in Table 8 are the average size of the GEM-T1 eigenvalues and the scaled average error (found through a scaling with R_e) of the eigenvalues in cm within each of the groupings. The group calibration factors for each of these test solutions are also given in Table 8. In general, the projected eigenvector calibration factors have stable behavior over these groupings, and as seen earlier with the coefficient uncertainties, these eigenvector calibration factors also cluster around 1 indicating GEM-T1's covariance is well calibrated.

All of the subset solutions were evaluated using this projected eigenvector assessment including those which used subsets of GEM-T1 and those where new data was added to the GEM-T1 normals. Table 9 compares the weighted rms calibration factor obtained as in equation (6.16) from the eigenvector analysis with that obtained earlier using the coefficient differences and their variances.

The eigenvector analysis was also performed on the GEM-T1 plus deep resonance information solution. Not surprisingly, there were exactly 60 independent significant eigenvectors in the covariance matrix of the combined solution minus GEM-T1 corresponding to the number of independent (lumped) observations introduced into the solution. But only 52 of the 60 eigenvectors were found to be well determined because 8 represented independent resonance effects determined from very similar orbits. For the 52 significant eigenvectors, a satisfactory calibration was achieved. The derived eigenvector calibration factor of 1.09 was based upon these 52 independent points and agrees well with the value of 1.14 presented earlier.

TABLE 8

GEM-T1 EIGENVALUE PROJECTED ERRORS AND CALIBRATION FACTORS

AVERAGED IN GROUPS OF 50

CASE A: GEM-T1 vs. GEM-T1 without 4-Lasers data

CASE B: GEM-T1 vs. GEM-T1 + Surface Gravity + Seasat Altimeter

	GEM-T1		K_i	K_i
EIGENVALUE GROUP	AVERAGE EIGENVALUE	$\langle \Delta h \rangle$ SCALED AVERAGE ERROR(cm)	CALIBRATION FACTORS CASE A	CALIBRATION FACTORS CASE B
1	.58E-20	0.05	1.01	2.12
2	.66E-19	0.16	0.89	1.19
3	.20E-18	0.29	0.83	1.65
4	.46E-18	0.43	1.14	1.58
5	.89E-18	0.60	1.09	1.40
6	.15E-17	0.79	0.85	1.56
7	.25E-17	1.01	0.93	1.65
8	.39E-17	1.25	1.00	1.32
9	.59E-17	1.55	1.16	1.48
10	.90E-17	1.91	0.99	1.16
11	.13E-16	2.31	1.17	1.25
12	.17E-16	2.66	0.84	1.01
13	.22E-16	3.01	1.09	0.92
14	.27E-16	3.29	1.14	0.77
15	.30E-16	3.47	1.12	0.89
16	.32E-16	3.62	0.96	0.83
17	.35E-16	3.79	1.12	0.94
18	.39E-16	3.97	0.98	1.10
19	.43E-16	4.16	0.78	1.23
20	.48E-16	4.39	0.89	0.93
21	.53E-16	4.63	1.05	0.83
22	.60E-16	4.92	0.93	0.81
23	.69E-16	5.28	0.96	0.91
24	.82E-16	5.75	1.03	0.93
25	.10E-15	6.47	0.88	0.85
26	.13E-15	7.34	0.98	0.83
27	.18E-15	8.47	0.79	0.74

We have similarly performed these calibrations using the models which contained a factor of 10 bias introduced in the data weighting. The eigenvector projections yielded a comparable indication of a poorly calibrated model (see Table 9).

There clearly is a good agreement between the two sets of results, indicating that both the variances and covariances of the GEM-T1 solution are well understood. Again, with the exception of LAGEOS' subset solution, all calibration factors shown are within 10% of the ideal value of 1.

6.4 Summary of Eigenvector Calibrations

The overall calibration for the eigenvector analysis is expected to agree somewhat with that obtained on the basis of the variances of the geopotential coefficients themselves. This is because of the invariance of the trace (sum of the variances) of the variance-covariance matrix under rotation. This is not surprising because for an overall calibration factor obtained from the complete set of coefficient differences it holds that:

$$k = \frac{\Delta C^T \Delta C}{Tr(\Delta V)} = \frac{\Delta y^T \Delta y}{\sum \lambda_{ii}}$$

and it is thus independent of the technique used to determine it. The individual calibration factors

$$k_i = \frac{|\Delta y_i|}{\sqrt{\lambda_{ii}}}$$

show significant variation among the different data subsets utilized and have provided a very interesting spectral decomposition of the errors. While it is important to know which parts of the field calibrate best and poorest from a statistical point of view, for our purposes it is even more important that the parts of the field which the TOPEX orbit is most sensitive to are those calibrated satisfactorily.

TABLE 9

SUMMARY OF SOLUTION CALIBRATION FACTORS FROM GEM-T1 FIELD ASSESSMENTS

	COEFFICIENT CALIBRATION FACTOR	RMS WEIGHTED PROJECTED EIGENVECTOR CALIBRATION FACTOR ONTO GEM-T1
• (GEM-T1) vs. (GEM-T1 minus DATA SUBSET)		
4-LASERS (GEOS 1,2,3, BE-C)	1.06	0.94
STARLETTE LASER	1.10	0.99
OSCAR + SEASAT DOPPLER	1.09	1.07
OPTICAL (11 SATS)	0.84	0.89
LAGEOS LASER	1.45	1.59
• GEM-T1 vs. GEM-T1 + SURFACE GRAVITY	0.95	0.92
• GEM-T1 vs. GEM-T1 + SURFACE GRAVITY + SEASAT ALTIMETRY	0.94	0.89
• GEM-T1 vs. SURFACE GRAVITY + SEASAT + ALTIM	0.99	0.90
• GEM-T1 minus LAGEOS vs. LAGEOS + SURFACE GRAVITY + SEASAT ALTIMETRY	0.95	0.88
• GEM-T1 vs. GEM-T1 + Lumped Resonance Data	1.00	1.06
• GEM-T1 with 10 times the Data Weight vs. GEM-T1 minus 4-LASERS with 10 times the Data Weight	2.75	2.45

Returning to the original question pertaining to the influence of collocation on the correlation of the model, our eigenvector analysis has shown that there has been no significant aliasing of the coefficient variances in the region of the field most important in orbit determination. Apparently, collocation controls only weakly determined parameters and has little or no effect on those which are well sensed by the data. This insight into the behavior of the field could not be gained without a detailed calibration of individual coefficients and their corresponding eigenvectors.

VII. DIRECT CALIBRATION OF GEM-T1 WITH 1071 5°x5° MEAN GRAVITY ANOMALIES FROM ALTIMETRY

The purpose of this phase of our analysis is to perform a calibration of GEM-T1's errors by comparing gravimetric observations directly with corresponding values computed from the GEM-T1 model and equating these residuals with the errors produced by the model scaled by a calibration factor (k). Previously, except for the direct satellite resonant calibration, all other tests performed herein were based on subtracting coefficients between two solutions which differed by a given subset of data. This difference was then equated to a scaled (k) difference of the error estimates (that is, to be more precise, the square root of the difference of the error variances). These previous calibrations therefore indirectly test the fields against their data. A possible concern with this indirect method of data calibration is that both geopotential solutions may be affected similarly by unmodeled effects and hence, these errors go undetected when forming the field difference. The direct calibration of gravity models with independent observations as undertaken here will avoid this pitfall.

Mean gravity anomalies ($\Delta\bar{g}$) for 5°x5° blocks are somewhat commensurate in field resolution with the 36x36 harmonic model of GEM-T1. These independent data were used to calibrate the model. Although commensurate, analysis of the truncation effects beyond degree 36 was considered for the 5°x5° mean anomaly $\Delta\bar{g}$ and this effect was found to be important. The 5° mean anomalies from altimetry have accuracies which are usually better than 1 milligal which is far better than the errors from the GEM-T1 model. The uncertainty ascribed to the altimeter gravity anomalies are presented in Figure 12, and are compared to the GEM-T1 model in Figure 13. These figures indicate that the large GEM-T1 errors are due to the effects of the higher degree terms which are less well known in satellite models. Therefore, the calibration will primarily test these harmonic terms.

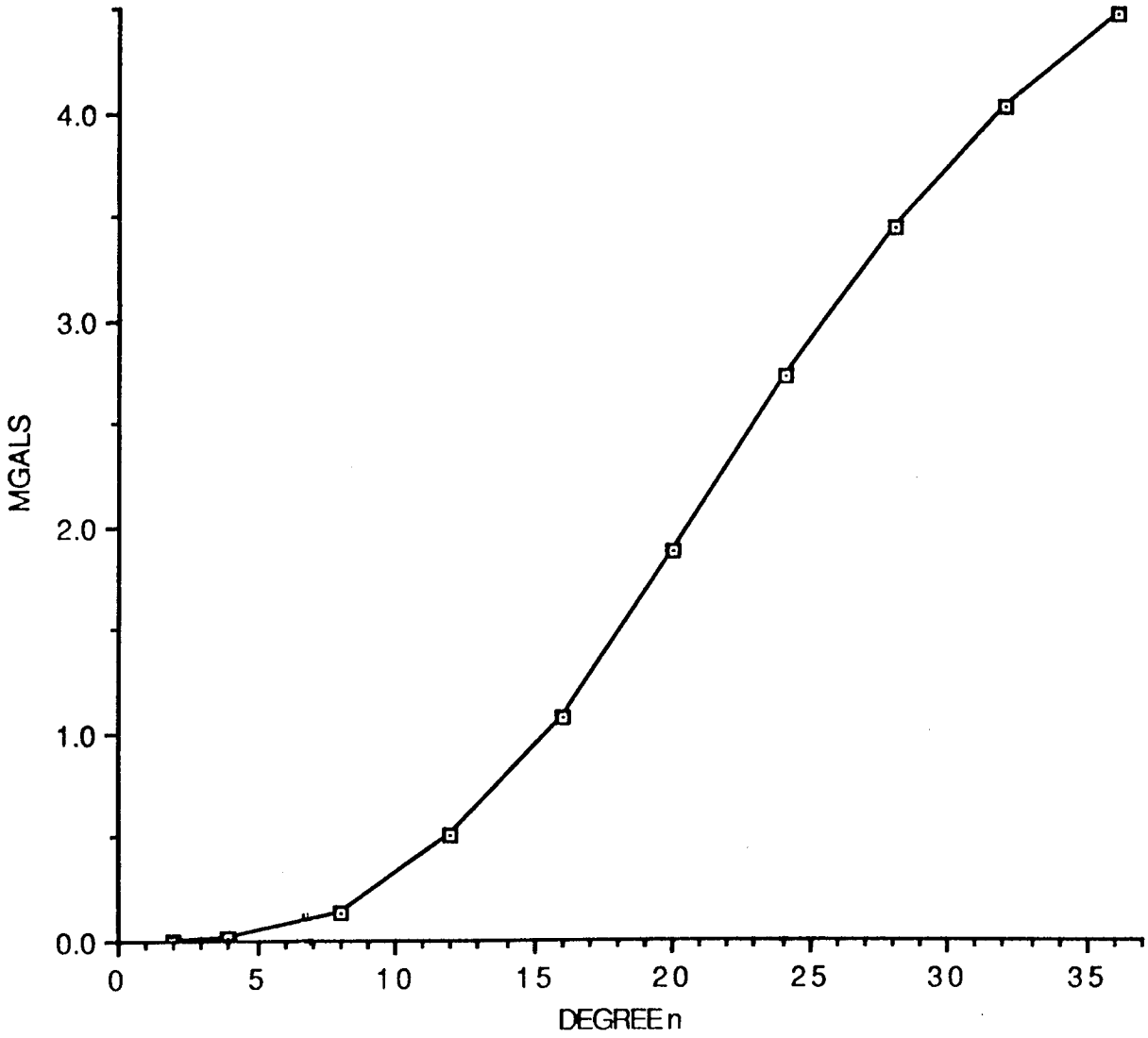

GEM-T1 ERROR SPECTRUM FOR 5° X 5°
GRAVITY ANOMALY ACCUMULATED TO DEGREE n

FIGURE 12

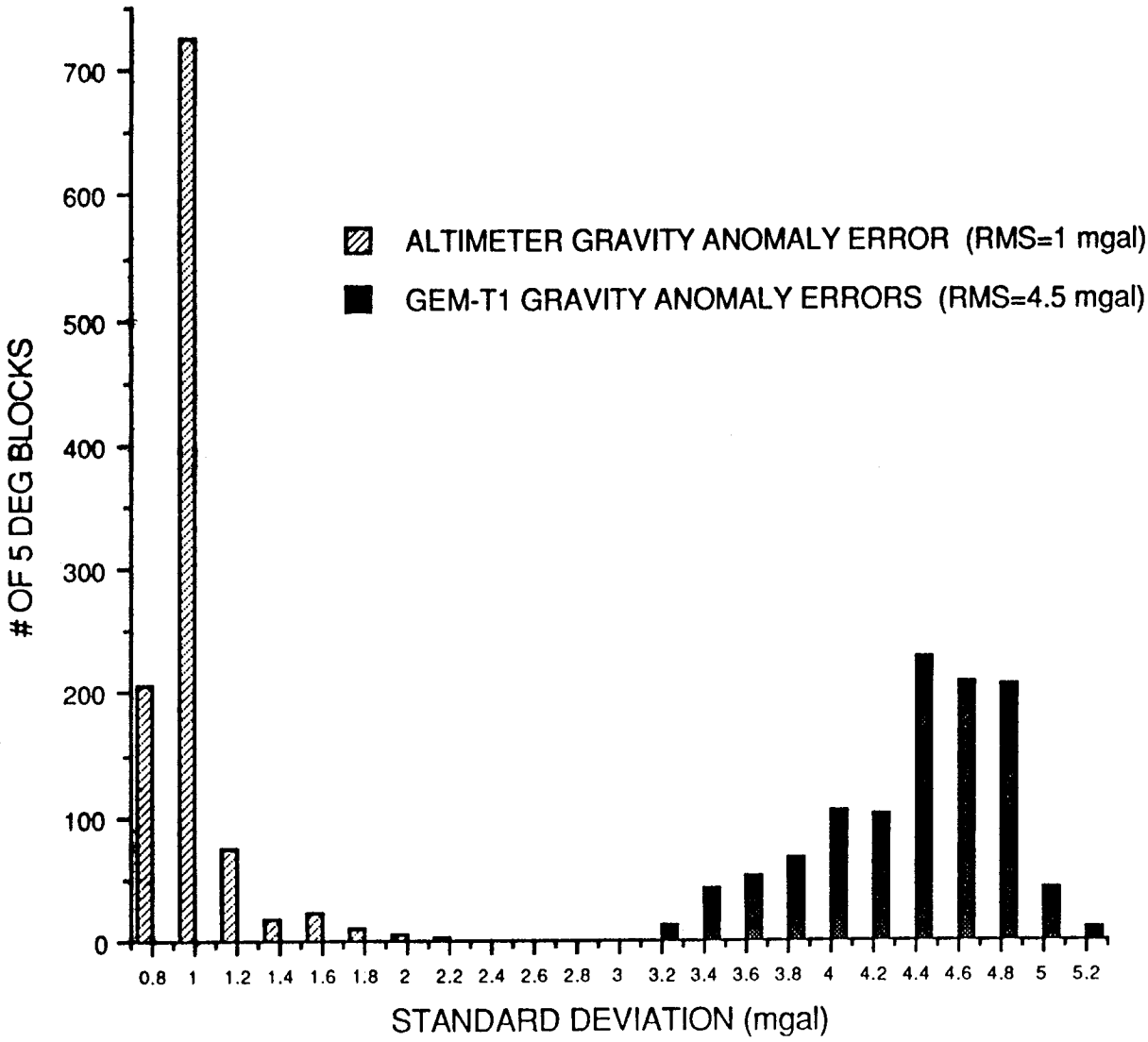

DISTRIBUTION OF STANDARD DEVIATIONS OF 5° X 5° BLOCKS OF GRAVITY ANOMALIES

FIGURE 13

7.1 Mean Gravity Anomaly Data for 5°x5° Blocks from Altimetry

Mean gravity anomalies $\bar{\Delta g}$ for 5°x5° blocks were obtained from a set of areal mean 1°x1° anomalies, which were derived from SEASAT and GEOS-3 altimetry by Rapp (1986). A set of 1071 5°x5° equal-angle $\bar{\Delta g}$ blocks were formed where each block had a complete set of 25 measured 1°x1° values. The set covered the entire ocean area and this type of data has been used previously to calibrate the earlier GEM models (Lerch et al., 1985b).

7.2 Initial Method of Calibration Excluding Truncation Effects

Because of the commensurability of observed 5°x5° anomaly blocks ($\bar{\Delta g}$) with those computed from the 36x36 model of GEM-T1 ($\bar{\Delta g}_c$) the effects of the truncation of higher degree terms were not included in the initial field calibrations. Values for the mean anomalies from GEM-T1 were obtained by averaging 1°x1° mean anomalies (Δg_c) to form 5°x5° mean anomaly blocks. The Δg_c (1°x1°) were computed (Heiskanen and Moritz, 1967) from harmonics of GEM-T1 evaluated at the center point of the 1°x1° block as follows:

$$\Delta g_c(1^\circ x 1^\circ) = \gamma \sum_{n=2}^{36} \sum_{m=0}^{n} \left(\frac{a_e}{r} \right)^n (n-1)\, P_n^m (\sin \phi) \cdot \left[C_{nm} \cos m\lambda + S_{nm} \sin m\lambda \right] \tag{7.1}$$

where r is evaluated on the reference ellipsoid with $\gamma = GM/r^2$. The 5°x5° mean anomaly blocks were formed as:

$$\bar{\Delta g}_c = \frac{\sum_{i=1}^{25} \Delta g_c\ (1^\circ x 1^\circ)_i}{25}$$

The calibration factor k is related to the mean gravity anomaly residual, $\Delta\bar{g} - \Delta\bar{g}_c$ and errors as follows:

$$E(\Delta g - \Delta\bar{g}_c)^2 = k^2\,\sigma^2(\Delta\bar{g}_c) + \sigma^2(\Delta\bar{g}) \qquad (7.2)$$

where $\sigma(\Delta\bar{g})$ and $\sigma(\Delta\bar{g}_c)$ are the errors in the mean anomaly data and the GEM-T1 errors respectively which are derived below. A global scale factor, k, can be obtained from (7.2) by averaging over the 1071 ocean points, namely

$$M[(\Delta\bar{g} - \Delta\bar{g}_c)^2] = k^2\,M[\sigma^2(\Delta\bar{g}_c)] + M[\sigma^2(\Delta\bar{g})]$$

where

$$k = \left| \frac{M[\Delta\bar{g} - \Delta\bar{g}_c)^2] - M[\sigma^2(\Delta\bar{g})]}{M[\sigma^2(\Delta\bar{g}_c)]} \right|^{1/2} \qquad (7.3)$$

and M denotes the mean square value.

The error for each 5°x5° mean anomaly $\sigma(\Delta\bar{g})$ was obtained from the 1°x1° errors given with the data as follows:

$$\sigma(\Delta\bar{g}) = \left| \sum_{i=1}^{25} \frac{\sigma^2(\Delta g\ 1^\circ x 1^\circ)_i}{25} \right|^{1/2} / 5 \ .$$

This assumes the errors for 1°x1° anomalies are random and uncorrelated. These errors are plotted in Figure 13 along with the GEM-T1 errors $\sigma(\Delta\bar{g}_c)$. The altimeter derived gravity anomaly errors are seen to be quite small (RMS = 1 mgal) as compared to the ones derived

from GEM-T1 (RMS = 4.5 mgal). For comparison purposes, a second global scale factor will be computed from (7.3) where the altimeter anomaly data errors are set to zero which will yield a conservative estimate of k. This result also shows that these relatively small altimeter block data errors are not very significant in the determination of k.

The calculation of the commission error $\sigma(\Delta\bar{g}_c)$ from GEM-T1 is now described. The mean anomaly errors were obtained from the GEM-T1 error covariance matrix (V) with the use of a spectral (Pellinen) smoothing operator β_n (Rapp and Jekeli, 1980). The operator enables errors for point values to be averaged over a capsize with area corresponding to a 5°x5° block. The error for $\Delta\bar{g}_c$ due to coefficient errors in GEM-T1 is given as:

$$\delta(\Delta g_c) = \gamma \sum_{n=2}^{36} \sum_{m=0}^{n} \beta_n \left(\frac{a_e}{r}\right)^n P_n^m(\sin\phi) \left[\Delta C_{nm} \cos m\lambda + \Delta S_{nm} \sin m\lambda\right]$$

$$\equiv A\ \Delta C\ ,$$

then

$$E\left[\delta^2(\Delta\bar{g}_c)\right] \equiv \sigma^2(\Delta\bar{g}_c) = AVA^T \qquad (7.4)$$

which is evaluated at the center point of the 5°x5° block. For a conservative estimate of the calibration factor, the β_n were computed using an area corresponding to the size of an equal-angle block at the equator. A more rigorous computation would account for the smaller 5°x5° areas remote from the equator.

The importance of the smoothing operator β_n may be seen by comparing $\sigma(\Delta\bar{g}_c)$ with point values of $\sigma(\Delta g_c)$ where $\beta_n = 1$. The histogram (Figure 13) for $\sigma(\Delta\bar{g}_c)$ shows an rms value of 4.5 mgals, which is the square root of the term being scaled by k^2 for the global calibration, namely $M[\sigma^2(\Delta\bar{g}_c)]$. For point values, $M[\sigma^2(\Delta g_c)]$

equals about 6.0 mgals^2. Hence, the effect of β_n provides for a more realistic calibration factor by the ratio of (6.0/4.5) or 1.33. This is still somewhat conservative since the smoothing for β_n is based upon equatorial areas (which yields both smaller β_n and $\sigma(\Delta\bar{g}_c)$).

7.3 Calibration Results

From the global calibration given by (7.3), the value of k computed was

$$k = 1.1 \ .$$

A histogram (Figure 14) using the global k value was obtained from individual calibration factors k_i for each mean anomaly as follows:

$$k_i = \frac{|\Delta\bar{g} - \Delta\bar{g}_c|_i}{[\ \sigma^2(\Delta\bar{g}) + k^2\ \sigma^2(\Delta\bar{g}_c)\ ]^{1/2}} \qquad (7.5)$$

Using a 3 sigma edit of 3.3 (based upon the global value of k = 1.1) 8 points with large residuals were edited yielding a new global calibration factor of:

$$k = 1.04 \qquad (7.6)$$

With use of this k an rms of k_i from (7.5) gave

$$\bar{k} = \left| \frac{\sum_i k_i^2}{1062} \right|^{1/2} \qquad (7.7)$$

$$= 1.03$$

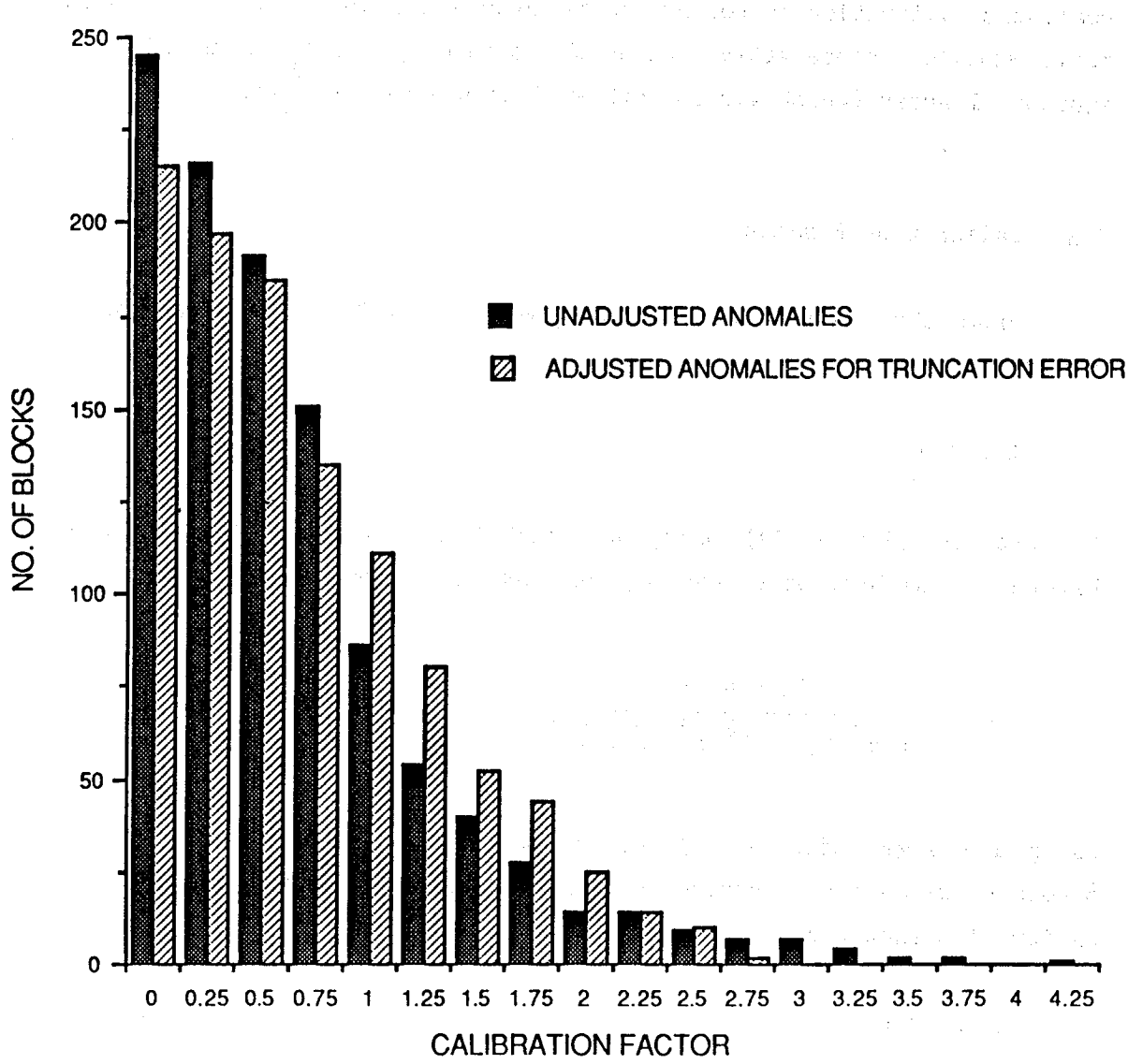

DISTRIBUTION OF BLOCK CALIBRATION FACTORS

GEM-T1 CALIBRATION WITH 1071 5° X 5° ALTIMETER GRAVITY ANOMALIES

FIGURE 14

The value for $\bar{k}$ rose to 1.07 when the data errors $\sigma(\Delta\bar{g})$ were set to zero, showing as predicted, that these errors are not very significant in this calibration; the commission error in GEM-T1 is much larger than these data errors.

The geographical distribution of the k_i calibration factors are shown in Figure 15 with the 8 points selected for editing shown in black. These edited points overlie areas of oceanic trenches. If the editing is tightened to 2 sigma, 34 points (Figure 16) are selected for editing using (2k = 2.2) as a residual cutoff. These blocks are all located in areas of steep geoidal variation, leading us to conclude that GEM-T1's truncation error is significant and the effect should be included in the calibration.

7.4 GEM-T1 Calibration with Adjustment for Truncation Effects

As a result of the relatively large values in the tail of the histogram (Figure 14), it was decided to adjust the gravity anomaly data for truncation effects, Δg_T, for terms beyond degree 36 in the harmonic expansion. These new calibrations used altimeter anomalies, Δg_A, defined as:

$$\Delta g_A\ (1^0 x 1^0) = \Delta g(1^0 x 1^0) - \Delta g_T(1^0 x 1^0) \qquad (7.8)$$

The mean anomalies over 5°x5° blocks, corrected for truncation effects, were computed as:

$$\Delta\bar{g}_A = \Delta\bar{g} - \Delta\bar{g}_T \qquad (7.9)$$

Using the gravitational model of Rapp and Cruz (1986a), which is complete in spherical harmonics through degree and order 360, a grid of $\frac{1}{2}^\circ$ x $\frac{1}{2}^\circ$ Δg_T values were computed for terms beyond degree 36. These Δg_T values were areally averaged to produce $\Delta g_T(1^0 x 1^0)$ anomaly corrections.

BLACK---block is edited

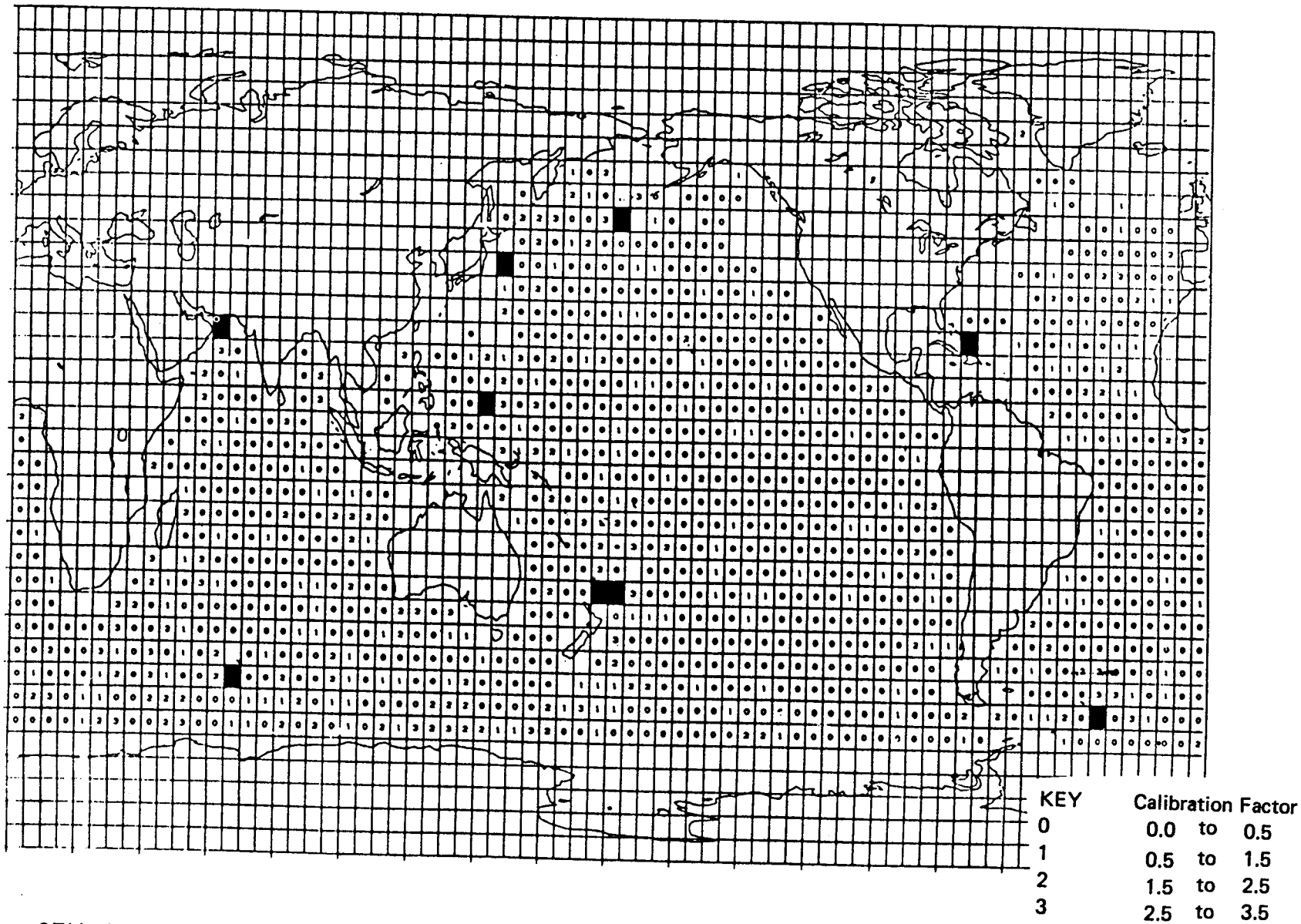

GEM-T1 BLOCK CALIBRATION FACTORS FOR SEASAT ALTIMETER 5 DEG. X 5 DEG. GRAVITY ANOMALIES

FIGURE 15.

BLACK --- 2 Sigma Edit Applied (2.2 edit cutoff)

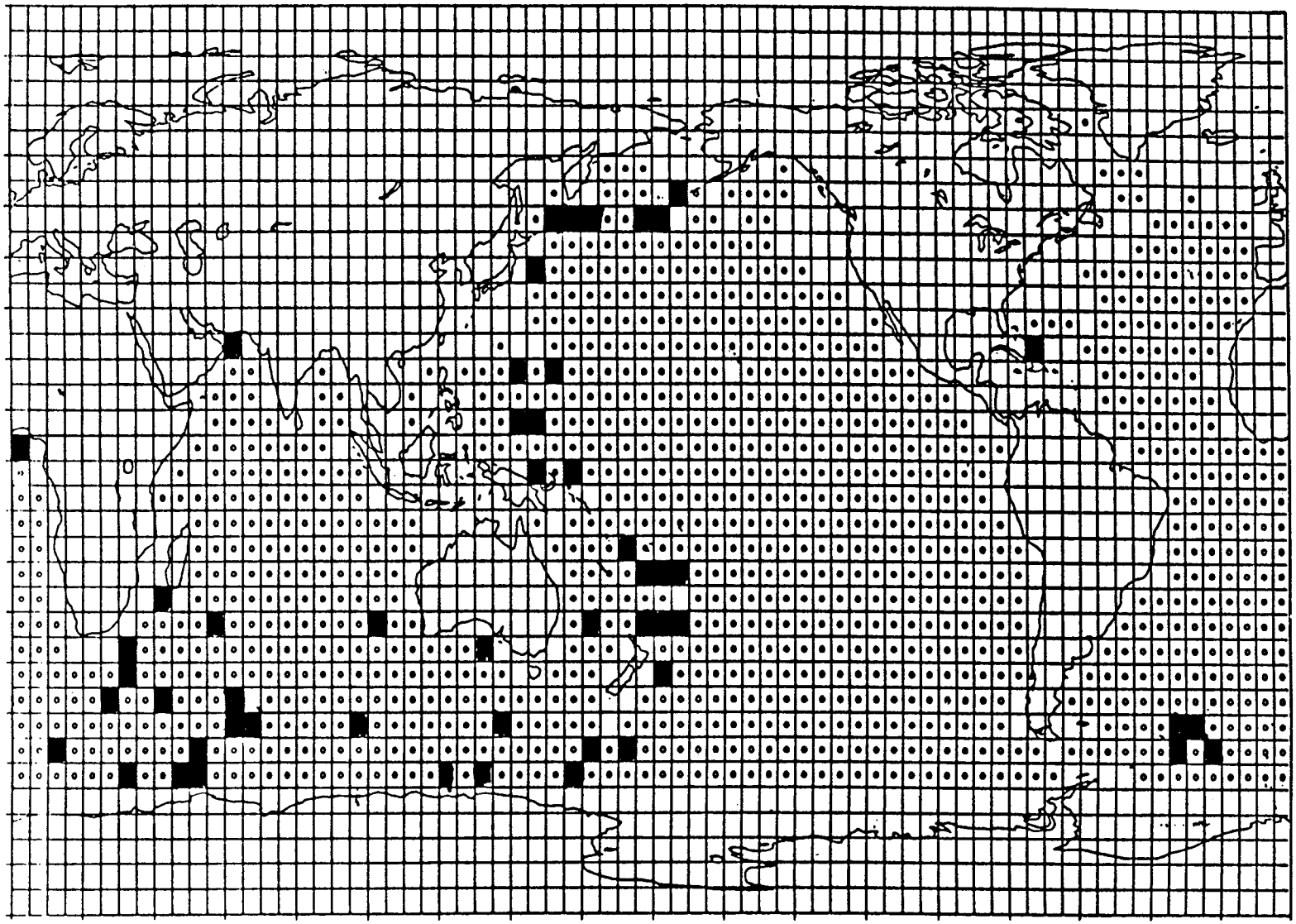

BLOCK CALIBRATION FACTORS WITH TIGHTER EDITING

FIGURE 16.

Using the adjusted 5°x5° mean anomalies $\Delta\bar{g}_A$ in place of $\Delta\bar{g}$ in (7.9), the calibration process was repeated. The new global value of k from (7.3) gave

$$k = .87 \tag{7.10}$$

which was based upon all 1071 adjusted anomalies with no editing. The new k_i from (7.5) corresponding to each adjusted mean anomaly $(\Delta\bar{g}_A)_i$ was plotted alongside the previous values in Figure 14. Note the tail of the new histogram shows significant improvement, with many fewer instances of large disagreements (which required editing for the previous calibration). Also, accounting for truncation improved the overall calibration factor indicating conservative estimates published for the commission error in GEM-T1.

7.5 Improved Comparisons of Gravity Models with Adjusted Gravity Anomalies

Based on this new set of 5° anomalies which have now been corrected for truncation effects (Δg_T), we have revised some earlier comparisons using older GEM models, applying these new anomalies instead. For each field the mean square residuals

$$M(\Delta\bar{g}_A) = \frac{\sum_i (\Delta\bar{g}_A - \Delta\bar{g}_c)^2_i}{1071}$$

are computed and compared to $M(\Delta\bar{g})$ for the original uncorrected anomaly data. Results are presented in Table 10 for comparison showing significant reductions in the mean square residuals.

7.6 Surface Gravimetry Calibration Conclusions

An oceanwide set of 1°x1° altimeter-derived gravity anomalies, when averaged to form 5°x5° mean gravity anomalies, were found to be quite productive in calibrating the GEM-T1 model. The truncation effect for 5°x5° mean anomalies was found to be an important contaminant in estimating the calibration factor for the 36x36 model. Estimations for the global calibration factor reduced k from 1.11 to 0.84 by applying estimates of the truncation effect for terms above degree 36 obtained from a high degree and order gravity model. This truncation effect, when used to correct the 1071 5°x5° mean gravity anomalies, gave a significantly improved anomaly data set for testing 36x36 geopotential models. The commission error in the field is better tested using these new anomaly values, which is the chief concern in field calibrations. These adjusted anomalies reduced the mean square residual misclosure between altimeter anomalies and GEM-T1 from 29 to 15 $mgals^2$.

Because of the greater sensitivity of the gravity anomaly to the higher degree harmonic terms, the calibration results obtained herein apply more directly to the higher degree (above degree 10) terms of GEM-T1.

Table 10. Improved Field Comparisons of 1071 5°x5° Mean Gravity Anomalies Based Upon Mean Square Residuals (MSR) Using Original Data ($\Delta\bar{g}$) and the Data Adjusted for Truncation Effect ($\Delta\bar{g}_A$)

Field	MSR($\Delta\bar{g}$)	MSR($\Delta\bar{g}_A$)
GEM-T1	25 $mgal^2$	15 $mgal^2$
COMBINED MODEL (GEM-T1 + SURF. GRAV. + ALTIMETER)	14	5
GEM-L2	40	29

Table 10. Improved Field Comparisons of 1071 5°x5° Mean Gravity Anomalies Based Upon Mean Square Residuals (MSR) Using Original Data ($\Delta\bar{g}$) and the Data Adjusted for Truncation Effect ($\Delta\bar{g}_A$)

Field	MSR($\Delta\bar{g}$)	MSR($\Delta\bar{g}_A$)
GEM-T1	25 $mgal^2$	15 $mgal^2$
COMBINED MODEL (GEM-T1 + SURF. GRAV. + ALTIMETER)	14	5
GEM-L2	40	29

VIII. ESTIMATED TOPEX ORBITAL ERRORS FROM GEOPOTENTIAL SOURCES

Figure 1.2 has indicated that there is a significant improvement in the level of coefficient accuracy which has been achieved with the development of GEM-T1. It is of interest to assess how these improvements translate into radial uncertainty performance on the TOPEX nominal orbit. This assessment is now possible since we have demonstrated in Section VI that the covariance of the GEM-T1 solution is well calibrated and gives a reliable estimate of model uncertainty in the presence of model correlation.

To make these calculations, the GSFC ERODYN Program (Englar et al, 1978) was used. This program is capable of propagating the full gravity model covariance error statistically into an rss position error of the satellite's trajectory as a function of time using the variational equations involving the partial derivatives of position with respect to the force model. The covariance matrices for GEM-L2 (Lerch et al., 1982), GEM-T1 and a combination solution containing GEM-T1 and surface gravimetry/altimetry were individually assessed. In this section we give only the radial error contributions from the gravitational field alone and consider no other sources of error such as those from the tracking systems.

Three days worth of Doppler data were simulated from a global network of 40 stations to provide observations for this analysis. These 'perfect' observations were made without any consideration for tracking system errors and merely reflect the likely data distribution for TOPEX from one of the possible tracking scenarios. These observations were based on our best knowledge of the nominal TOPEX orbital characteristics and were reduced in our standard mode to yield gravitational normal equations and the variational matrix of force model derivatives as they are computed within our orbit determination program, GEODYN (Martin et al., 1987). The covariance matrix of the geopotential solutions completed the information required by ERODYN to give a picture of the TOPEX orbit errors in time over this tested three day interval arising from geopotential uncertainty.

TABLE 11

Radial Orbital Errors (RMS) for Three Day Arc Lengths Using Calibrated Covariance Matrices

Geopotential Model	Radial RMS Error (cm)
GEM-L2	65
GEM-T1	25
GEM-T1 + Surface Gravimetry + Altimetry	17

Table 11 summarizes these results. Shown in this table is the rms radial error due only to geopotential effects for the TOPEX orbit over this three-day arc length. The results displayed as a function of time, are presented in Figure 17. They indicate that GEM-T1 has made considerable progress in reducing the likely gravitational modeling problems for TOPEX. And with the further addition of altimeter/surface gravity data types, these errors should be substantially reduced still further. While they are preliminary, these findings are grounds for cautious optimism.

Figure 18 shows a breakdown of the GEM-T1 radial errors on TOPEX for terms of the same degree and those of the same order. The strongest signal is seen from an evaluation of the geopotential error contributions by order, where two very significant peaks are found. These high error sources are due to the m=1 and m=13 terms. The m=13 harmonics are those which have primary resonance with TOPEX and even a small amount of TOPEX data will be capable of resolving them to a high level of accuracy for they act at a limited and very narrow frequency band. Likewise, the m=1 effects are largely due to the so-called "m-daily" perturbations which give rise to perturbations with a period of nearly one cycle per day for m=1 terms. Again, limited amounts of TOPEX data can effectively resolve these "lumped" harmonic effects. Therefore, while the overall performance of the fields seems to be improving, this preliminary assessment of the most "TOPEX-orbit" sensitive part of the error spectrum indicates that limited amounts of TOPEX tracking data (a few month's worth) should yield a satisfactory orbit (radial errors ~10 cm) even with current models shortly after TOPEX flies.

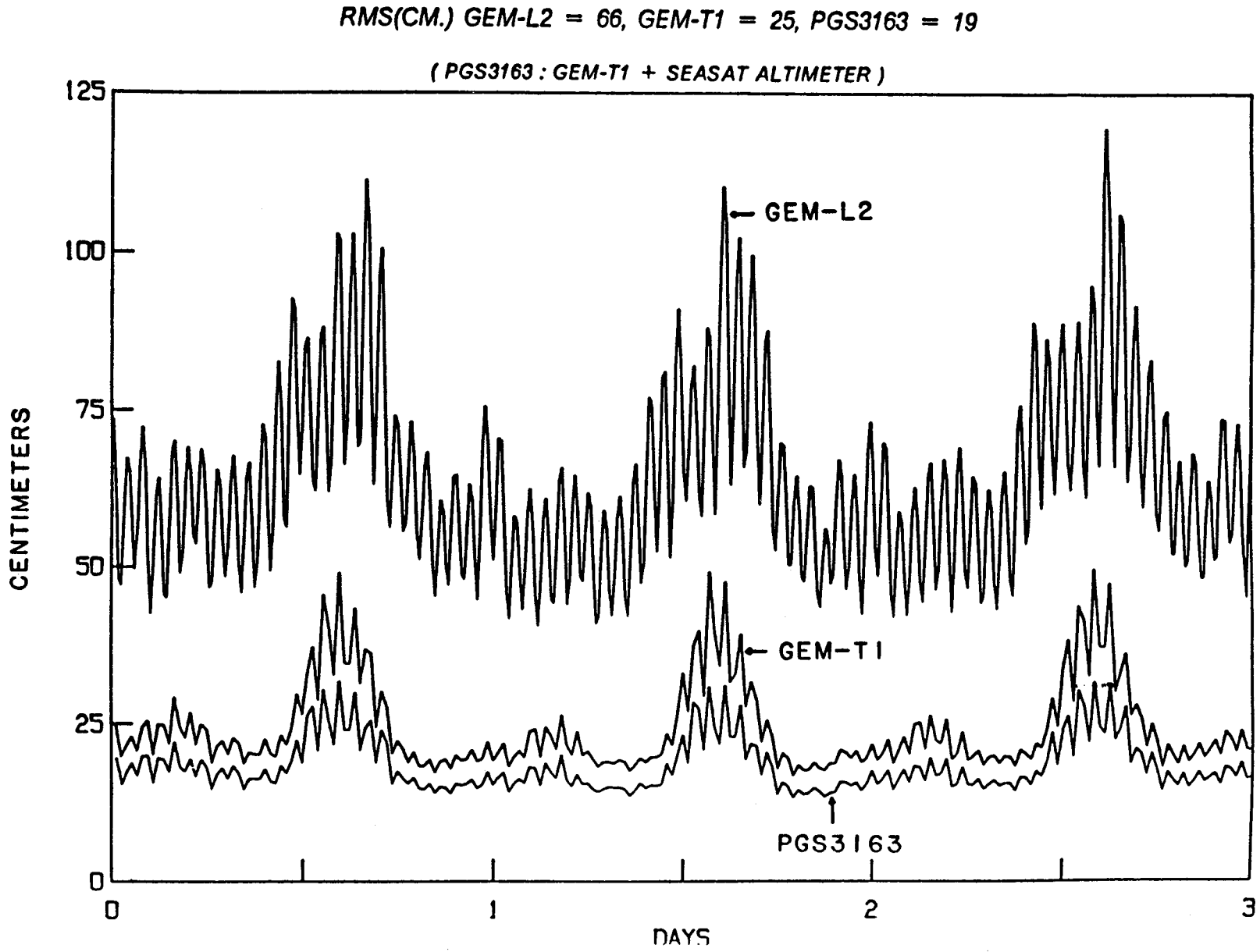

TOPEX PROJECTED RADIAL ERRORS

FIGURE 17

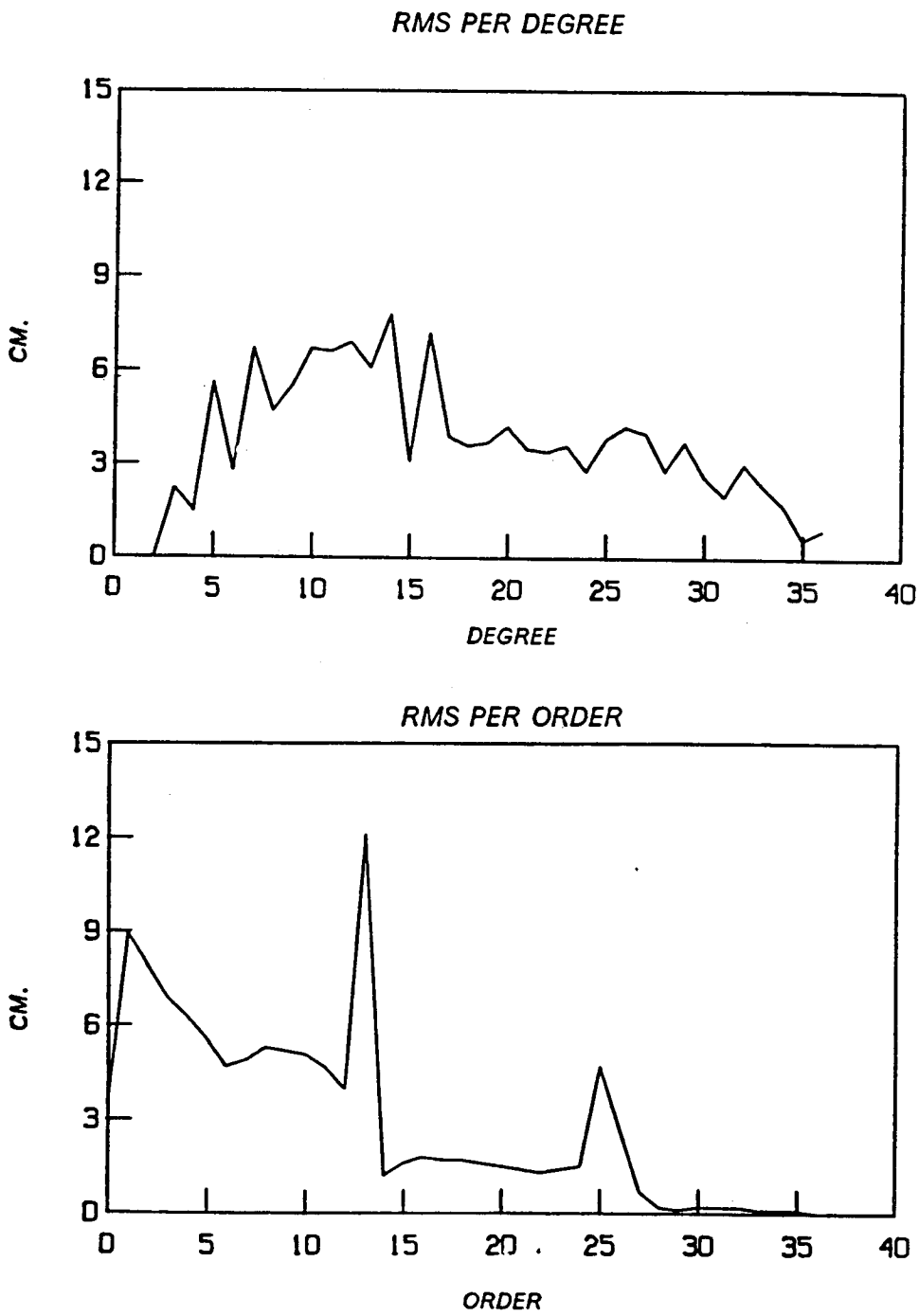

TOPEX PROJECTED RADIAL ERRORS GEM-T1

FIGURE 18

IX. SUMMARY

This report documents the derivation of calibration techniques using independent and dependent data sets incorporating both variance and eigenvector analyses. It details their application in assessing the accuracy and calibration of the error covariances of the GEM-T1 gravitational model. Taking full advantage of the "super-computing" environment available at NASA/Goddard Space Flight Center, many solutions have been compared providing a completeness of field testing heretofore impossible within earlier computing environments. The results show a model remarkably consistent in stability for the calibration of its errors. With the exception of a few known and understood high-order resonance terms (and the limitations of the high altitude Lageos satellite providing data suitable for the calibration of a full 36x36 field), the calibrations show a stability in error assessment at the 10% level for each of the major data subsets employed in this evaluation. The published coefficient uncertainties for GEM-T1 and its error covariance matrix are herein found to be reasonably well calibrated and reliable. For example, the average calibration factor (k) for GEM-T1 using nine major sets of data in Table 9 (excluding the anomalous result for LAGEOS data) gave k=0.99 (± .08) for the coefficient calibration and k=0.95 (± .09) for the eigenvector calibration. This is a gratifying result, particularly, since formal least squares error formulae based on random variables were employed with compensating downweighting factors to account for more general formulae involving error sources with unknown systematic effects. Appendix A analyzes the mathematical validity of the error estimation techique for the gravity model, develops an optimal weighting technique with internal self-calibration of the error model, and shows that GEM-T1 approximates this process.

ACKNOWLEDGEMENTS

The authors would like to thank C.K. Shum, John Ries and Byron Tapley of the Center of Space Research, University of Texas, for their thoughtful reading and constructive comments in the preparation of this report. George Rosborough of the University of Colorado likewise made valuable comments. The authors would like to also thank Dick Rapp and Nick Pavlis of Ohio State University for their assistance in processing and helping us successfully utilize the surface gravimetry.

APPENDIX A

F.J. Lerch and E.C. Pavlis

WEIGHTING, ERROR COVARIANCE, AND OPTIMIZED CALIBRATION FOR BIASED DATA IN GEM-T1

The least-squares or modified least-squares linearized adjustment methods are commonly used to estimate a set of parameters (the solution) from a linear combination of observation residuals. The residuals (difference between the observations and the computed observables from a model) consist of, in addition to the errors arising from the modeled parameters, a systematic effect due to unadjusted parameters and a random noise component. While the exact cause of these systematic effects (biases) is unknown, we will show that they can be accommodated for in the solution statistics through the proper weighting of the data. It is shown that the ensemble of biases in the GEM-T1 observation residuals also have some form of randomness so that the linear combination of the data errors tend to average towards zero; this is necessary for the signal to be recovered well in the solution. The analysis in this appendix is an attempt to (1) characterize the bias errors, (2) weight their effects along with the noise errors, (3) develop an approximate form of the error covariance, and (4) provide an optimized technique for weighting the various data subsets. The calibration of the error estimates for our solutions hinges on deriving the optimal data weights; we use a combination of solutions which use data subsets in these assessments.

The estimation technique for the GEM-T1 solution is a weighted least squares process with a priori constraints on the size of the adjusting coefficients. The inverse of the weighted least-squares normal equations (N) is used as the error covariance of the estimated parameters. This process is common in least-squares solutions in a formal sense, and it is formally correct when the mathematical model is complete and thus the computed residuals are unbiased. Since the GEM-T1

observation residuals display a biased behavior due to unmodeled effects, a special weighting of the normal equations is employed to make the simplified error estimation (N^{-1}) applicable as an approximation for the error estimate of the solution. An optimization of this weighting process is developed herein which automatically provides for a well calibrated error estimate of the gravity parameters. The appendix is presented in three parts:

A1. Weighting for Biased Data

A2. Error Covariance for Biased Data Reduced to Simplified Form (N^{-1}), and

A3. Optimization of Weighting With Error Calibration

There is also a Summary section to the appendices.

A1. WEIGHTING FOR BIASED DATA

A1.1 Experimental Analysis

The characteristics of the weighting system are based upon the actual performance of the observation residuals. The tracking data is post-processed, in this case using GEM-T1, over orbital arc lengths used in the GEM-T1 solution, and the data residuals are analyzed to determine the systematic characteristics seen in the passes of tracking data. Let the residuals r be denoted as

$$r = r_s + n \qquad \text{(A1-1)}$$

where r_s is the systematic part of the residual and n is the random noise. Typically the systematic effects appear as a straight line (when the residual is plotted against the observation derivative in time). For example, for laser ranges (R) over a pass of NOBS points

$$r_s = r_o + \dot{R}\,\tau \qquad \text{(A1-2)}$$

where r_o is an offset constant, τ is a timing constant, and $\dot{R}$ is the range rate. Let the average data residual per pass represent a bias

$$b = \frac{\Sigma r}{NOBS} = \frac{\Sigma r_s}{NOBS} + \frac{\Sigma n}{NOBS} \qquad \text{(A1-3)}$$

where the symbol (Σ) indicates summation over the components in the vectors (r, r_s, and n).

Since the random noise will largely average out over the typical number of points seen in a pass, the significant effect is given by

$$E(b) = \frac{\Sigma r_s}{NOBS} \neq 0. \qquad \text{(A1-4)}$$

Note that for symmetric coverage about $\dot{R} = 0$, (point of closest approach):

$$E(b) \simeq r_o.$$

In the analysis presented here using a sample of passes (Brown, 1988) fit with GEM-T1, it was found that the biases (as in (A1-3)) are the dominant part of the systematic effects seen in r_s (from (A1-2)) which may be associated with a bias in the measurements. For example, on 450 passes of laser tracking acquired on GEOS-1 during 1977 and 1978 (mostly SAO/NASA tracking), the rms of the residuals, $\sigma(r)$, and the biases $\sigma(b)$ for all the passes were

$\sigma(r) \equiv \sigma_t = 70$ cm
$\sigma(r_s) = 60$ cm
$\sigma(b) = 50$ cm
NOBS = 60 average pts. per pass (after data sampling)

where σ_t refers to the residuals for a specific satellite data type t (i.e., GEOS-1 laser ranges).

The histogram of the biases for the 450 passes appear as a normal distribution with an average bias

$$\bar{b} = 0.2 \text{ cm.}$$

Inspection of the biases (per pass) in time plots on a daily basis show fluctuations that appear random. At this point it is unimportant to characterize whether these biases are in the data themselves or whether they are a result of unmodeled (or poorly modeled) force modeling effects. What is important is that these errors yield data residuals which are quite systematic over a pass and are describable using the model given in (A1-2).

During the 1980 period the laser data on GEOS-1 was not used in GEM-T1, but a similar analysis of these data gave an improved set of residuals: $\sigma_t = 35$ and $\sigma(b) = 25$. This result is typical for the laser systems, especially for the SAO systems which were improved over this time interval. Similar analysis on a pass-by-pass basis is being developed for other satellites. Preliminary results on Starlette and Lageos indicate that much smaller and less biased residuals are obtained. Because of the significant improvement in the residuals and biases on GEOS-1 laser data between 1977 vs. 1980 with the same gravity model, it would appear that a significant source of the biases for the earlier time frame is the measurements themselves (or related pre-processing).

A1.2 Effects of Biased Data on Least Squares Estimation

To examine the effect of biased data (unmodeled effects) on the solution, a single pass of tracking data with residuals r contributes to the overall weighted least-squares solution (as in GEM-T1), as

$$Q = f\, r^T W r \qquad \text{N points for the pass} \qquad \text{(A1-5)}$$

where

$W = [1/\sigma_t^2]$ diagonal weight matrix

σ_t = rms of residuals for satellite data type t

f = scale factor to be estimated to account for effects of biased data in the solution

Let the bias* be constant per pass and random from pass to pass with variance for a given data type as

$$E(b^2) = \sigma^2(b)$$

Denote the residual r as

$$r = Ax + b + n$$

$$= r_s + n \qquad \text{(A1-6)}$$

where

x = gravity and other unknowns

*The bias b and other constants are used interchangeably as a constant and a vector constant.

n = random noise

b = bias

r_s = systematic effect as in (A1-2).

For simplicity, consider the systematic part of r from (A1-6) as

$$r_s = Ax + b$$

$$Ax = \bar{g} + \Delta g \qquad \text{(A1-7)}$$

where

$$\bar{g} = \frac{\Sigma A_i x}{NOBS} \qquad \text{average offset (i = 1 to NOBS)} \qquad \text{(A1-8)}$$

and let $\bar{g}$ be estimated from the biased data. Minimizing Q wrt $\bar{g}$ will give the normal equations as

$$f\ G^T W G\ \bar{g} = f\ G^T W r \qquad \text{(A1-9)}$$

$$M = f\ G^T W G \quad \text{normal matrix} \qquad \text{(A1-10)}$$

where $G^T = (1,1,1\ldots1)$ NOBS ones for the pass. From (A1-6 through A1-9)

$$\hat{\bar{g}} = \frac{\Sigma r}{NOBS} = \frac{\Sigma Ax}{NOBS} + \frac{\Sigma(n+b)}{NOBS}$$

$$= \bar{g} + b + \frac{\Sigma n}{NOBS}$$

with error and variance respectively as

$$\hat{\bar{g}} - \bar{g} = b + \frac{\Sigma n}{NOBS}$$

$$\sigma^2(\bar{g}) = \sigma^2(b) + \frac{\sigma^2(n)}{NOBS} \qquad \text{(A1-11)}$$

From (A1-10) the least-squares error estimate of the variance is

$$\sigma^2(\bar{g}) = M^{-1} = \frac{\sigma_t^2}{f\ NOBS} \qquad \text{(A1-12)}$$

Equating (A1-11) and (A1-12) gives the scale factor

$$f = \frac{\sigma_t^2}{\sigma^2(n) + NOBS\ \sigma^2(b)} \qquad \text{(A1-13)}$$

$$\simeq \frac{1}{N}\left[\frac{\sigma_t}{\sigma(b)}\right]^2 \qquad \text{(A1-14)}$$

since the effect of the noise is small compared to NOBSxσ^2(b).

Noting that $\sigma^2(b)$ varies with the data type

$$\sigma_t(b) \equiv \sigma(b)$$

and since it is a significant part of the rms of the residuals, $\sigma_t(r)$, then

$$\frac{\sigma_t}{\sigma(b)} \equiv \frac{\sigma_t(r)}{\sigma_t(b)} \simeq 1 \qquad \text{(A1-15)}$$

Hence (A1-14) becomes, using (A1-15)

$$f \simeq \frac{1}{NOBS} \qquad \text{(A1-16)}$$

which is a factor used to downweight the data to account for the unmodeled bias in the pass.

For GEM-T1, f=.02 was found to be optimal; this corresponds to N=50 on average which agrees well with the overall distribution of GEM-T1's data. This is especially true for the sampling used for the SAO laser data where a typical pass contained 50 to 60 observations (Brown, 1988).

A1.3 Optimal Estimation By Adjustment of Bias Per Pass of Data

Herein, we will analyze the effect of the bias adjustment on the weighting and error estimation from a pass of data as defined in Section A1.2. From (A1-6) the residuals r are unadjusted for bias. Designate the adjusted residuals for bias as

$$\hat{r} = r - \hat{b} = n + Ax + b - \hat{b}$$

where as before

$$r = n + b + Ax$$

An a priori constraint $\sigma_A \equiv \sigma(b)$ is applied to the bias in the adjustment. Using the symbols and definitions of Section A1.2 we first minimize Q_b (similar to equation (A1-5)) wrt b, solve for an a priori value of b, and transform Q_b by back substitution for b as follows:

$$Q_b = \hat{r}^T W \hat{r} + \hat{b}^2/\sigma_A^2$$

$$\frac{1}{2} Q_b = -G^T W \hat{r} + \frac{\hat{b}}{\sigma_A^2} = 0$$

$$\hat{b} = + \frac{\Sigma r}{NOBS+q}$$

$$q = (\sigma_t/\sigma_A)^2$$

$$Q_b = \frac{r^T W r}{NOBS+q} + \frac{(N+q-1) \Sigma r^2 - (\Sigma r)^2}{\sigma_t^2 (NOBS+q)} \qquad (A1\text{-}17)$$

Note that if the residuals are dominated by the bias b, then $\sigma_t(r) \simeq \sigma_A$ or q=1. In this case, with q=1 and

r = constant bias over the pass, then

$$Q_b = \frac{r^T W r}{NOBS+1} . \qquad (A1\text{-}18)$$

This result is very similar to the weighting in (A1-5) where by (A1-15) and (A1-16)

$$Q \simeq Q_b$$

with

$$f \simeq \frac{1}{NOBS}$$

For GEM-T1, f=.02 corresponding to NOBS=50 on average. Hence the weighting in GEM-T1 is near optimum for the case where the laser residuals are dominated by a bias and all passes would ideally have 50 points.

If, in addition to a bias, we consider a timing error τ (as in (A1-2)) in the residuals with balanced sampling about $\dot{R}$=0 (i.e., a pass

C-2

which is symmetric about the point of closest approach of the satellite to the station) where

$$r = r_s = b + \dot{R}\,\tau$$

then (with q=1) in (A1-17)

$$Q_b \simeq \frac{r^T W r}{NOBS+1} + \frac{\Sigma(\dot{R}\,\tau)^2}{\sigma_t^2} \qquad \text{(A1-19)}$$

This case shows that the downweighting factor f only principally influences the bias. The approach would still be optimum if the timing errors were largely attributed to the gravity field signal.

Therefore, this method is ideal when biases dominate the measurement residuals. It has great benefit in the proper relative weighting of the data, particularly when there is significant variability in the number of points per pass and in the magnitude of the biases $\sigma_t(b)$. The bias variability can be systematic chronologically as will happen as the laser systems are improved. Of most benefit, this approach reveals the reduction of the adjusted residuals $\sigma_t(\hat{r})$ when biases are removed as compared to the $\sigma_t(r)$ when biases are not removed. Based upon this approach for error estimation, a reduction of the ratio of $\sigma_t(\hat{r})/\sigma_t(r)$ should occur in the errors (which is a significant reduction for laser tracking when normal points are employed) since $\sigma_t(\hat{r})$ would be small.

It should be noted that A1.2 accounts for the effect of bias on the solution when it is not modeled whereas A1.3 considers its effect when it is modeled, which is the recommended approach. Since our solution (GEM-T1) does not adjust for biases (per pass), this situation is analyzed in the subsequent sections.

A2. ERROR COVARIANCE FOR BIASED DATA REDUCED TO SIMPLIFIED FORM (N^{-1})

A2.1 FORMAL LEAST-SQUARES ERROR ESTIMATE

The weighted least-squares solution of the normal equations with random observation errors (n) and complete modeling of parameters in the solution ($\underline{\bar{X}}$) gives a simplified form of the error covariance matrix V(x). A more general form is given when the observation or modeling errors (e) have systematic effects (e_s) in addition to the pure random errors attributable to (n).

The following development is given for the error estimation, namely:

$$\hat{r} \equiv O - \hat{C} \qquad \text{observed minus computed quantities from solution } \underline{\hat{\bar{X}}}$$

$$e \equiv O - C \qquad C \text{ computed from true values } \underline{\bar{X}}$$

$$= n + e_s \qquad n - \text{random noise}; \; e_s - \text{systematic error}$$

$$x = \underline{\hat{\bar{X}}} - \underline{\bar{X}} \qquad \text{error in solution} \qquad \text{(A2-1)}$$

$$\hat{C} = C + A\,x \qquad A \text{ is matrix of partials for Taylor's expansion (linear) about the true } \underline{\bar{X}}.$$

From the above

$$\hat{r} = O - C - A\,x$$

$$= e - A\,x \qquad \text{(A2-1a)}$$

The least-squares weighted normal equations with weight matrix W (to be defined) become from (A2-1, 1a).

$$A^T \hat{Wr} = A^T We - A^T W A x = 0 \qquad \text{(A2-2)}$$

with error

$$x = (A^T W A)^{-1} A^T We \qquad \text{(A2-3)}$$

Note that if e is biased, then x is expected to be biased, as is the case within our solution. The error matrix for the solution is

$$V(x) \equiv E(x\, x^T) = E[x-E(x)][x-E(x)]^T + E(x)\, E(x)^T$$

$$= (A^T WA)^{-1} A^T W\, E(ee^T)\, WA(A^T WA)^{-1} \qquad \text{(A2-4)}$$

We will refer to V(x) as the error covariance. For the most generalized case where e has systematic effects let

$$W^{-1} = E(ee^T) \quad \text{which is non-diagonal,}$$

then

$$V(x) = (A^T WA)^{-1} = N^{-1} \qquad \text{(A2-5)}$$

This case is not generally useful since W is non-diagonal and generally unknown given our lack of knowledge of all the unmodeled errors. For the most simplified case let

$$e = n$$

then

$$W^{-1} = [\sigma_n^2] \quad \text{which is a diagonal matrix}$$

and

$$V(x) = [A^T WA]^{-1} = N^{-1} \qquad \text{(A2-6)}$$

which is the formal least squares error covariance estimate.

Our solution for the error x is a mixture of (A2-5) and (A2-6). We cannot apply W^{-1} of (A2-5) to the solution (A2-3) since the weight matrix is non-diagonal and unknown. Further we cannot apply (A2-6) since the error covariance is assumed to be diagonal and our errors by definition include biases which are strongly correlated within a pass of tracking data. Hence our errors follow (A2-4) where ideally we model

$$W = f\left[1/\sigma_t^2(e)\right] \qquad \text{which, again, is a diagonal matrix.} \quad \text{(A2-7)}$$

Here f is a downweighting factor accounting for the correlated systematic error effects in modeling the data and $\sigma_t^2(e)$ is estimated from the rms of the residuals of a given data type for a given satellite based upon its post-solution performance. It remains for us to show that (A2-4) with (A2-7) can be approximated by (A2-6) under empirical conditions, albeit, which are reasonably simplified.

A2.2 EMPIRICAL MODELING OF SYSTEMATIC EFFECTS

For our case consider systematic effects (e_s) on a pass-by-pass basis for a given satellite's data. We typically find these systematic signatures to exhibit a straight-line character as follows (see Section A1.1):

$$e = n + e_s \qquad \text{(A2-8)}$$

$$e_s = b + \Delta\dot{e}_s \, \tau \qquad \text{(A2-9)}$$

$$\Delta\dot{e}_s = \dot{e}_s(t) - \dot{e}_s(t_m)$$

where

e_s - straight-line fit

b - constant offset centered at the midpoint (t_m) of the straight line

τ - constant timing error

$\dot{e}_s$ - time rate of e_s

n - random uncorrelated noise

For each data type the biases over all passes can be characterized as (see Section A1.1)

$$E(b^2) = \sigma^2(b) \qquad \text{(A2-10)}$$

and our experience has shown that it is reasonable to assume these systematic trends are uncorrelated among passes (certainly, for weighting purposes), then

$$E(b_i\ b_j) = 0,\ i \neq j\ . \qquad \text{(A2-11)}$$

We will further assume that within a pass the bias b is orthogonal to the timing error term

$$b\Sigma\ \Delta\dot{e}_s\ \tau = 0 \qquad \text{(A2-12)}$$

which is reasonable (in our case) since the orbits are nearly circular and the coverage is usually somewhat symmetric about the midpoint t_m of the straight line.

A2.3 ERROR COVARIANCE AND SIMPLIFIED MODELING

Let the contributions to the least-squares normal matrices be defined as follows:

(a) for each tracking pass p of observations of a given data type, t, with the number of observations equal to $NOBS_p$

$$N_{p,t} = (A^T W A)_{p,t} \qquad \text{(A2-13)}$$

$$R_{p,t} = (A^T W e)_{p,t}$$

where from (A2-7) with $f = f_{p,t}$

$$W = W_{p,t} = [f_{p,t} / \sigma_t^2(e)]$$ which is a diagonal matrix of dimension $NOBS_p$

(b) for each data type t

$$N_t = \Sigma N_{p,t} \qquad \text{(A2-14)}$$

$$R_t = \Sigma R_{pt}$$

(c) for all data types

$$N = \Sigma N_t$$

$$R = \Sigma R_t \qquad \text{(A2-15)}$$

The normal equations with solution x are

$$N x = R$$

$$x = N^{-1} R \qquad \text{(A2-16)}$$

and the error covariance is (a priori constraints to be added later)

$$V(x) = E(x\ x^T)$$

$$= N^{-1}\ E(R\ R^T)\ N^{-1} \qquad \text{(A2-17)}$$

We will show that

$$E(R\ R^T)\ N^{-1} \simeq I \qquad \text{(A2-18)}$$

and hence (A2-17) is simplified to

$$V(x) = N^{-1} \qquad \text{(A2-18a)}$$

From (A2-11), (A2-12), (A2-8,-9), and the condition of uncorrelated random noise (n) we have

$$E[R_{p,t}\ R^T_{q,t'}] = 0 \qquad p \neq q \text{ or } t \neq t' \qquad \text{(A2-19)}$$

$$= E[R_{p,t}\ R^T_{p,t}] \qquad p=q \text{ and } t=t'$$

hence, using (A2-13) through (A2-16)

$$E\ [R\ R^T] = E\ [(\Sigma\ R_t)\ (\Sigma\ R_t)^T] = E\ [\sum_t R_t\ R_t^T] \qquad \text{(A2-20)}$$

$$= E\ [\sum_t \sum_p (R_{p,t}\ R^T_{p,t})]\ ,$$

$$E\ [R_t\ R_t^T] = E\ [\sum_p (R_{p,t}\ R^T_{p,t})]$$

$$= E[\sum_p (A^T We)_p\ (A^T We)^T_p]_t\ , \qquad \text{(A2-21)}$$

and

$$(R_{p,t}\ R^T_{p,t}) = (A_p^T\ W_p\ e_p\ e_p^T\ W_p\ A_p)_t \qquad \text{(A2-22)}$$

For each pass of data, from (A2-1, -8, -9)

$$(O\text{-}C)_p = e_p = n_p + e_{s,p} \qquad \text{(A2-23)}$$

$$(O\text{-}\hat{C})_p = \hat{r}_p = e_p - A_p\, x$$

for $NOBS_p$ data points.

Since gravity and other parameters modeled in the solution ($A_p x$) produce misclosure errors in the residuals $\hat{r}_p$ within a pass of data which (like e_s) largely fit to a straight line (see equations A1-1,-7,-8), we will average the signature A_p over the pass (A1-8) for each component k of the solution. Thus for each data type let

$$A_p = [A_p^k]$$

$$\bar{A}_p^k = \frac{\sum_i (A_p^k)_i}{NOBS_p}$$

$$A_p = [A_p^k] \approx [\bar{A}_p^k\, G] \equiv \bar{A}_p \qquad \text{(A2-24)}$$

where

$G^T = (1, 1, 1 \ldots 1)$ $NOBS_p$ ones

$k = 1$ to K solution parameters.

Note that in (A2-12), with b replaced by $\bar{A}_p$, the orthogonality holds.

Using (A2-24) and (A2-8,-9,-11,-12,-21) in (A2-22) with $A_p \equiv \bar{A}_p$, then

$$E\left(R_{p,t}\, R_{p,t}^{T}\right) = E\left[A_p^T\, W_p\, e_p\, e_p^T\, W_{p2}\, A_p\right]_t$$

$$= \left[A_p^T\, W_p\, A_p\right]_t \qquad \text{(A2-25)}$$

where

$$W_{p,t} = \left[f_{p,t} \,/\, \sigma_t^2(e)\right]$$

$$f_{p,t} = \frac{\sigma_t^2\,(e)}{\sigma_t^2(n) + NOBS_{p,t}\, \sigma_t^2(b)} \,. \qquad \text{(A2-26)}$$

Notice that (A2-26) may be approximated by

$$f_{p,t} \simeq \frac{1}{NOBS_{p,t}} \qquad \text{(A2-27)}$$

if we assume (as found in Section A1.1) that the variance of the bias, $\sigma_t^2(b)$, dominates the errors $\sigma_t^2(e)$ for a typical pass. (In the presence of biases of weighting this type tends to equalize the data by passes instead of by number of observations.)

Using the result (A2-25) in (A2-20) and (A2-21), then with $A_p \equiv \bar{A}_p$

$$E\left[R\, R^T\right] = \sum_t \sum_p \left(A_p^T\, W_p\, A\right)_t \qquad \text{(A2-28)}$$

This simply gives from (A2-13, -14, -15)

$$E\left[R\, R^T\right] = N \qquad \text{(A2-29)}$$

yielding the desired result (A2-18) and hence

$$V(x) = N^{-1}. \qquad \text{(A2-30)}$$

This represents the simplified form of the weighted least-squares inverse.

For practical application, the weighting $W_{p,t}$ in (A2-26) can be optimally achieved by solving for a bias per pass as indicated in Section A1.3 (see equation A1-19). The next level of simplification is shown in Section A3 of the Appendix. Here an average factor of $f_{p,t}$ in (A2-26) is employed which may be represented by

$$f_t = \bar{f}_{p,t} = \frac{\sigma_t^2(e)}{\sigma_t^2(n) + \overline{NOBS}_t \, \sigma_t^2(b)} \qquad \text{(A2-31)}$$

where a mean number of points per pass ($\overline{NOBS}_t$) for each data type t is employed. In Section A3 the weighting factor f_t in actual practice is resolved for each data type t from analysis of subset solutions associated with each data type requiring the condition (A2-30).

A2.4 MODELING THE A PRIORI KAULA CONSTRAINT

Before showing further simplification of the weighting used in GEM-T1, it is desirable to introduce the Kaula constraint equations which we may regard as data type t=0. The equations for the errors in the solution are obtained directly from the constraints on the coefficients (C) as follows:

firstly, denote the coefficients of degree ℓ as

$$C_\ell = \begin{bmatrix} C_{\ell m} \\ S_{\ell m} \end{bmatrix} \qquad m = 0 \text{ to } \ell \ (S_{\ell 0}=0), \qquad \text{(A2-32)}$$

the entire set by

$$C = [\ C_\ell\ ]$$

the solution errors ΔC (a subset of x) by

$$\Delta C = \hat{C} - C\ ,$$

then the error e_o and residual $\hat{r}_o$ (data type t=o) are

$$e_o = 0(\text{zero}) - C \tag{A2-33}$$

$$\hat{r}_o = 0(\text{zero}) - \hat{C} = e_o + \Delta C$$

The contributions to the normal equations for t=o become

$$N_o\ \Delta C = R_o$$

$$N_o = W_o = [f_o/\sigma^2_\ell\ (e_o)] \tag{A2-34}$$

$$R_o = W_o e_o$$

$$\sigma^2_\ell\ (e_o) = \frac{1}{2}\ (10^{-5}/\ell^2)^2 \qquad \text{(Kaula's rule).}$$

The weighting factor $f_o \simeq 1$ can be contrasted to the actual tracking data types, where $f_t \simeq .02$ was found to be appropriate. From equation (A2-27) each coefficient behaves like a bias with one observation point as in (A2-33).

We statistically treat the coefficients C in the error equation e_o, (A2-33), similar to the biases for the tracking data, namely

$$E\ (C_i\ C_j) = 0 \qquad i \neq j$$

$$E\ (C_i^2) = \sigma^2_\ell(C_i) \tag{A2-35}$$

$$C_i = C_{\ell m} \text{ or } S_{\ell m}$$

With this treatment the normal equations (A2-34) with the error e_o (A2-33) may be combined as data type t=o in (A2-15, -16, -17) resulting in (A2-18a).

A2.5 RANDOMNESS TESTS FOR THE ENSEMBLE OF BIAS PARAMETERS AND COEFFICIENTS

The degree of randomness of the biases and the coefficients (as with random noise) is important for the error solution x in (A2-16), which is a linear combination of all these error effects. The effect of randomness, with proper weighting, permits (x) to average toward zero. A measure of the randomness of the biases and the coefficients is given.

A measure of the randomness of the ensemble of the biases for a given data type t is

$$Z = \frac{|\bar{b}_t|}{\sigma(\bar{b}_t)} \leq 2 \qquad \text{(A2-36)}$$

where

$$\bar{b}_t = \frac{\Sigma\, b_i}{NB_t}$$

$$\sigma(\bar{b}_t) = \frac{\sigma_t(b)}{(NB_t)^{1/2}} ,$$

with NB_t being the number of passes.

Similarly, for the randomness of the coefficients

$$\bar{C}_\ell = \frac{\sum_m (C_{\ell m} + S_{\ell m})}{2\ell + 1} \qquad \text{(A2-37)}$$

$$\text{(Modified Kaula's Rule)} = \sigma(c_\ell) = 10^{-5}/\sqrt{2}/\ell^2$$

$$\sigma(\bar{C}_\ell) = (10^{-5}/\sqrt{2}/\ell^2)/(2\ell+1)^{1/2}$$

$$Z(\ell) = \frac{\bar{C}_\ell}{\sigma(\bar{C}_\ell)}$$

Some results are available.

From Section A1.1, the biases for the GEOS-1 (1977-78) laser data employed in GEM-T1 gave (for 450 passes) the following values:

$$\bar{b}_t = .2 \text{ cm}$$

$$\sigma_t(b) = 50 \text{ cm}$$

$$\sigma(\bar{b}_t) = 2 \text{ cm}$$

$$Z = 0.1$$

A time ordered plot of the biases is given in Figure A2-1 and a randomness test per tracking site for these biases is given in Table A2-1 showing strong indication of stochastic behaviour from pass to pass.

Using a solution (PGS-3325) which is a combination of GEM-T1 normals, surface gravity, and altimeter data, the statistics in (A2-37) for the randomness of the coefficients are listed in Table A2-2. Since the constraint dominates the higher-degree terms in GEM-T1, it is important that the $Z(\ell)$ improve with degree ℓ, which is supported by the tabulated results. The random behaviour of the coefficients causes a minimal error in the solution when the "apparent" biases (C) in (A2-33)

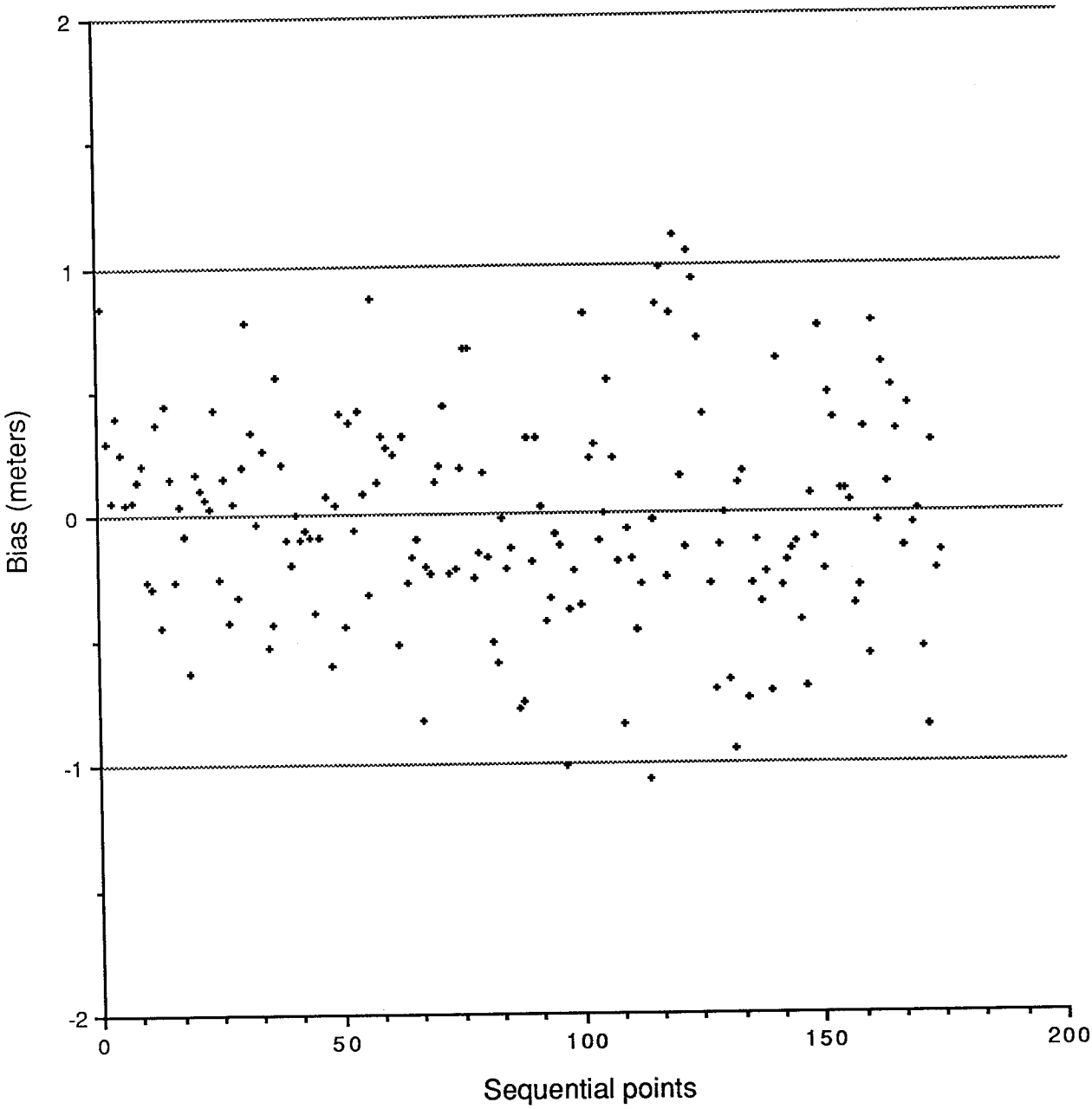

Figure A2-1. Pass Biases
GEOS-1 Laser Tracking Stations
(187 passes - 8 months, 1977)

TABLE A2-1

BIAS RANDOMNESS TEST PER LASER SITE

($Z \leq 2.5$)

LASER STATION	PASSES	CENTIMETERS $\sigma(b)$	$\bar{b}$	$\sigma(\bar{b})$	Z
AREQUI91	68	54	9	6.5	1.4
HOPLAS91	43	40	11	6.1	1.8
ORRORL91	46	41	-15	6.0	-2.5
RAMLAS1	4	57	3	28.5	.1
STALAS1	6	17	-2	7.0	-.3
NATAL91	15	98	-15	25.3	-.6
GORF1001	4	42	-34	21.0	-1.6
GORF0652	1	177	177	—	—
AVG	(187)	54	1	3.9	.3

TABLE A2-2

Randomness Test for Potential Coefficients*
of Degree ℓ ($Z \leq 2.5$)
(Coeff. units of 10^{-9})

Degree ℓ	No. of Coeff.	RMS (Coeff.)	Kaula x 0.7	$\bar{C}_\ell$	$O(\bar{C}_\ell)$	Z
3	7	1122.7	785.7	807.90	296.96	2.72
4	9	529.2	441.9	161.19	147.31	1.09
5	11	351.4	282.8	-105.43	82.28	-1.24
6	13	251.3	196.4	-158.04	54.48	-2.90
7	15	193.2	144.3	23.43	37.26	0.63
8	17	118.9	110.5	25.65	26.80	0.96
9	19	97.7	87.3	10.50	20.03	0.52
10	21	77.7	70.7	-26.82	15.43	-1.74
11	23	53.5	58.4	-19.00	12.19	-1.56
12	25	31.2	49.1	6.17	9.82	0.63
13	27	45.7	41.8	8.49	8.05	1.05
14	29	26.0	36.1	0.89	6.70	0.13
15	31	25.3	31.4	2.38	5.64	0.42
16	33	23.3	27.6	-3.87	4.81	-0.81
17	35	20.0	24.5	-0.06	4.14	-0.01
18	37	18.6	21.8	-0.84	3.59	-0.23
19	39	15.2	19.6	0.35	3.14	0.11
20	41	13.7	17.7	1.06	2.76	0.39
21	43	15.1	16.0	2.03	2.45	0.83
22	45	14.0	14.6	1.39	2.18	0.64
23	47	11.7	13.4	-0.79	1.95	-0.41
24	49	10.1	12.3	-0.15	1.75	-0.09
25	51	11.5	11.3	-0.12	1.58	-0.08
26	53	8.8	10.5	1.23	1.44	0.86
27	55	7.8	9.7	0.59	1.31	0.45
28	57	8.8	9.0	0.47	1.19	0.40
29	59	7.6	8.4	-1.59	1.09	-1.45
30	61	8.2	7.9	-0.66	1.01	-0.65
31	63	8.0	7.4	-0.10	0.93	-0.11
32	65	6.9	6.9	0.06	0.86	0.07
33	67	6.9	6.5	-0.51	0.79	-0.64
34	69	7.2	6.1	-0.51	0.74	-0.70
35	71	6.7	5.8	-0.72	0.69	-1.05
36	73	5.7	5.5	-0.18	0.64	-0.28

* PGS-3326: 50 x 50 model GEM-T1 without Kaula constraint with surface gravimetry and SEASAT altimetry.

are properly weighted. Hence, any downweighting of f_o from unity in (A2-34) or misuse of $\sigma_\ell(e_o)$ by ignoring the scale factor of 1/2 will allow the errors in the coefficients to increase and falsely represent their power. Note that when the Kaula constraint is present, the power in the coefficients should become zero for high degree ℓ at the point when the satellite tracking data just begins to have negligible effect on the solution.

A2.6 APPLICATION TO GEM-T1

In the GEM-T1 solution, a more simplified case of the weighting of $W_{p,t}$ and $f_{p,t}$ in (A2-26) was employed. The more general weighting in (A2-26) is based upon $NOBS_{p,t}$ (points per pass) while the simplified weighting is based upon an average $\overline{NOBS}$ over all passes and data types in the solution, namely

$$W_t = f/\sigma_t^2(e) \qquad \text{(A2-38)}$$

$$f = 1/\overline{NOBS} \qquad \text{(A2-39)}$$

$$= 1/50 \quad \text{(for GEM-T1)}$$

In GEM-T1, $\sigma_t^2(e)$ was approximated basically by the rms of the observation residuals from iterative test solutions. It was allowed to vary from the rms by use of tests with other data, in order to account for the variability in $\overline{NOBS}$ for different data types ($\overline{NOBS}_t$) and other variable effects in (A2-26). Furthermore, in the special case of the optical data where considerably fewer points per pass were taken than the laser data, an effective f = 1/10 was employed by applying $\sigma_t^2(e)$ to 1/5 of its corresponding rms residual value so these optical data retain some influence on the solution.

Since the weighting represents an average for the different satellite data types and since the simplified form of V(x) in (A2-28a) is an approximation, an optimal technique for iterating on a weighting factor per data type

$$w_t = f_t/\sigma_t^2(e) \qquad \text{(A2-40)}$$

and a scale factor (k) for the error covariance V(x) has been developed and is presented in the next section. GEM-T1 followed this procedure in somewhat of a piecewise fashion and hence the model may be further refined with use of this more rigorous optimal weighting approach.

The data type t should be considered broadly in general applications of this approach. There is variability in the precision and accuracy among the different laser tracking sites, hence the data type in (A2-40) should reflect this situation. The general improvement seen in modern tracking performance as time progresses is another consideration. Although the former condition has not been generally applied to develop station specific weights in (A2-40) in GEM-T1, the latter condition is considered in the individual weighting factors applied to the normal equations for orbital arcs of tracking data which sequentially span periods of time. In GEM-T2, which will employ some 30 different satellites, we utilize variable weighting factors for satellite tracking data of a similar type. In particular, the laser data from GEOS-1 and GEOS-3 spanning 1975 through 1978 is given smaller weight than the newer data in 1980 (see Section A1.3).

A2.7 SUMMARY

If a more generalized description of the different data types is utilized for the application of the weighting in (A2-26), the better the approximation of the simplified inverse N^{-1} in (A2-30) will become. In summary, N^{-1} is the inverse of the least-squares weighted normal equations and represents, as an approximation, the complete error covariance expression of the solution parameters in (A2-17), namely

$$V(x) = N^{-1} \sum_{t,p} (A_p^T W_p e_p e_p^T W_p A_p)_t N^{-1}$$

$$= N^{-1} \qquad \text{(A2-41)}$$

$$V(x) = \left| \overline{\sum_{t,p}} \left(A_p^T W_p A_p \right)_t \right|^{-1} .$$

The result is considered an approximation because it is based upon an average signature $A_p = \overline{A}_p$ over each pass p of tracking data for the gravity parameters and other modeled parameters. Furthermore, the errors (e_p), in addition to random noise, were assumed to have systematic effects which were empirically modeled as a bias and a timing error for each pass of tracking data. The result has also considered the effect of the Kaula constraints by modeling it as data type t=0 as given in Section A2.4.

A3. OPTIMIZATION OF WEIGHTING AND AUTOMATIC CALIBRATION

There are two major concerns in the proper weighting of least-squares normal equations:

(a) weighting of individual observations corresponding to the expected accuracy of the observation residuals (σ_t) for a given data type t (σ_t is computed from the iterated, rms of the observation residuals), and

(b) the effects of unmodeled biases and forces on the solution by applying a downweighting factor (w_t) for the normal equations (see Table 1 for GEM-T1 weights).

The normal least-squares approach, given σ_t, accounts for (a) but not for the effect of (b) without some special analysis and downweighting process. In our approach we obtain σ_t on a few test arcs for each data type based upon trial (iterative) solutions of the weighted normal equations (w_t). It is the purpose of this section to derive the weights w_t. We will show that these weights can be obtained in a process that automatically calibrates the error estimates of the gravity model.

The optimized process of determining the weights (w_t) for each data type in the solution (with an automatic calibration of the error model) is a refinement in the determination of the GEM-T1 solution. As before, this process is based upon forming subset solutions and comparing these solutions with the complete solution. The subset solution is formed by deleting a given satellite data type from the complete solution. The weighting and calibration is then established by requiring that the difference between the solutions and the error estimates be compatible. It will be shown that in the process of converging the weights (w_t), one automatically obtains a calibration of the error estimates. Hence this process, when applied to GEM-T1 data sets, can then be tested by calibrating the new (refined) GEM-T1 solution with independent surface gravity data by the method given in Section VII of this report.

Solutions are formed after summing the weighted least-squares normal equations. For simplicity let each subset of normal equations (N_t) correspond to the reduced normals, where only the gravity parameters x remain, and assume all other parameters have been accounted for through the back substitution process. Denote the subset normals for a given data type by

$$w_t N_t \hat{x} = w_t R_t \qquad t = 0 \text{ to } T \text{ representing all of the data in the solution,}$$

where t=0 corresponds to the Kaula constraint equations with $w_o = 1/\sigma_\ell^2$ (see Section A2.4).

It is convenient to write

$$w_t = f_t / \sigma_t^2$$

where σ_t is given by (a) above and f_t accounts for the downweighting effect in (b). Note for the case where biases are the dominating errors in the data, equations (A1-15) and (A1-16) show that f_t is expected to correspond somewhat to the reciprocal of the average number of points in a pass for the given data type. For the case of GEM-T1 (Section A2) the overall value of f=.02 would correspond to an average of 50 points per pass for all data types.

Denoting x as the solution (S) for all data subsets and x_t as the subset solution (S_t) of all data except data type t, the difference in the solutions corresponds to the difference in the errors between the solutions, namely

$$x - x_t = [\hat{X} - X(\text{true})] - [\hat{X}_t - X(\text{true})] = \hat{X} - \hat{X}_t$$

Hence, for the analysis we will assume as in (A2-1)

$$x = X - X \text{ (true)}$$

$$x_t = X_t - X \text{ (true)}$$

The following quantities are defined from the weighted normal equations associated with the solutions S and S_t:

$$w_t N_t \hat{x} = w_t R_t \qquad \text{subset normals for data type t}$$

$$N_t = A_t^T A_t \qquad (A3\text{-}1)$$

$$R_t = A_t^T e_t$$

$$\bar{N} = \sum_{j \neq t} w_j N_j \qquad \text{data type t removed} \qquad (A3\text{-}2)$$

$$\bar{R} = \sum_{j \neq t} w_j R_j$$

$$\bar{N} x_t = \bar{R} \qquad \text{subset solution } S_t \qquad (A3\text{-}3)$$

$$(\bar{N} + w_t N_t) x = \bar{R} + w_t R_t \qquad \text{complete solution S} \qquad (A3\text{-}4)$$

$$V(x_t) \equiv \bar{N}^{-1} \qquad \text{error variance of } x_t$$

$$V_{(x)} \equiv (\bar{N} + w_t N_t)^{-1} \qquad \text{error variance of x}$$

$$x = V(x) (\bar{R} + w_t R_t)$$

$$x_t = V(x_t) \bar{R}$$

$$V(x_t - x) = E[x_t - x) (x_t - x)^T] \qquad \text{error variance } x - x_t$$

$$= V(x_t) - V(x) \qquad (A3\text{-}5)$$

$$V(x-x_t) = \bar{N}^{-1} - (\bar{N} + w_t N_t)^{-1}$$

$$\simeq w_t \bar{N}^{-1} N_t \bar{N}^{-1} \qquad t \neq 0 \qquad \text{(A3-6)}$$

Letting Tr denote the trace of a matrix

$$Q_t = (x_t-x)^T(x_t-x) = \mathrm{Tr}\left[(x_t-x)(x_t-x)^T\right] \qquad \text{(A3-7)}$$

then a scale factor, k_t, is defined as

$$Q_t = k_t E(Q_t) = k_t \, \mathrm{Tr}\, E\left[(x_t-x)(x_t-x)^T\right]. \qquad \text{(A3-8)}$$

Since k_t scales the variances of the errors, $V(x-x_t)$, it will be inversely proportional for scaling the weights. Hence, an adjusted weight w_t' is

$$w_t' = k_t^{-1} w_t \, .$$

This result can be shown more directly from use of (A2-25, -26, -31) where

$$w_t R_t = \sum_p R_{p,t}$$

$$= A_t^T w_t e_t$$

$$W_t = w_t I$$

then, with use of an updated weight w_t' ,

$$E(R_t R_t^T) = E[A^T e_t e_t^T A] = \frac{1}{w_t'} N_t \, , \qquad \text{(A3-9)}$$

for which, as in (A3-1)

$$N_t = A_t^T A_t \ .$$

In order to establish the result we need $(x-x_t)$ to the same approximation as (A3-6), namely

$$x-x_t \simeq w_t \bar{N}^{-1} R_t$$

which gives from (A3-5), (A3-6), and (A3-9)

$$(x-x_t)(x-x_t)^T \simeq \frac{w_t}{w_t'} w_t \bar{N}^{-1} N_t \bar{N}^{-1}$$

$$= \frac{w_t}{w_t'} V(x-x_t) \qquad \text{(A3-10)}$$

and then from (A3-8)

$$k_t = \frac{w_t}{w'_t} \qquad \text{(A3-11)}$$

In the above development all the formulae are based upon the <u>a priori</u> weighting (w_t) with the exception of (A3-9) where the updated weight (w_t') is based upon the observation errors e_t including unnmodelled effects. Thus, the adjustment of the weights is obtained from $x-x_t$ which is a linear combination of these errors e_t.

In summary, the adjusted weight for each data type t can be computed from

$$w_t' = k_t^{-1} w_t \qquad \text{(A3-12)}$$

where from (A3-8)

$$k_t = \frac{Q_t}{Tr\ V(x_t - x)} \qquad \text{(A3-13)}$$

This process should be iterated until the weights converge for all t (k_t=1). An overall calibration factor k from (A3-12) when summed over all t is given as

$$k = \frac{\Sigma\ Q_t}{\Sigma\ Tr\ V(x_t - x)} = 1 \qquad \text{(A3-14)}$$

when the weights converge, since k_t=1 for all t.

SUMMARY

A summary is given for the three areas of analysis in the Appendix (A1,A2, and A3). Appendix A1 has shown that the solution scaling factor for overall weighting of the data, f=0.02, found to be optimal for GEM-T1, is attributable to the non-random characteristics of the tracking data residuals in post-fit analyses of these data. While the specific cause of this anomalous data behaviour is not presently known, the net result is that each pass of data, and not the original observations themselves, is more nearly the fundamental data "unit" within our solution. It was shown that the scaling factor represents f=1/n, where n=50, and approximates reasonably well the average number of observations found within a pass of electronic and laser tracking data in GEM-T1. For optical tracking, an n=10 was used through a rescaling of data weights by a factor of 5; this was applied to properly reflect the lower data density found within this observation type.

Appendix A2 has developed a general mathematical form of the error covariance for the GEM-T1 solution parameters which includes effects of unmodeled biases within the data. It was shown that the simplified inverse of the weighted least-squares normal equations (N^{-1}) can approximate the error covariance by downweighting the data to account for the unmodeled bias effects. The weighting should account for the effect of a bias per pass of tracking data to be most complete. However, it is reasonable to statistically account for the biases by applying an average weighting factor to each different satellite data type. This latter process was achieved somewhat in GEM-T1 to approximate the error covariance matrix. It was also shown that the use of least squares collocation (a priori constraint on the size of the coefficients using Kaula's rule) which introduces its own bias-like influence on the coefficient solution (favoring zero power) is well accommodated by the simplified inverse. The process was also shown to perform well because the biases behave largely in a random way across the solution.

Appendix A3 developed an optimized technique for estimating a weighting factor for the different data types in the weighted least-squares solution. The algorithm indicates that by iterating the data-weights to a converged solution, the error covariance matrix (N^{-1}) will automatically be calibrated. A solution which properly combines the subsets of data at their appropriate weights will also be achieved. Again, GEM-T1 was shown to approximate this process in the estimation of its data weighting factors.

Some of the benefits and recommendations which can be made on the basis of the three parts of Appendix A are:

1) It was shown that the more recent data has a diminished biased behaviour which leads us to believe that older data sets can be replaced as new data becomes available; the solution will likewise improve.

2) We are attempting to understand the modeling errors and system causes for these biases so that they can be either eliminated or specifically recovered within the solution, thusly reducing the need for any downweighting of the least-squares normal equations.

3) We will use the methods developed herein as an algorithm for optimal data weighting. Future GEM models will be easier to develop and less difficult to optimize given the analysis performed here.

REFERENCES

Brown, R.D., Characterization of the GEOS-1 Laser Ranging Residuals (1976-1980), STX Contract Report 8801, Oct. 1988.

Englar, T.S., Estes, R.H., Chin, D.C., and Maslyar, G.A., ERODYN Program Mathematical Description Version 7809, BTS Contractor Report BRT-TR-78-69, Greenbelt, Maryland, September 1978.

Estes, R.H. and Majer, V., SOLVE Program Mathematical Description, BTS Contractor Report prepared under NAS 5-27656, Greenbelt, Maryland, March 1986.

Heiskanen, W. and H. Moritz, Physical Geodesy, W.H. Freeman, New York, 1967.

Jekeli, C. and Rapp, R.H., Accuracy of the Determination of Mean Anomalies and Mean Geoid Undulations from a Satellite Gravity Field Mapping Mission, Report No. 307, Department of Geodetic Science, OSU, August 1980.

Kaula, W.M., Theory of Satellite Geodesy, Blaisdell Press, Waltham, Mass., 1966.

Lerch, F.J., Error Spectrum of Goddard Satellite Models for the Gravity Field, Geodynamics Branch Annual Report-1984, NASA TM86223, August 1985.

Lerch, F.J., Klosko, S.M., Laubscher, R.E. and Wagner, C.A., Gravity Model Improvement Using Geos-3, GSFC Document X-921-77-246, Goddard Space Flight Center, Greenbelt, Maryland, 1977.

Lerch, F.J., Klosko, S.M., Laubscher, R.E. and Wagner, C.A., Gravity Model Improvement Using GEOS-3, (GEM-9 and 10), J. Geophys. Res., Vol. 84 (138), pp. 3897-3915, 1979.

Lerch, F.J., Klosko, S.M. and Patel, G.B., Gravity Model Development From Lageos, Geophys. Res. Letters, 9, (11), pp. 1263-1266, 1982.

Lerch, F.J., Klosko, S.M. and Wagner, C.A., Comments on Lambeck and Coleman: 'The Earth's Shape and Gravity Field: A Report of Progress from 1958 to 1982', Geophys. J. Roy. Astron. Soc., Vol. 86, pp. 651-664, 1986.

Lerch, F.J., Klosko, S.M., Wagner, C.A. and Patel, G.B., On the Accuracy of Recent Goddard Gravity Models, J. Geophys. Res., 90, (B11), pp. 9312-9334, 1985.

Lerch, F.J., B.H. Putney, C.A. Wagner and S.M. Klosko, Goddard Earth Models for Oceanographic Applications (GEM 10B and 10C), Marine Geodesy, 5, 2, pp. 145-187, 1981.

Lerch, F.J., Wagner, C.A., Richardson, J.A. and Brownd, J.E., Goddard Earth Models (5 and 6), GSFC X-921-74-145, Greenbelt, MD, 1974.

Marsh, J.G., et al., An Improved Model of the Earth's Gravitational Field: GEM-T1, NASA TM 4019, July 1987.

Marsh, J.G., et al., A New Gravitational Model for the Earth from Satellite Tracking Data: GEM-T1, J. Geophys. Res. 93, B6, 6169-6215, 1988.

Moritz, H., Least Squares Collocation, Rev. Geophys., 16, 421-430, 1978.

Moritz, H., Advanced Physical Geodesy, Abacus, Tunbridge Wells Kent, Kent, England, 1980.

Pavlis, N.K., Modeling and Estimation of a Low Degree Geopotential Model from Terrestial Gravity Data, Report No. 386, Department of Geodetic Science, OSU, March 1988.

Rapp, R.H., Gravity Anomalies and Sea Surface Heights Derived from a Combined GEOS-3/SEASAT Altimeter Data Set, J. Geophys. Res. 91, E5, 4867-4876, 1986a.

Rapp, R.H. and Cruz, J.Y., Spherical Harmonic Expansions of the Earth's Gravitational Potential to Degree 360 using 30' Mean Anomalies, Report No. 376, Department of Geodetic Science, OSU, 1986b.

Rapp, R.H., Private Communications, OSU, 86 Normals for Gravity, 1987.

Reigber, C.H., Balmino, G., Moynot, B. and Mueller, H., The GRIM3 Earth Gravity Field Model, Manuscripta Geodaetica, 8, pp. 93-138, 1983.

Reigber, C.H., "Bestimmungsgleichungen fur Resonanzparameter der Ordnung 13 aus der Analyse Von Bahnen der Satelliten GEOS B, BEC und D10," Deutsche Geodatische Kommission, Reihe C, Haft 198, 1974.

Wagner C.A., The Accuracy of the Low-Degree Geopotential: Implications for Ocean Dynamics, J. Geophys. Res., 88, (B6), pp. 5083-5090, 1983.

Wagner, C.A. and Colombo, O., Gravitational Spectra from Direct Measurements, J. Geophys. Res., 84, p. 4709, 1979.

Wagner, C.A. and Lerch, F.J., The Accuracy of Geopotential Models, Planet. Space Sci., Vol. 26, pp. 1081-1140, 1978.

Wagner, C.A. and S.M. Klosko, "Gravitational Harmonics from Shallow Resonant Orbits," Celestial Mechanics, (16), 1977.

NASA
National Aeronautics and Space Administration

Report Documentation Page

1. Report No.	2. Government Accession No.	3. Recipient's Catalog No.
NASA TM-100713		

4. Title and Subtitle	5. Report Date
An Improved Error Assessment for the GEM-T1 Gravitational Model	November 1988
	6. Performing Organization Code: 621.0

7. Author(s)	8. Performing Organization Report No.
F. J. Lerch, J. G. Marsh, S. M. Klosko, E. C. Pavlis, G. B. Patel, D. S. Chinn, and C. A. Wagner	89B0021
	10. Work Unit No.

9. Performing Organization Name and Address	11. Contract or Grant No.
Goddard Space Flight Center Greenbelt, Maryland 20771	
	13. Type of Report and Period Covered: Technical Memorandum

12. Sponsoring Agency Name and Address	14. Sponsoring Agency Code
National Aeronautics and Space Administration Washington, D.C. 20546-0001	

15. Supplementary Notes: Authors Klosko and Pavlis--EG&G/Washington Analytical Services Center, Lanham, MD; Authors Patel and Chinn--STX, Lanham, MD; Author Wagner--NOAA/National Geodetic Survey, Rockville, MD; and Authors Lerch and Marsh--GSFC, Greenbelt, MD.

16. Abstract

Several tests have been designed to determine the correct error variances for the GEM-T1 gravitational solution which was derived exclusively from satellite tracking data. The basic method employs both wholly independent and dependent subset data solutions and produces a full field coefficient estimate of the model uncertainties. The GEM-T1 errors have been further analyzed using a method based upon eigenvalue-eigenvector analysis which calibrates the entire covariance matrix. Dependent satellite and independent altimetric and surface gravity data sets, as well as independent satellite deep resonance information, confirm essentially the same error assessment. These calibrations (utilizing each of the major data subsets within the solution) yield very stable calibration factors which vary by approximately 10% over the range of tests employed. Measurements of gravity anomalies obtained from altimetry were also used directly as observations to show that GEM-T1 is calibrated. The mathematical representation of the covariance error in the presence of unmodeled systematic error effects in the data is analyzed and an optimum weighting technique is developed for these conditions. This technique yields an internal self-calibration of the error model, a process which GEM-T1 is shown to approximate.

17. Key Words (Suggested by Author(s))	18. Distribution Statement
Gravity Model Accuracy Laser Tracking Geopotential Satellite Geodesy Error Estimation Error Calibration	Unclassified-Unlimited Subject Category 46

19. Security Classif. (of this report)	20. Security Classif. (of this page)	21. No. of pages	22. Price
Unclassified	Unclassified		